
Masters Theses

Student Theses and Dissertations

Summer 2024

Development of a Novel Bioink for Human Vascularized Organoids

Bradley Allen Bromet

Missouri University of Science and Technology

Follow this and additional works at: https://scholarsmine.mst.edu/masters_theses



Part of the [Biology Commons](#)

Department:

Recommended Citation

Bromet, Bradley Allen, "Development of a Novel Bioink for Human Vascularized Organoids" (2024).
Masters Theses. 8190.

https://scholarsmine.mst.edu/masters_theses/8190

This thesis is brought to you by Scholars' Mine, a service of the Missouri S&T Library and Learning Resources. This work is protected by U. S. Copyright Law. Unauthorized use including reproduction for redistribution requires the permission of the copyright holder. For more information, please contact scholarsmine@mst.edu.

DEVELOPMENT OF A NOVEL BIOINK FOR HUMAN VASCULARIZED
ORGANOIDS

by

BRADLEY ALLEN BROMET

A THESIS

Presented to the Graduate Faculty of the

MISSOURI UNIVERSITY OF SCIENCE AND TECHNOLOGY

In Partial Fulfillment of the Requirements for the Degree

MASTER OF SCIENCE

in

BIOLOGICAL SCIENCES

2023

Approved by:

Julie Semon, Co-Advisor
Katie Shannon, Co-Advisor
Krishna Kolan

© 2023

Bradley Allen Bromet

All Rights Reserved

PUBLICATION THESIS OPTION

This thesis consists of the following four articles, formatted in the style used by the Missouri University of Science and Technology:

Paper I, found on pages 3–29, has been edited and resubmitted to the *Journal of Biomedical Materials Research: Part A*, under the title of “The Angiogenic Potential of pH Neutral Borophosphate Bioactive Glasses.”

Paper II, found on pages 30–61, is intended for submission to the *Journal of Tissue Engineering and Regenerative Medicine*, under the title “Adipose Stem Cell Response to Borophosphate Bioactive Glass.”

Paper III, found on pages 62–85, is intended for submission to *Tissue Engineering, Parts A, B and C, or Bioprinting*, under the title “Functional Hydrogel BioInk Modified with Borophosphate Glasses.”

Paper IV, found on pages 86–103, is intended for submission to *Tissue Engineering, Parts A, B and C*, under the title “Development of Novel Bioink for Sizable Organoids via Inner Gelation.”

ABSTRACT

There is a need for a model to better mimic human physiology in the clinic, so the objective was to develop a novel bioink for a 3D tissue model to study human disease and development in a dynamic 3D environment. The results from each corresponding study helped in developing a novel bioink for use in a bioprinted human vascularized organoid. The bioink composed of alginate with other natural hydrogels to function as extracellular matrix and with the addition of borophosphate bioactive glasses (BPBGs) to replace growth factors, can be used with multiple cell types to bioprint the proposed organoid.

Bioactive glass with varying borate-to-phosphate can be added to release therapeutic ions to support multiple types of cells without significantly altering the local pH *in vivo* and *in vitro*. First, the biological effects of these BPBGs were investigated by multiple assays *in vitro* and *in vivo*. The results conclude that the pH neutral BPBGs supported endothelial cell proliferation and migration in cell culture and had greater blood vessel formation in the *in vivo* model, while BPBGs can directly influence viability, differentiation, and migration in adipose stem cells (ASCs) and their secretome. Next, BPBGs were used in an alginate-gelatin hydrogel bioink with ASCs in bioprinted scaffolds. This resulted in the creation of a bioink in which the BPBGs release desired ionic species that stimulate desired cellular responses and can control the bioink viscosity for optimized printing of scaffolds. Finally, a novel bioink made via inner gelation with fibrin instead of gelatin to create a more human-like bioink for the fabrication of a vascularized organoid. Eventually, the organoid can be included in a microphysiological system to facilitate studying developmental biology and disease mechanisms.

ACKNOWLEDGMENTS

I would like to express my sincere gratitude to my committee members Dr. Julie Semon, Dr. Katie Shannon, and Dr. Krishna Kolan. Thank you, Dr. Semon, for being my research advisor and for your guidance, patience, and enthusiasm, throughout my undergraduate research and my master's study. She is the reason I chose to pursue research in academia, taught me how to think like a scientist, and how to conduct proper research. Next, I am grateful to Dr. Shannon for always providing helpful assistance whenever I had any issues. She helped encourage my interest in imaging during my time as her GRA for the confocal microscope in the Center for Biomedical Research (CBR). Finally, to Dr. Krishna Kolan, I want to express my appreciation for your help and guidance in my research. He is the reason I became interested in bioprinting. Overall, I want to make sure to express my appreciation for the continuous support and valuable life advice which Julie, Katie, and Krishna have provided. They have been extremely patient and supportive, especially during the period in which I struggled with mental health. helped make me the person I am today.

I would also like to thank our collaborators in the Materials Science department, Dr. Richard Brow and his graduate students Parker Freudenberger and Rebekah Blatt for their advice, expertise and providing us with the bioactive glass used in my studies. Additionally, I want to acknowledge CBR for funding my GRA and the Biology department for allowing me to come back and finish my last year partly funded by the GTA positions they provided.

TABLE OF CONTENTS

	Page
PUBLICATION THESIS OPTION.....	iii
ABSTRACT.....	iv
ACKNOWLEDGMENTS	v
LIST OF ILLUSTRATIONS.....	xi
LIST OF TABLES.....	xiii
NOMENCLATURE	xiv
 SECTION	
1. INTRODUCTION.....	1
1.1. BIOACTIVE GLASS	1
1.2. CELLS	1
1.3. HYDROGELS	2
 PAPER	
I. THE ANGIOGENIC POTENTIAL OF PH NEUTRAL BOROPHOSPHATE BIOACTIVE GLASSES.....	3
ABSTRACT.....	3
1. INTRODUCTION.....	4
2. MATERIAL AND METHODS	5
2.1. GLASS PREPARATION	5
2.2. DISSOLUTION STUDIES.....	6
2.3. CELL CULTURE.....	7
2.4. CELL PROLIFERATION	7

2.5. CELL MIGRATION.....	8
2.6. CHICK CHORIOALLANTOIC MEMBRANE (CAM).....	8
2.7. BIOACTIVE GLASS ADMINISTRATION AND QUANTIFICATION.....	9
2.8. STATISTICS	10
3. RESULTS.....	10
3.1. GLASS PROPERTIES	10
3.2. EFFECTS OF BOROPHOSPHATE BGS ON HUVEC PROLIFERATION.....	11
3.3. BOROPHOSPHATE BGS INCREASE ENDOTHELIAL MIGRATION	12
3.4. BOROPHOSPHATE BGS STIMULATE ANGIOGENESIS IN VIVO.....	15
4. DISCUSSION	20
5. CONCLUSIONS	24
REFERENCES.....	25
II. ADIPOSE STEM CELL RESPONSE TO BOROPHOSPHATE BIOACTIVE GLASS	30
ABSTRACT.....	30
1. INTRODUCTION.....	31
2. MATERIALS AND METHODS	33
2.1. GLASS PREPARATION	33
2.2. CELL CULTURE.....	33
2.2.1. Adipose Stem Cells.	33
2.2.2. Dermal Microvascular Endothelial Cells.	34
2.3. GLASS CHARACTERIZATION	34

2.4. CELL VIABILITY	35
2.5. DIFFERENTIATION	35
2.6. MIGRATION	36
2.7. CYTOKINE ARRAY	37
2.8. STATISTICS	38
3. RESULTS.....	38
3.1. GLASS PROPERTIES	38
3.2. HIGH CONCENTRATION OF BPBGS REDUCED ASCS VIABILITY AT 72 HOURS	40
3.3. BPBGS AFFECTS ASCS DIFFERENTIATION	42
3.4. PH-NEUTRAL BPBGS ATTRACT ASCS WHILE ASCS TREATED WITH BASIC BPBGS ATTRACT ECS	44
3.5. BPBG ALTERS ASC SECRETOME	45
4. DISCUSSION	46
5. CONCLUSION	55
REFERENCES	55
III. FUNCTIONAL HYDROGEL BIOINK MODIFIED WITH BOROPHOSPHATE GLASSES	62
ABSTRACT	62
1. INTRODUCTION.....	63
2. METHODS.....	64
2.1. GLASS PREPARATION	64
2.2. HYDROGEL PREPARATION	65
2.3. CHEMICAL TESTING	66

2.4. MECHANICAL TESTING	66
2.5. MICROSTRUCTURE OBSERVATION.....	67
2.6. CELL CULTURE.....	67
2.7. SCAFFOLD FABRICATION	68
2.8. CELL VIABILITY	68
2.9. STATISTICAL ANALYSIS	69
3. RESULTS.....	69
3.1. PH CHANGE, GLASS DISSOLUTION, AND ION RELEASE	69
3.2. VISCOELASTIC BEHAVIOR OF BOROPHOSPHATE GLASSES.....	74
3.3. COMPARISON OF X40 AND CROSSLINKING ON HYDROGEL MICROSTRUCTURE.....	78
3.4. CELL VIABILITY WITH BIOINK AND GLASS	80
4. DISCUSSION	83
REFERENCES.....	84
IV. DEVELOPMENT OF NOVEL BIOINK FOR SIZABLE ORGANOIDS VIA INNER GELATION	86
ABSTRACT.....	86
1. INTRODUCTION.....	87
2. MATERIALS AND METHODS	89
2.1. FABRICATION OF HYDROGEL INKS	89
2.1.1. Fabrication of Alginate-Gelatin Hydrogel.	89
2.1.2. Fabrication of Alginate-Fibrinogen Hydrogel.....	89
2.1.3. Crosslinking of Hydrogels.....	90
2.2. SCAFFOLD FABRICATION	91

2.3. ALGINATE-FIBRINOGEN HYDROGEL CHARACTERIZATION	91
2.4. BOROPHOSPHATE BIOACTIVE GLASSES	93
3. RESULTS.....	94
3.1. EXTERNAL VS INTERNAL CROSSLINKING	94
3.2. FTIR CONFIRMATION FOR UNIFORM MIX OF ALGINATE- FIBRINOGEN HYDROGEL.....	96
3.3. COMPARISON OF VARYING CONCENTRATIONS OF INTERNAL CROSSLINKER IN BIOINK FOR PRINTABILITY	97
4. DISCUSSION	100
REFERENCES.....	102
SECTION	
2. CONCLUSIONS AND FUTURE DIRECTIONS.....	104
BIBLIOGRAPHY.....	105
VITA.....	107

LIST OF ILLUSTRATIONS

PAPER I	Page
Figure 1. Borophosphate BGs did not increase proliferation but did attract and stimulate cells more than the dissolution product.	13
Figure 2. Borophosphate BGs stimulated angiogenesis in chick CAM.	16
Figure 3. Dopants decreased viability of chick CAMs but increased width of vasculature.	21
PAPER II	
Figure 1. Schematic of the experimental setup for migration assays.	37
Figure 2. A high concentration of BPBGs reduced ASCs viability at 72 hours under static conditions.	41
Figure 3. BPBGs influence ASC differentiation.....	43
Figure 4. BPBGs affect cell migration.....	45
Figure 5. Effect of BPBGs on the ASCs secretory profile.	47
Figure 6. Boron concentration influenced ASC secretome.	49
Figure 7. Representative hierarchal heatmap clustering the proteins based on function.....	52
PAPER III	
Figure 1. pH shifts for borophosphate glasses dissolved in water after more than 8 days.....	70
Figure 2. pH change of gels with differing wt% glass in SBF at 1 and 7 days.	71
Figure 3. Ion release rates for the major elements that compose each glass type.....	72
Figure 4. Glass dissolution rates for borophosphate glasses with Ca and P ion release profile at 1 and 7 days.	73

Figure 5. Shear rate dependence of alginate-gelatin hydrogels doped with and without BPBG particles.	75
Figure 6. Hydrogel recovery with borophosphate glasses.	76
Figure 7. Elastic & viscous modulus of the different components of the hydrogel.	77
Figure 8. Elastic & viscous modulus of the different glass compositions.	78
Figure 9. Internal cross section of hydrogels with and without crosslinker or X40 glass.	79
Figure 10. Microstructure of alginate-gelatin \pm X40 with and without crosslinker by Environmental SEM at 50x and 400x magnification.	80
Figure 11. Scaffold fabrication using borophosphate glasses.	81
Figure 12. Cell viability after 7 days in static culture for scaffolds printed with hydrogels doped with different borophosphate glasses.	82
Figure 13. Cell viability measurements for scaffolds printed with undoped hydrogels and hydrogels doped with borophosphate glasses.	83
 PAPER IV	
Figure 1. Extrusion-based 3D printing and components of the bioinks.	92
Figure 2. External vs internal crosslinking of alginate in alginate-gelatin hydrogel.	94
Figure 3. Lateral cross section of external vs. internal crosslinked samples.	96
Figure 4. FTIR confirmation of uniform mix for alginate-fibrinogen hydrogel.	98
Figure 5. Printability of differing CaCO ₃ concentrations in alginate-fibrinogen hydrogel ink.	99
Figure 6. Comparison between varying concentrations of internal crosslinking in alginate-fibrinogen samples at multiple time points.	101

LIST OF TABLES

	Page
PAPER I	
Table 1. Bioactive glass compositions.....	6
Table 2. pH change and percent weight loss of glass.	11
Table 3. Percentages of chick CAMs with histological phenomenon with X0 examples.	18
Table 4. Summary of glass responses in vitro and in vivo.	24
PAPER II	
Table 1. Bioactive glass compositions.....	33
Table 2. pH change and ion release in CCM with or without cells.	39
Table 3. Protein secretion levels, presented in pg/ml and mean±SD.....	50
PAPER III	
Table 1. Bioactive glass compositions.....	65
PAPER IV	
Table 1. Bioactive glass compositions.....	93

NOMENCLATURE

ACA	6-aminocaproic acid
Alg	Alginate
ASCs	Adipose stem cells
B3	13-93B3
B	Boron
BG	Bioactive Glass
BPBG	Borophosphate Bioactive Glass
C	Carbon
Ca	Calcium
CaCl ₂	Calcium Chloride
CaCO ₃	Calcium Carbonate
CAM	Chick chorioallantoic membrane
CCM	Complete Culture Media
Co	Cobalt
Cu	Copper
EC	Endothelial cells
ECM	Extracellular matrix
EM	Endothelial medium
DMEM	Dulbecco's Modified Eagle Medium
DP	Dissolution product
DSLR	Digital Single Lens Reflex

Fib	Fibrinogen
FTIR	Fourier-transform infrared spectroscopy
G'	Storage modulus (can be either tensile or shear)
G''	Loss modulus (can be either tensile or shear)
GDL	D-(+)-Gluconic acid d-lactone
Gel	Gelatin
H	Hydrogen
HA	Hydroxyapatite
HUMVEC-d	Human dermal microvascular endothelial cells
HUVEC	Human umbilical vein endothelial cell
Na	Sodium
O	Oxygen
P	Phosphorus
PBS	Phosphate Buffer Saline
SBF	Simulated Body Fluid
SEM	Scanning electron microscope
Si	Silicon
VEGF	Vascular endothelial growth factor
Wt%	Weight percent
Zn	Zinc

1. INTRODUCTION

1.1. BIOACTIVE GLASS

Bioactive glasses are a biomaterial that react and can release ions to produce desired physiological responses in the body. The first bioactive glasses, BGs, were based on silicate chemistries developed 50 years ago but now include borate and phosphate glasses[1-5]. Borate BGs have been shown to stimulate angiogenesis in tissues in various applications and be able to promote the bone precursor, hydroxyapatite by creating a local alkaline environment, but the basic conditions created by this glass can have detrimental effects on cells in vitro if not pretreated[6-8]. The development of a pH-neutral glass by the addition of phosphate would be of beneficial use when culturing cells[5]. Adding phosphate to BGs to create different borate-phosphate ratios can lead to acidic conditions instead of alkaline and allow for the control of the local pH microenvironment.

1.2. CELLS

The cells used in the studies included in this thesis are adipose stem cells and endothelial cells. Adipose stem cells (ASCs) are easily isolated from adipose tissue and are used in regenerative medicine due to their ability to hone to damage and their immunomodulatory effects[8–10]. These stem cells also can self-renew, differentiate into multiple cell types, are endogenous to the stromal vascular fraction, and secrete growth factors, cytokines, and other signaling molecules[11]. ASCs are widely used in tissue engineering due to aft for mentioned effects, including being used with bioactive glass[8,12,13]. Endothelial cells are required for angiogenesis, the process by which new

blood vessels develop from pre-existing vessels and an important part of tissue engineering, to proliferate, migrate, and form tubes[14]. Since bioactive glass has been shown to increase EC migration and stimulate angiogenesis by local pH[6,15], both human umbilical vein endothelial cell, HUVECs and Human dermal microvascular endothelial cells, HUMVEC-d will be used during this thesis, as results from Wesson et al. demonstrated that microvascular cells from the kidney and the heart secreted different levels of an angiogenic factor when the local pH was reduced[16].

1.3. HYDROGELS

Hydrogels are either natural or synthetic polymers that are a network of 3D structures with the ability to absorb and retain a significant amount of water and have comparable properties to natural tissues when swollen[17]. The networks are formed via crosslinking, whether by ionic, covalent, or other means[18]. When hydrogels are used together with cells, they can be used to create inks for 3D printing. The inks or bioinks should have the following biological and mechanical aspects for optimal use: biocompatibility with cells, biodegradation, permeability for O₂ and nutrients, and tissue regeneration and gelation, viscoelasticity, shear thinning, and printability[19–21]. Only natural hydrogels, such as alginate and gelatin, were used to form bioinks in this thesis. Alginate has nontoxic and noninflammatory properties and can provide structure since due to no degradation in vivo, however its cell adhesion is poor and mechanical characteristics are insufficient when used alone[17,22]. Alginate needs divalent cations to cross-link. Gelatin on the other hand crosslinks by temperature and is usually physically blended with alginate to provide cell adhesion and to support cell proliferation[17,20].

PAPER

I. THE ANGIOGENIC POTENTIAL OF PH NEUTRAL BOROPHOSPHATE BIOACTIVE GLASSES

Bradley A. Bromet^a, Nathaniel P. Blackwell^a, Nada Abokefa^a, Parker Freudenberger^b,
Rebekah L. Blatt^b, Richard K. Brow^b, Julie A. Semon^a

^a Department of Biological Sciences, Missouri University of Science and Technology,
Rolla, MO, USA

^b Department of Material Science and Engineering, Missouri University of Science and
Technology, Rolla, MO, USA

ABSTRACT

Borate bioactive glasses have gained attention in recent years due to their therapeutic and regenerative effects in vivo. However, borate bioactive glasses release alkaline ions, increasing the local pH and creating a toxic environment for cell culture studies. A partial compositional substitution of phosphate for borate can create a pH neutral glass that does not significantly affect the local pH while still releasing therapeutic ions. In the present study, a series of Na-Ca-borophosphate bioactive glasses with different borate-to-phosphate ratios was evaluated in vitro and in vivo for cytotoxicity and angiogenic effects. The pH neutral glasses supported endothelial proliferation and migration and stimulated greater blood vessel formation in a chick chorioallantoic membrane model, compared to more basic borate glasses. The results from this study indicate that these pH neutral glasses are promising angiogenic biomaterials for use in tissue engineering and regenerative medicine.

Keywords: Angiogenesis, Borophosphate, Bioactive glass, Endothelial cells

1. INTRODUCTION

Bioactive glasses (BGs) react in the body to stimulate desired physiological responses. The original bioactive glasses, including the 45S5 composition developed over 50 years ago by Hench[1], were based on silicate chemistries. Since then, BGs have been developed from many different glass compositional families, including those based on borate and phosphate chemistries[2–7]. Borate BGs have been of particular interest in applications for vascularized tissues because it has been shown that borate ions stimulate the secretion of pro-angiogenic growth factors[8–16]. Consequently, borate BGs are a promising therapy to repair tissues that require a high degree of vascularization. However, when borate BGs react in aqueous environments, the local pH of the solution, or the region near the glass surface, quickly increases due to the release of alkali ions that form strong bases (NaOH and $\text{Ca}(\text{OH})_2$) and borate ions that form a weak acid (H_3BO_3)[17]. The development of localized alkaline conditions promotes the formation of hydroxyapatite[18], a desired outcome for many biomedical applications. However, there are other situations where having localized neutral or acidic conditions around a bioactive glass would be beneficial, including the ability to study the effects that BGs have on cells in vitro. Furthermore, because they create local alkaline conditions when first exposed to aqueous solutions, BGs are often pre-reacted before exposure to cell cultures[14,19,20], a step that complicates potential clinical applications of the glass.

A silicate BG modified with significant concentrations of phosphate was reported to create locally neutral pH conditions that increased the viability of a pre-osteoblastic cell line, compared to the more conventional phosphate-free silicate BG that created locally alkaline conditions[7]. Phosphoric acid released by the dissolution of the glass can counter the effects of the concomitant release of alkaline ions. Adding phosphate to borate BGs can also control the local pH conditions, from alkaline to acidic, depending on the borate-to-phosphate ratio. In the present study, we show how those local conditions affect the function of endothelial cells in vitro and in vivo.

2. MATERIAL AND METHODS

2.1. GLASS PREPARATION

Glasses with the nominal molar composition $16\text{Na}_2\text{O}-24\text{CaO}-x\text{B}_2\text{O}_3-(60-x)\text{P}_2\text{O}_5$ (mol%) were produced, where $x = 0, 10, 20, 30, 40,$ and 60 , and several were doped with different concentrations of CuO and CoO, as indicated in Table 1. The borate bioactive glass 1393-B3 (B3)[8], with the nominal composition $6\text{Na}_2\text{O}, 12\text{K}_2\text{O}, 5\text{MgO}, 20\text{CaO}, 4\text{P}_2\text{O}_5, 53\text{B}_2\text{O}_2$ (wt%), was also produced. Reagent grade batch materials were calcined at 300°C for at least 4 hours and then melted for an hour in platinum crucibles at $1000-1150^\circ\text{C}$, depending on composition. Melts were stirred on the half hour with a platinum rod, then quenched in graphite molds. Samples were annealed at 350°C for one hour then allowed to cool to room temperature and stored in a vacuum desiccator until use. Glasses were analyzed by x-ray diffraction, using a PANalytical X'Pert Multipurpose

diffractometer with a Cu K- α source and a PIXcel detector, and all compositions were found to be amorphous.

Table 1. Bioactive glass compositions. Nominal compositions in mol% of the borophosphate glasses used in this study.

Glass Designation	Na ₂ O	CaO	B ₂ O ₃	P ₂ O ₅	CuO	CoO
X0	16	24	-	60	-	-
X10	16	24	10	50	-	-
X20	16	24	20	40	-	-
X20Co	16	20	20	40	-	4
X20Cu	16	20	20	40	4	-
X20CuCo	16	20	20	40	2	2
X30	16	24	30	30	-	-
X40	16	24	40	20	-	-
X40Co	16	20	40	20	-	4
X40Cu	16	20	40	20	4	-
X40CuCo	16	20	40	20	2	2
X60	16	24	60	-	-	-

2.2. DISSOLUTION STUDIES

Glass particles (75-150 microns) in the amount of 150 ± 1 mg were sealed in nylon mesh bags with $45 \mu\text{m}$ openings, then immersed in 50 ml of either deionized water or

simulated body fluid[21] contained in high density polyethylene centrifuge tubes in a shaker bath at 37°C. The bags were removed after 24 hours, dried and weighed, and the solution pH was measured. Ion concentrations in the dissolution solutions were analyzed using Inductively Coupled Plasma – Optical Emission Spectroscopy (ICP-OES), using a Perkin-Elmer Avio 200. These pH and ion concentration measurements were done in triplicate and the average values are reported with their respective standard deviations.

2.3. CELL CULTURE

Human umbilical vein endothelial cells (HUVECs, pooled donors) and adult dermal microvascular endothelial cells (HMVEC-d) were obtained from Lonza (Walkersville, MA). Endothelial cells were grown in endothelium media (EM), with HUVECs grown in Endothelial Cell Basal Medium-2 and HMVEC-d grown in Endothelial Cell Basal Medium-2MV, both from Lonza. Cells were fed every 3-4 days and utilized when confluent.

2.4. CELL PROLIFERATION

HUVECs were plated at 5500 cells/cm² in a 96-well plate and incubated at 37°C, 5% CO₂ overnight. Media was removed and glass was added at 2.5 or 10mg/ml in EM under static conditions for 24 hours. For glass dissolution product (DP), 2.5 or 10mg/ml of glass was added to EM and incubated at 37°C while rocking for 24 hours. The medium was then filtered to remove any residual glass, and then media was added to HUVECs and incubated under static conditions for 24 hours. Wells were gently washed 3-5 times in pre-warmed PBS, and DNA was quantified with CyQuant (ThermoFisher; Waltham, MA), according to manufacturer's instructions and measured using a fluorescent

microplate reader (FLUOstar optima; BMG Labtech Inc.; Durham, NC). Each experiment was performed in triplicate.

2.5. CELL MIGRATION

To evaluate the ability of the glass to attract ECs, migration assays were performed in 96-well transwells with 8 μ m pore membrane inserts (MilliporeSigma; Burlington, MA). Glass was suspended in EM at 2.5 or 10mg/ml and 100 μ l of that solution was added to the bottom of the transwell. For glass DP, 2.5 or 10mg/ml of glass was added to EM and incubated at 37°C while rocking for 5 hours. The solution was then filtered to remove any glass particulates, and 100 μ l of that solution was added to the bottom of the transwell. On the top of the membrane insert, $\sim 2 \times 10^4$ ECs were loaded into each well insert in triplicate. After incubating 5 hours at 37°C with 5% humidified CO₂, the insert was rinsed with PBS, and the cells that had migrated to the bottom of the insert were enzymatically removed and quantified for DNA using CyQuant and a fluorescent microplate reader. Each experiment was performed in triplicate.

2.6. CHICK CHORIOALLANTOIC MEMBRANE (CAM)

White Leghorn chicken Spf fertile eggs (Charles River, East Roanoke, IL) were acclimated to room temperature for 4-6 hours after delivery (Day 0) and then incubated at 37.5°C with constant humidity for 3 days. After incubation (Day 3), eggs were cracked by gently breaking against a sterilized hex wrench and transferred into an 88 x 88 x 23mm weigh boat. A piece of eggshell was added to the embryo to ensure normal chick development. Weigh boats with chick embryos were placed into individual humidity chambers, which were prepared by placing Kimwipes (Kimberly-Clark Worldwide, Inc.,

Roswell, GA) and 100mL of Milli-Q® (MilliporeSigma, Burlington, MA) purified water inside of a 6.5 x 6.5 x 4” polypropylene container. The humidity chambers with chick embryos were placed in incubators at 37.5°C and allowed to develop 7 additional days (Day 10).

2.7. BIOACTIVE GLASS ADMINISTRATION AND QUANTIFICATION

Bioactive glass was added to chick CAMs on Day 10. A sterilized 10mm diameter poly-band ring was placed in an area on the chick embryo with no major vessels. Approximately 2.5mg of -20µm glass was suspended in 20µL PBS and immediately added inside the poly-band rings. Either 2 or 3 samples were placed on each egg. An overall image at 1x and a magnified image at 2x for each sample were captured on days 1 and 5 after the administration of glass using a Leica StereoZoom® S8 AP0 and Leica software (Leica Microsystems Inc, Buffalo Grove, IL). Quantification of CAM images were performed using Wimasis (Córdoba, Spain). Images were digitally divided into sections to quantify observed pathologies, with scoring criteria adapted from Raga et al[22,23]. Vessels that appeared white due to a lack of blood flow were classified as “ghost” vessels. If ghost vessels were seen in at least ½ of the sections ($\geq 50\%$ of the surface area of the image), they were classified as progressive[22,23]. They were considered preliminary if identified on less than half of the sections. An accumulation of blood at the microcapillary level resulting in petechial hemorrhaging and blood droplets was classified as hyperemia. Hyperemia was classified as minimal if identified in less than ¼ of the sections, moderate in ¼ to ½ of the sections, and severe if greater than ½ of sections.

2.8. STATISTICS

Analysis was performed using Minitab® Statistical Software (State College, Pennsylvania, USA). The statistical differences among two or more groups were determined by ANOVA, followed by post-hoc Tukey's honest significant difference for CAM assay and T-test for in vitro tests versus the respective control group.

3. RESULTS

3.1. GLASS PROPERTIES

Table 2 summarizes changes in the pH and the weight losses from glass particles immersed for 24 hours at 37°C in either water or simulated body fluid (SBF). For samples immersed in water, there is a clear trend in solution pH, with the phosphate-rich glasses producing acidic solutions and the borate-rich glasses, including B3, producing more basic solutions. The shifts in the pH of buffered SBF are smaller after 24 hours of reaction, although both X60 and B3 glasses produce more alkaline solutions. It is worth noting that the addition of up to 30 mol% B₂O₃ (X30) to the borate-free Na-Ca-phosphate glass (X0) reduces the dissolution rate in SBF, with the X10 glass having the lowest. The borate-rich glasses (X40, X60, and B3) dissolve much more rapidly, and the X60 glass is almost completely dissolved after 24 hours. The slower dissolution kinetics of the X10, X20, and X30 glasses help explain why these glasses had less effect on SBF pH, whereas the fast-reacting, but pH neutral, X40 glass did not shift SBF pH the way the basic X60 and B3 glasses did.

Table 2. pH change and percent weight loss of glass. Change in pH and percent weight loss of glass particles (3mg/ml) after 24 hours in 37°C water or simulated body fluid (SBF, original pH=7.4±0.02 (SD)). ND = not detected.

Glass	Water pH	SBF pH	Weight Loss (SBF)	B Concentration, ppm (SBF)	Total B release, % (SBF)
X0	2.6±0.01	7.4±0.01	17.6±0.39%	ND	ND
X10	3.1±0.00	7.4±0.03	1.8±0.08%	ND	ND
X20	3.8±0.00	7.5±0.04	3.4±1.79%	1.7±0.19	1.2±0.14
X30	6.3±0.02	7.5±0.11	4.0±0.07%	2.2±0.29	0.98±0.38
X40	7.1±0.00	7.1±0.01	56.2±0.29%	290.3±3.37	89.1±1.03
X60	9.6±0.00	8.2±0.09	81.4±2.11%	503.1±19.23	84.2±3.22
B3	9.4±0.01	8.1±0.03	65.0±5.9%	480.6±50.0	91.0±9.5
No glass	6.02±0.00	7.5±0.08		ND	ND

3.2. EFFECTS OF BOROPHOSPHATE BGS ON HUVEC PROLIFERATION

Figure 1A shows the effects of 2.5 and 10mg/ml glass on the proliferation of endothelial cells (ECs). At 2.5mg/ml, the acidic and pH neutral glasses (X0, X20, and X40) did not affect HUVEC proliferation when compared to that measured for the endothelial media (EM), whereas cell proliferation was significantly lower for the two alkaline glasses (X60 and B3). In general, HUVEC proliferation was reduced at a higher glass concentration of 10mg/ml, although not always significantly.

Glass particles at 2.5mg/ml were also reacted in EM in a shaker bath at 37°C for 24 hours, and the resulting dissolution product (DP) was then fed to HUVECs. The DP from the two most reactive glasses (X40 and X60) decreased HUVEC proliferation

compared to the direct administration of each glass (Figure 1B). There were also smaller, but statistically insignificant, decreases in cell proliferation associated with the DPs from the X0 and X20 glasses.

Two pH neutral glasses, X20 and X40, were doped with metal cations (4 mol%) reported to promote angiogenesis[24–27] and the effects of these glasses on HUVEC proliferation are shown in Figure 1C. For both base glasses, CoO additions decreased HUVEC proliferation, whereas the addition of CuO had no statistically meaningful effect. Interestingly, the CuO/CoO combination increased HUVEC proliferation, although not in a statistically meaningful way, compared to the respective base glasses. Figure 1C also compares the effects of glass DP on HUVEC proliferation to the direct contact data. As was the case for the undoped glasses (Figure 1B), the DPs typically reduced HUVEC proliferation compared with the direct contact conditions.

3.3. BOROPHOSPHATE BGS INCREASE ENDOTHELIAL MIGRATION

The results of the endothelial migration tests for X20 and X40, both in direct contact and DP conditions are summarized in Figure 1D. For both conditions, X40 was associated with statistically greater migration than was found for the EM baseline, whereas the X20 results were not statistically different from the EM results. The metal doped X40 glasses promoted greater cell migration for both direct and DP conditions than did the X20 glasses. As was found for the HUVEC proliferation experiments, endothelial migration was greater under the direct contact conditions than the DP conditions, although those results were statistically meaningful for only a few metal dopants.

While HUVECs are commonly used endothelial cells, they have characteristics that are distinct compared to endothelial cells from other sources, particularly microvascular endothelial cells[28–30]. It has also been shown that extracellular pH has different effects on endothelial cells acquired from different sources[31].

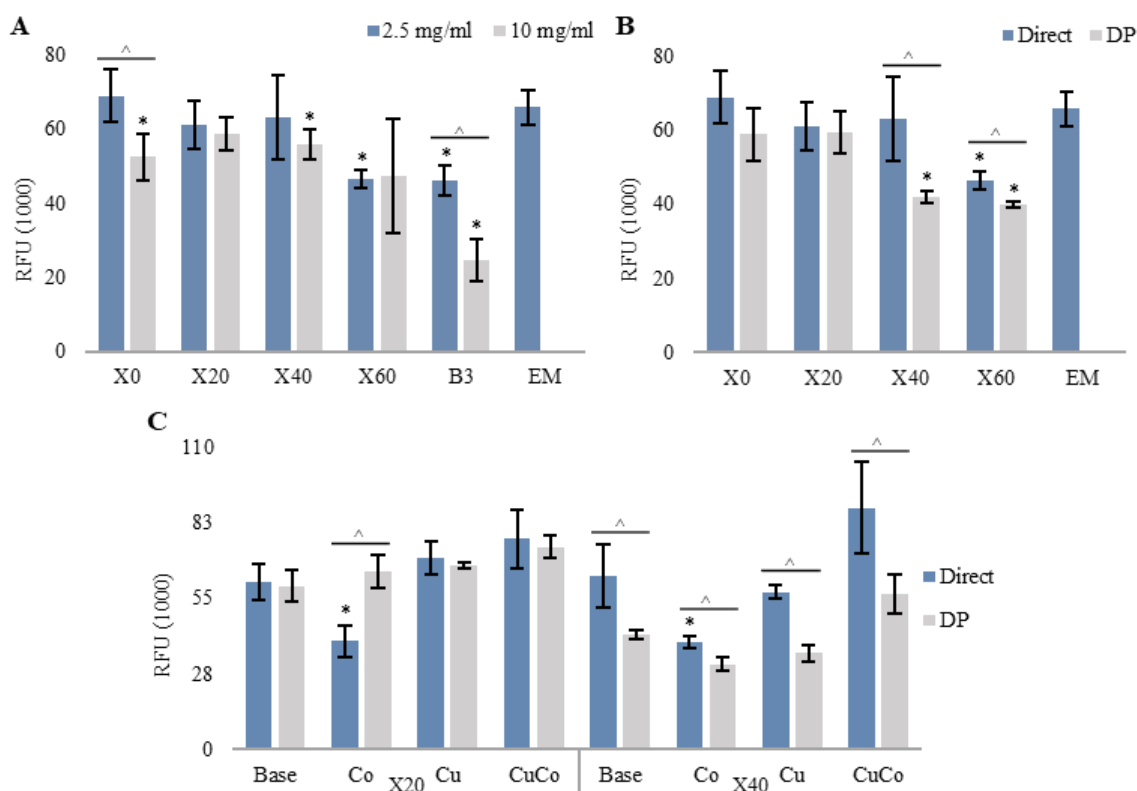


Figure 1. Borophosphate BGs did not increase proliferation but did attract and stimulate cells more than the dissolution product. Glasses were added to HUVECs in a 96-well plate, and cell numbers were measured by DNA content 24-hrs later. (A) Glasses at two different concentrations were evaluated, with the higher concentration showing reduced cell viability. (B) Glass DP was compared to the direct addition of glass on HUVEC proliferation, with the direct addition having higher HUVEC viability. (C) The DP of doped glasses were compared to base glasses for and shown to have lower cell viability for all except X20Co. For cell migration, DP or direct glass was added to the bottom insert of a 96-well transwell, with endothelial cells plated on top and incubated for 5 hours at 37°C. HUVECs (D) and HUMVEC-d (E) migrated more to the direct glass. Mean \pm SD; * $p < 0.01$ compared to EM (A, B, D, E) or base composition (C); ^ $p < 0.05$ compared to concentrations of the same glass composition (A), to direct addition of glass for that composition (B, D, & E), or to respective base compositions (C).

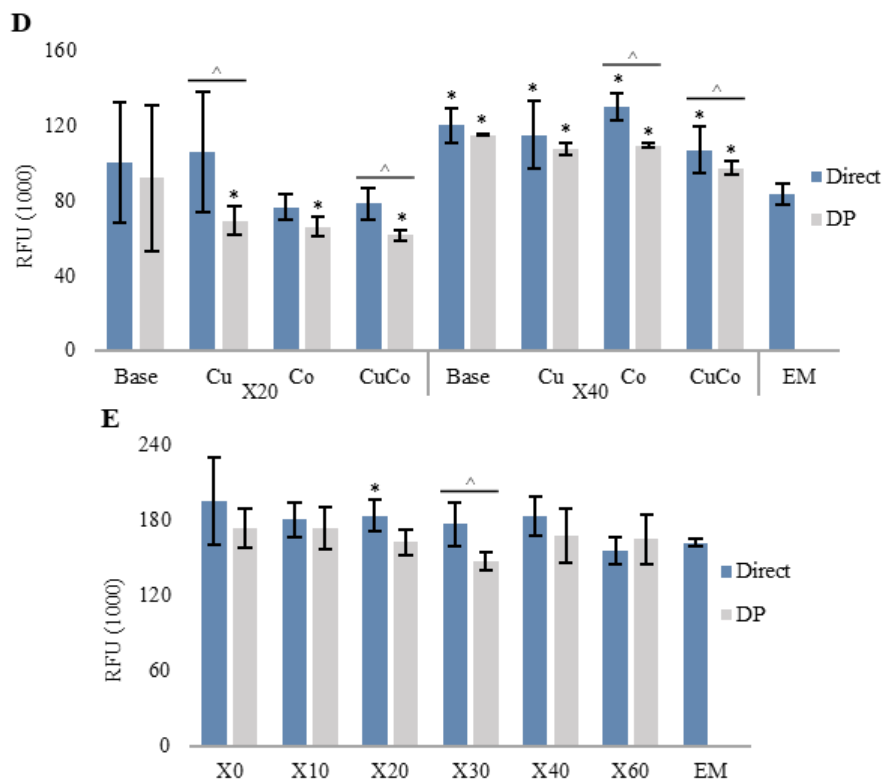


Figure 1. Borophosphate BGs did not increase proliferation but did attract and stimulate cells more than the dissolution product. Glasses were added to HUVECs in a 96-well plate, and cell numbers were measured by DNA content 24-hrs later. (A) Glasses at two different concentrations were evaluated, with the higher concentration showing reduced cell viability. (B) Glass DP was compared to the direct addition of glass on HUVEC proliferation, with the direct addition having higher HUVEC viability. (C) The DP of doped glasses were compared to base glasses for and shown to have lower cell viability for all except X20Co. For cell migration, DP or direct glass was added to the bottom insert of a 96-well transwell, with endothelial cells plated on top and incubated for 5 hours at 37°C. HUVECs (D) and HUMVEC-d (E) migrated more to the direct glass. Mean \pm SD; * $p < 0.01$ compared to EM (A, B, D, E) or base composition (C); ^ $p < 0.05$ compared to concentrations of the same glass composition (A), to direct addition of glass for that composition (B, D, & E), or to respective base compositions (C) (cont.).

Because the migration of endothelial cells is critical for angiogenesis, a second type of endothelial cell, microvascular endothelial cell from the skin (HMVEC-d), was also tested in the 5-hour transwell migration assay, and those results are shown in Figure 1E for the six base glasses and the EM controls. In general, there were no statistically significant differences in HMVEC-d migration for any of the glasses in the direct contact

experiments, although the X60 glasses had the lowest levels of HMVEC-d migration. As was found with other assays, the glass DPs attracted fewer cells than did the direct contact glass particles.

3.4. BOROPHOSPHATE BGS STIMULATE ANGIOGENESIS IN VIVO

The developing chick chorioallantoic membrane (CAM) is a popular model to evaluate in vivo angiogenic responses to biomaterials, including bioactive glass[32–35]. The developing CAM provides a large network of arterioles, venules, and capillaries that can be easily imaged and used to investigate the in vivo vascular effects of these borophosphate glasses. After the eggs were incubated for 10 days, 2.5mg/ml of bioactive glass was suspended in PBS, added to the CAM, and imaged with a stereomicroscope 1, 3, and 5 days after administration.

Figure 2A shows representative images of the CAM on Days 1 and 5 after the administration of different borophosphate glasses, the alkaline glass B3, and a PBS control. Figure 2 (B-D) summarizes Day 1 metrics used to evaluate blood vessel formation. In general, the acidic glasses (X0) had significantly lower average vessel densities and total branching points than pH neutral (X40) and alkaline glasses (X60 and B3). The trend did not continue with segment width, however. Segment widths were significantly larger for the X20 and X60 glasses compared to the PBS control. X20 also had increased widths compared to X0, X40, and B3 glasses.

The more acidic X0 glass had an acute effect on the CAM, generating prominent, but nonuniform regions of ghost vessels (Table 3). Ghost vessels were found to be devoid of blood flow and appeared clear under the microscope. On Day 1 after administration,

100% of the CAMs treated with X0 displayed progressive ghost vessels (Table 3). However, by Day 3 after administration, only 14% of CAMs treated with X0 samples had progressive ghost vessels (ghost vessels on >50% of the surface area of the CAM), whereas 43% had preliminary (<50% of treated CAM) ghost vessels.

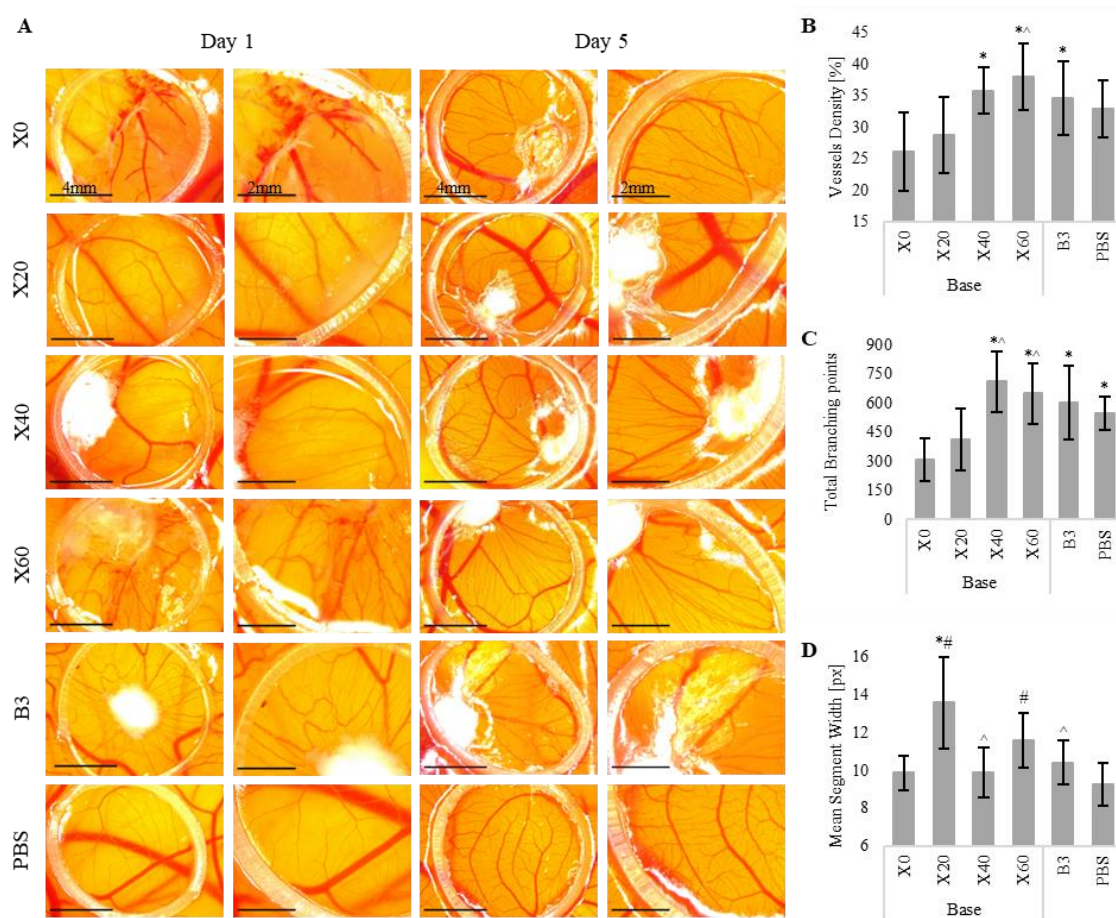


Figure 2. Borophosphate BGs stimulated angiogenesis in chick CAM. Approximately 2.5mg of -20 μ m glass was suspended in 20 μ L PBS and immediately added to 10-day old chick CAMs. Images were taken on days 1 and 5 after the administration of glass (A). CAMs were evaluated by vessel density (B), total branching points (C), and vessel width (D) at 24 hours. Values are mean \pm SD; * $p < 0.05$ compared to X0, ^ $p < 0.05$ compared to X20, and # $p < 0.05$ compared to PBS. Scale bar: overall image taken at 1x = 4mm, magnified image taken at 2x = 2mm.

Ghost vessels were further reduced by Day 5 with only 17% of CAMs treated with X0 having preliminary ghost vessels and none having progressive ghost vessels. It is unclear to us if the reduction in ghost vessels is due to the sprouting of new vessels or revascularization of functional ghost vessels. Ghost vessels were not detected in the CAMs treated with X20 and X40 base glasses but were detected in some samples treated with X60 (Table 3). To our knowledge, this is the first time any bioactive glass has been associated with the creation of ghost vessels in CAMs.

A similar phenomenon occurred with hyperemia, which is an increased blood flow at the microcapillary level. On Day 1 after administration, 100% of the CAMs treated with acidic X0 displayed moderate to severe hyperemia (Table 3). Fewer examples of hyperemia were noted for CAMs treated with the X20 and X40 base glass particles, and somewhat more were associated with samples treated with X60 glass (Table 3). Numerous blood pools formed along the arteriole length and capillary terminals. Initially, it was assumed that such an increase in blood flow may have produced too much damage on the sprouting vessels, resulting in anoxia in the developing embryo. However, the survival rate of the eggs remained high throughout the study. Additionally, by Day 3, 100% of the CAMs treated with X0 had only minimal hyperemia, which then was reduced to 17% by Day 5. This suggests that the acidic X0 glass produces a burst of angio-suppression that does not compromise mortality.

The pH neutral glasses, X20 and X40, were both doped with CoO, CuO, or a combination of the two (CuCo). The dopants decreased the viability of the chick CAMs (Figure 3A). For both series of base glasses, all dopants had less than 100% survivability by Day 1, < 60% by Day 3, and < 30% by Day 5. Both CoO and CuO had lower survival

rates than CuCo after Day 2. Furthermore, these dopants had some acute effects on the CAM with more ghost vessels and hyperemia than their respective base glasses (Figure 3B-E; Table 3), although most of these pathological features disappeared by Day 5 after administration.

Table 3. Percentages of chick CAMs with histological phenomenon with X0 examples. Approximately 2.5mg of -20 μ m glass was suspended in 20 μ L PBS and immediately added to 10-day old chick CAMs. Images were taken on Days 1, 3, and 5 after the administration of glass (A). The pathologies are characterized as ghost vessels (black arrow) or hyperemia (white arrow). Scale bar: overall image taken at 1x (top row) = 4mm, magnified image taken at 2x (bottom row) = 2mm. Most severe pathologies were observed on Day 1 and diminished by Day 5 (B).

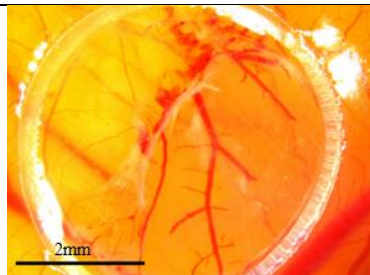
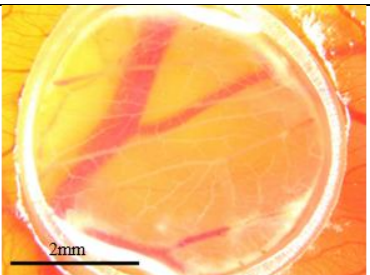
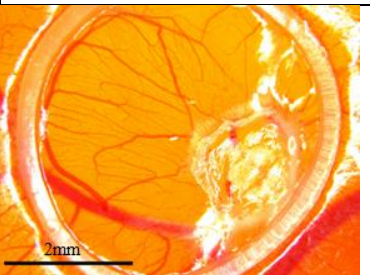
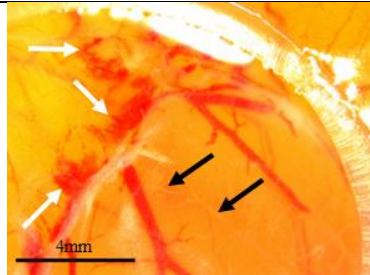
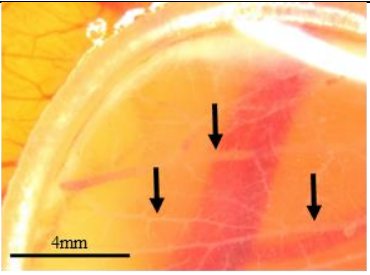
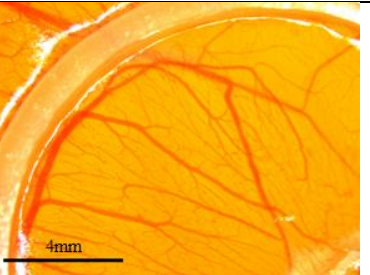
A) Day 1		Day 3						Day 5								
																
																
B)	Dopant	Ghost Vessels						Hyperemia								
	Glass	Preliminary			Progressive			Minimal			Moderate			Severe		
Day(s) after adding glass		1	3	5	1	3	5	1	3	5	1	3	5	1	3	5
X0	Base	0	43	17	100	14	0	0	100	17	50	0	0	50	0	0

Table 3. Percentages of chick CAMs with histological phenomenon with X0 examples.

Table 3. Approximately 2.5mg of -20 μ m glass was suspended in 20 μ L PBS and immediately added to 10-day old chick CAMs. Images were taken on Days 1, 3, and 5 after the administration of glass (A). The pathologies are characterized as ghost vessels (black arrow) or hyperemia (white arrow). Scale bar: overall image taken at 1x (top row) = 4mm, magnified image taken at 2x (bottom row) = 2mm. Most severe pathologies were observed on Day 1 and diminished by Day 5 (B) (cont.).

X20	Base	0	0	0	0	0	0	10	0	0	0	0	0	0	0	0
	Co	0	0	0	0	0	0	63	0	0	13	0	0	0	0	0
	Cu	22	0	0	11	0	0	22	0	0	0	0	0	0	0	0
	CuCo	30	0	0	0	0	0	60	13	20	30	0	0	0	0	0
X40	Base	0	0	0	0	0	0	20	0	0	0	0	0	0	0	0
	Co	10	0	0	0	0	0	50	25	25	10	25	25	0	0	0
	Cu	50	0	0	38	33	0	63	67	50	13	0	0	0	0	0
	CuCo	30	0	0	30	0	0	40	0	0	30	0	0	0	0	0
X60	Base	25	0	0	0	0	0	50	14	0	29	0	0	17	0	0
B3	Base	10	0	0	0	0	0	50	0	0	13	0	0	14	0	0

Cu-ions are noted to be angiogenic[25,26], but the amount of Cu²⁺ in these glasses (4 mol% CuO) may have been too much for developing vessels in the CAM, reducing viability, and may have a different effect on established vessels. The X40Cu sample agglomerated on the CAM, making overall imaging and quantification impossible. Interestingly, the X20Co glass increased the angiogenic indicators but decreased mean segment width over the X20 base composition, whereas the X40Co glass decreased angiogenic indicators and increased segment width over its base composition. For both the X20 and X40 compositions, doping with CuCo increased vessel density and

branching points. However, when compared to the respective base composition, X40CuCo increased mean segment width while X20CuCo was comparable.

4. DISCUSSION

Both Na-Ca-borate and Na-Ca-phosphate glasses dissolve congruently in neutral pH solutions, releasing boric and phosphoric acid to the solution, respectively[17,36]. At these time scales (<48 hours), borophosphate glasses also dissolve congruently. As shown in Table 2, phosphate-rich glasses create acidic environments, borate-rich glasses create basic environments, and the intermediate compositions can retain pH neutral environments. Similar pH-control effects have been reported for the substitution of P₂O₅ for SiO₂ in Na-Ca-silicate glasses[7].

In addition to altering local solution pH, the ion release rates of the X-series base glasses vary significantly (Table 2). In SBF, X20 dissolves at a rate that is about 30 times slower than X0, which itself dissolves about 10 times slower than X40, and X40 dissolves about half as fast as X60. Because these glasses dissolve congruently at these time scales, the release of the constituent ions, including metal ion dopants, will vary accordingly. For example, ions are released from X40 about 350 times faster than from X20. The weight loss fractions from the undoped X40 and B3 glasses (56% and 65%, respectively, Table 2) were significantly less than the respective fractions of borate released to solution (89% and 91%). This is consistent with the precipitation of calcium phosphate phases on the surfaces of these glasses[18]. The weight loss and borate release fractions from the other glasses are similar, indicating that the precipitation of similar

phases did not occur over the course of 24 hours in SBF. The ability to tailor the time-release kinetics should allow biomaterial designers to use materials like these for different applications.

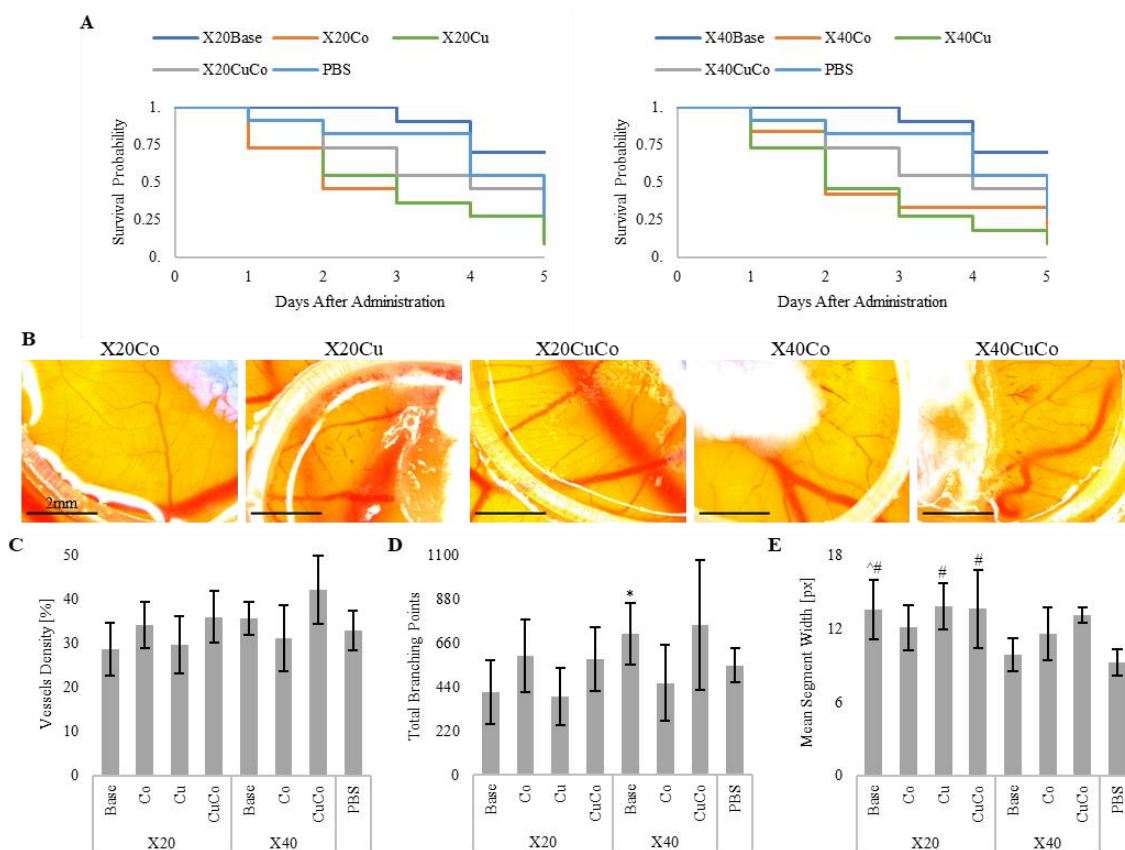


Figure 3. Dopants decreased viability of chick CAMs but increased width of vasculature. Approximately 2.5mg of $-20\mu\text{m}$ doped glass was suspended in $20\mu\text{L}$ PBS and immediately added to 10-day old chick CAMs. The addition of dopants reduced the viability of chick CAMs, with the combination of dopants having better survivability than single doped glasses (A). Images were taken 1 day after the administration of glass (B). CAMs were evaluated by vessel density (C), total branching points (D), and vessel width (E) at 24 hours. Dopants had little effect on angiogenesis compared to base glasses and the control. Values are mean \pm SD; * $p < 0.01$ compared to X20 base, ^ $p < 0.01$ compared to X40 base, and # $p < 0.001$ compared to PBS. Scale bar = 2mm.

Angiogenesis, the process by which new blood vessels develop from pre-existing vessels, requires EC to proliferate, migrate, and form tubes[38]. A previous report showed that borate BGs did not stimulate HUVEC proliferation but did increase endothelial migration[14]. Similarly, our glass series did not stimulate HUVEC proliferation, but the glasses with higher borate contents increased HUVEC migration. It is interesting to note that while the X20 glass did not increase HUVEC migration (Figure 1D), it did increase HMVEC-d migration (Figure 1E), suggesting that local pH and ion concentrations may have different effects on distinct regions of the vascular system. This coincides with results from Wesson et al. who demonstrated that microvascular cells from the kidney and the heart secreted different levels of an angiogenic factor when the local pH was reduced[39].

Previous studies have reported that an acidic pH can increase angiogenesis to poorly vascularized sites under both normal and pathological conditions[38]. This may be due to an acidic extracellular environment upregulating GPR4, a proton-sensing receptor expressed on endothelial cells, or it could be that the acidic extracellular environment increases VEGF binding[24–26,31,40]. In this work, the acidic X0 glass produced the most ghost vessels and hyperemia on chick CAMs one day after being administered. However, these features disappeared by Day 5, and the viability of the chick was unaffected throughout the experiment. Although the reasons for this are unclear, the capillary endothelium does undergo considerable morphological change in this stage of chick development, with developing vasculature having discontinuous basement membranes, increased mitosis in days 8–10, and relatively undifferentiated endothelial cells[34]. It would be interesting to compare the results here for the developing vascular

network of a chick CAM to an established vascular network and evaluate if an acidic bioactive glass might have increased therapeutic applications related to angiogenesis.

Less is known about the vascular effects of an alkaline environment, like those created by X60 or B3. The earliest reports of alkaline reactions in vascular cells showed differing effects on capillaries compared to medium-sized arterioles, as well as differences in phosphatase activity in the capillaries of different organs[41]. Other studies showed that an alkaline agent, such as sodium bicarbonate, increased the percentage of endothelial cells expressing VEGFR-2 and provided stronger anti-cancer activity when combined with an anti-cancer drug[31]. Similar to Faes et al who witnessed an increase in mean vessel density with sodium bicarbonate treatment[31], the CAM treated with X60 particles in this study also increased mean vessel density (Figure 2B).

EC proliferation and migration to the DP unexpectedly decreased compared to the direct glass. Except for X20Co, the DP of the doped glasses did not stimulate HUVEC proliferation as much as the direct administration of glass (Figure 1C). Though further investigations are needed to explain this phenomenon, it may be that ions are precipitating out of solution more quickly in the absence of cells, reducing the remaining ions in the DP and, therefore, having an insignificant effect on cell behavior.

An overall summary of our results for all the borophosphate glass base compositions is given in Table 4. X10 and X30 Of all the compositions tested in this study, X40, a fast-reacting, pH neutral glass, was the most angiogenic and had the least amount of pathology (ghost vessels and hyperemia) associated with the chick CAM. Consequently, X40 was further investigated by doping with CuO, CoO, or CuCo, all which had previously been shown to increase angiogenesis[26,27]. There was not an

increase in angiogenesis with the CuO-doped glasses, though such a result was expected. The concentration of CuO may not have been optimized for developing vessels and may have different results in established vessels. On the other hand, a previous study observed that CuO-doped borophosphate BG decreased viability of adipose stem cells, demonstrating the need for further understanding of CuO-doped BGs[42].

Table 4. Summary of glass responses in vitro and in vivo. Double arrows indicate progressive / severe pathology. Dash indicates no change. NA = not available because not tested for.

Glass	HUVEC Proliferation	HUVEC Migration	HMVEC-d Migration	Angiogenesis	Ghost Vessels
X0	↑	NA	↑	↑	↑↑
X20	—	—	↑	↓	—
X40	—	—	↑	↑	—
X60	—	NA	↑	↑	↑

5. CONCLUSIONS

There have been few investigations of BGs that degrade in a pH neutral manner. In this study, we evaluated the angiogenic potential of a series of novel borophosphate BGs with different borate-to-phosphate ratios. Of these glasses, the pH neutral X40 glass, with 20 mol% P₂O₅ and 40 mol% B₂O₃ was shown to have a better angiogenic potential than either its acidic (X0, 60 mol% P₂O₅) or basic (X60, 60 mol% B₂O₃) counterparts. Compared to the other compositions, X40 increased HUVEC and HUVEC-d migration,

increased vessel density, increased total branching points, and had no pathologies for the base composition in the CAM assay. The in vitro and in vivo results from this study demonstrated that these pH neutral glasses are promising candidates as angiogenic biomaterials for future use in regenerative medicine and tissue engineering.

REFERENCES

- L.L. Hench, The story of Bioglass®, *J. Mater. Sci. Mater. Med.* 17 (2006) 967–978. <https://doi.org/10.1007/s10856-006-0432-z>.
- G. Kaur, O.P. Pandey, K. Singh, D. Homa, B. Scott, G. Pickrell, A review of bioactive glasses: Their structure, properties, fabrication and apatite formation, *J. Biomed. Mater. Res. A.* 102 (2014) 254–274. <https://doi.org/10.1002/jbm.a.34690>.
- F. Baino, S. Hamzehlou, S. Kargozar, Bioactive Glasses: Where Are We and Where Are We Going?, *J. Funct. Biomater.* 9 (2018). <https://doi.org/10.3390/jfb9010025>.
- A. Hoppe, N.S. Güldal, A.R. Boccaccini, A review of the biological response to ionic dissolution products from bioactive glasses and glass-ceramics, *Biomaterials.* 32 (2011) 2757–2774. <https://doi.org/10.1016/j.biomaterials.2011.01.004>.
- M.N. Rahaman, D.E. Day, B. Sonny Bal, Q. Fu, S.B. Jung, L.F. Bonewald, A.P. Tomsia, Bioactive glass in tissue engineering, *Acta Biomater.* 7 (2011) 2355–2373. <https://doi.org/10.1016/j.actbio.2011.03.016>.
- S. Kargozar, F. Baino, S. Hamzehlou, R.G. Hill, M. Mozafari, Bioactive Glasses: Sprouting Angiogenesis in Tissue Engineering, *Trends Biotechnol.* 36 (2018) 430–444. <https://doi.org/10.1016/j.tibtech.2017.12.003>.
- A. Li, Y. Lv, H. Ren, Y. Cui, C. Wang, R.A. Martin, D. Qiu, In vitro evaluation of a novel pH neutral calcium phosphosilicate bioactive glass that does not require preconditioning prior to use, *Int. J. Appl. Glass Sci.* 8 (2017) 403–411. <https://doi.org/10.1111/ijag.12321>.
- Y. Lin, R.F. Brown, S.B. Jung, D.E. Day, Angiogenic effects of borate glass microfibers in a rodent model, *J. Biomed. Mater. Res. A.* 102 (2014) 4491–4499. <https://doi.org/10.1002/jbm.a.35120>.

- Revolution in wound care? Inexpensive, easy-to-use cotton candy-like glass fibers appear to speed healing in initial venous stasis wound trial, *Am. Ceram. Soc.* (2011). <https://ceramics.org/ceramic-tech-today/revolution-in-wound-care-inexpensive-easy-to-use-cotton-candy-like-glass-fibers-appear-to-speed-healing-in-initial-venous-stasis-wound-trial> (accessed September 8, 2020).
- P. Balasubramanian, T. Büttner, V. Miguez Pacheco, A.R. Boccaccini, Boron-containing bioactive glasses in bone and soft tissue engineering, *J. Eur. Ceram. Soc.* 38 (2018) 855–869. <https://doi.org/10.1016/j.jeurceramsoc.2017.11.001>.
- S. Zhao, L. Li, H. Wang, Y. Zhang, X. Cheng, N. Zhou, M.N. Rahaman, Z. Liu, W. Huang, C. Zhang, Wound dressings composed of copper-doped borate bioactive glass microfibers stimulate angiogenesis and heal full-thickness skin defects in a rodent model, *Biomaterials.* 53 (2015) 379–391. <https://doi.org/10.1016/j.biomaterials.2015.02.112>.
- Q. Yang, S. Chen, H. Shi, H. Xiao, Y. Ma, In vitro study of improved wound-healing effect of bioactive borate-based glass nano-/micro-fibers, *Mater. Sci. Eng. C* 55 (2015) 105–117. <https://doi.org/10.1016/j.msec.2015.05.049>.
- A. Yao, D. Wang, W. Huang, Q. Fu, M.N. Rahaman, D.E. Day, In Vitro Bioactive Characteristics of Borate-Based Glasses with Controllable Degradation Behavior, *J. Am. Ceram. Soc.* 90 (2007) 303–306. <https://doi.org/10.1111/j.1551-2916.2006.01358.x>.
- L.A.H. Durand, A. Góngora, J.M.P. López, A.R. Boccaccini, M.P. Zago, A. Baldi, A. Gorustovich, In vitro endothelial cell response to ionic dissolution products from boron-doped bioactive glass in the $\text{SiO}_2\text{--CaO--P}_2\text{O}_5\text{--Na}_2\text{O}$ system, *J. Mater. Chem. B* 2 (2014) 7620–7630. <https://doi.org/10.1039/C4TB01043D>.
- L. Pizzorno, Nothing Boring About Boron, *Integr. Med. Clin. J.* 14 (2015) 35–48.
- F.H. Nielsen, Update on human health effects of boron, *J. Trace Elem. Med. Biol.* 28 (2014) 383–387. <https://doi.org/10.1016/j.jtemb.2014.06.023>.
- K.L. Goetschius, M.A. Beuerlein, C.M. Bischoff, R.K. Brow, Dissolution behavior of ternary alkali-alkaline earth-borate glasses in water, *J. Non-Cryst. Solids.* 487 (2018) 12–18. <https://doi.org/10.1016/j.jnoncrysol.2018.02.011>.
- S. Chen, Q. Yang, R.K. Brow, K. Liu, K.A. Brow, Y. Ma, H. Shi, In vitro stimulation of vascular endothelial growth factor by borate-based glass fibers under dynamic flow conditions, *Mater. Sci. Eng. C Mater. Biol. Appl.* 73 (2017) 447–455. <https://doi.org/10.1016/j.msec.2016.12.099>.

- F.E. Ciraldo, E. Boccardi, V. Melli, F. Westhauser, A.R. Boccaccini, Tackling bioactive glass excessive in vitro bioreactivity: Preconditioning approaches for cell culture tests, *Acta Biomater.* 75 (2018) 3–10. <https://doi.org/10.1016/j.actbio.2018.05.019>.
- A. El-Ghannam, P. Ducheyne, I.M. Shapiro, Bioactive material template for in vitro, synthesis of bone, *J. Biomed. Mater. Res.* 29 (1995) 359–370. <https://doi.org/10.1002/jbm.820290311>.
- T. Kokubo, H. Kushitani, S. Sakka, T. Kitsugi, T. Yamamuro, Solutions able to reproduce in vivo surface-structure changes in bioactive glass-ceramic A-W, *J. Biomed. Mater. Res.* 24 (1990) 721–734. <https://doi.org/10.1002/jbm.820240607>.
- D.D. Raga, A.B. Alimboyoguen, C.-C. Shen, A.A. Herrera, C.Y. Ragasa, Triterpenoids and an Anti-Angiogenic Sterol from *Ardisia pyramidalis* Cav. *Pers.* 94 (2011) 9.
- D.D. Raga, A.A. Herrera, A.B. Alimboyoguen, C.-C. Shen, C.Y. Ragasa, Angio-Suppressive Effect of Sterols from *Ardisia Pyramidalis* (Cav.) *Pers.*, *Pharm. Chem. J.* 51 (2017) 683–689. <https://doi.org/10.1007/s11094-017-1674-4>.
- L.A. Durand, G.E. Vargas, R. Vera-Mesones, A. Baldi, M.P. Zago, M.A. Fanovich, A.R. Boccaccini, A. Gorustovich, In Vitro Human Umbilical Vein Endothelial Cells Response to Ionic Dissolution Products from Lithium-Containing 45S5 Bioactive Glass, *Materials.* 10 (2017). <https://doi.org/10.3390/ma10070740>.
- S.N. Rath, A. Brandl, D. Hiller, A. Hoppe, U. Gbureck, R.E. Horch, A.R. Boccaccini, U. Kneser, Bioactive Copper-Doped Glass Scaffolds Can Stimulate Endothelial Cells in Co-Culture in Combination with Mesenchymal Stem Cells, *PLOS ONE.* 9 (2014) e113319. <https://doi.org/10.1371/journal.pone.0113319>.
- M.A. Saghiri, J. Orangi, A. Asatourian, C.M. Sorenson, N. Sheibani, Functional role of inorganic trace elements in angiogenesis part III: (Ti, Li, Ce, As, Hg, Va, Nb and Pb), *Crit. Rev. Oncol. Hematol.* 98 (2016) 290–301. <https://doi.org/10.1016/j.critrevonc.2015.10.004>.
- S. Bose, G. Fielding, S. Tarafder, A. Bandyopadhyay, Understanding of dopant-induced osteogenesis and angiogenesis in calcium phosphate ceramics, *Trends Biotechnol.* 31 (2013) 594–605. <https://doi.org/10.1016/j.tibtech.2013.06.005>.
- H. Dib, P. Chafey, G. Clary, C. Federici, M.L. Gall, J. Dwyer, J. Gavard, N. Tamas, G. Bussone, C. Broussard, L. Camoin, V. Witko-Sarsat, M.C. Tamby, L. Mouthon, Proteomes of umbilical vein and microvascular endothelial cells reflect distinct biological properties and influence immune recognition, *PROTEOMICS.* 12 (2012) 2547–2555. <https://doi.org/10.1002/pmic.201200060>.

- J.-T. Chi, H.Y. Chang, G. Haraldsen, F.L. Jahnsen, O.G. Troyanskaya, D.S. Chang, Z. Wang, S.G. Rockson, M. van de Rijn, D. Botstein, P.O. Brown, Endothelial cell diversity revealed by global expression profiling, *Proc. Natl. Acad. Sci.* 100 (2003) 10623–10628. <https://doi.org/10.1073/pnas.1434429100>.
- J.A. Semon, L.H. Nagy, C.B. Llamas, H.A. Tucker, R.H. Lee, D.J. Prockop, Integrin expression and integrin-mediated adhesion in vitro of human multipotent stromal cells (MSCs) to endothelial cells from various blood vessels, *Cell Tissue Res.* 341 (2010) 147–158. <https://doi.org/10.1007/s00441-010-0994-4>.
- S. Faes, E. Uldry, A. Planche, T. Santoro, C. Pythoud, N. Demartines, O. Dormond, Acidic pH reduces VEGF-mediated endothelial cell responses by downregulation of VEGFR-2; relevance for anti-angiogenic therapies, *Oncotarget.* 7 (2016) 86026–86038. <https://doi.org/10.18632/oncotarget.13323>.
- A.A. Gorustovich, G.E. Vargas, O. Bretcanu, R.V. Mesones, J.M.P. López, A.R. Boccaccini, Novel bioassay to evaluate biocompatibility of bioactive glass scaffolds for tissue engineering, *Adv. Appl. Ceram.* 107 (2008) 274–276. <https://doi.org/10.1179/174367508X306541>.
- P. Nowak-Sliwinska, T. Segura, M.L. Iruela-Arispe, The chicken chorioallantoic membrane model in biology, medicine and bioengineering, *Angiogenesis.* 17 (2014) 779–804. <https://doi.org/10.1007/s10456-014-9440-7>.
- L.K. Dunn, S.K. Gruenloh, B.E. Dunn, D.S. Reddy, J.R. Falck, E.R. Jacobs, M. Medhora, Chick chorioallantoic membrane as an in vivo model to study vasoreactivity: Characterization of development-dependent hyperemia induced by epoxyeicosatrienoic acids (EETs), *Anat. Rec. A. Discov. Mol. Cell. Evol. Biol.* 285A (2005) 771–780. <https://doi.org/10.1002/ar.a.20212>.
- D. Ribatti, The chick embryo chorioallantoic membrane (CAM). A multifaceted experimental model, *Mech. Dev.* 141 (2016) 70–77. <https://doi.org/10.1016/j.mod.2016.05.003>.
- L. Ma, R.K. Brow, M.E. Schlesinger, Dissolution behaviour of sodium calcium polyphosphate glasses, *Phys. Chem. Glas. Eur. J. Glass Sci. Technol. Part B.* 59 (2018) 205–212. <https://doi.org/10.13036/17533562.59.5.018>.
- E1: Acid Dissociation Constants at 25°C, *Chem. Libr.* (2014). https://chem.libretexts.org/Bookshelves/Ancillary_Materials/Reference/Reference_Tables/Equilibrium_Constants/E1%3A_Acid_Dissociation_Constants_at_25C (accessed October 8, 2020).
- A.L. Goerges, M.A. Nugent, pH Regulates Vascular Endothelial Growth Factor Binding to Fibronectin A MECHANISM FOR CONTROL OF EXTRACELLULAR MATRIX STORAGE AND RELEASE, *J. Biol. Chem.* 279 (2004) 2307–2315. <https://doi.org/10.1074/jbc.M308482200>.

- H. Jin, S.-H. Chang, C.-X. Xu, J.-Y. Shin, Y.-S. Chung, S.-J. Park, Y.-S. Lee, G.-H. An, K.-H. Lee, M.-H. Cho, High Dietary Inorganic Phosphate Affects Lung through Altering Protein Translation, Cell Cycle, and Angiogenesis in Developing Mice, *Toxicol. Sci.* 100 (2007) 215–223. <https://doi.org/10.1093/toxsci/kfm202>.
- C.E. Camalier, M. Yi, L.-R. Yu, B.L. Hood, K.A. Conrads, Y.J. Lee, Y. Lin, L.M. Garneys, G.F. Bouloux, M.R. Young, T.D. Veenstra, R.M. Stephens, N.H. Colburn, T.P. Conrads, G.R. Beck, An integrated understanding of the physiological response to elevated extracellular phosphate, *J. Cell. Physiol.* 228 (2013) 1536–1550. <https://doi.org/10.1002/jcp.24312>.
- C. Stähli, N. Muja, S.N. Nazhat, Controlled Copper Ion Release from Phosphate-Based Glasses Improves Human Umbilical Vein Endothelial Cell Survival in a Reduced Nutrient Environment, *Tissue Eng. Part A.* 19 (2012) 548–557. <https://doi.org/10.1089/ten.tea.2012.0223>.
- A. Mishra, M. Ojansivu, R. Autio, S. Vanhatupa, S. Miettinen, J. Massera, In-vitro dissolution characteristics and human adipose stem cell response to novel borophosphate glasses, *J. Biomed. Mater. Res. A.* 107 (2019) 2099–2114. <https://doi.org/10.1002/jbm.a.36722>.

II. ADIPOSE STEM CELL RESPONSE TO BOROPHOSPHATE BIOACTIVE GLASS

Nada A. Abokefa^a, Bradley A. Bromet^a, Rebekah Blatt^b, Makenna S. Pickett^a, Richard K. Brow^b and Julie A. Semon^a.

^a Department of Biological Sciences, Missouri University of Science and Technology, Rolla, MO, USA

^b Department of Material Science and Engineering, Missouri University of Science and Technology, Rolla, MO, USA

ABSTRACT

Silicate and borate bioactive glasses have been reported to create alkaline solutions by the rapid release of ions when degrading. At certain levels, this alkaline solution can negatively affect cell viability. Adding phosphate ions to the glass composition can control the degradation rate of bioactive glasses and create a neutral pH environment. In this study, we evaluated a series of novel borophosphate bioactive glass (BPBGs) compositions that varied based on the borate-to-phosphate ratios. Borate-free, borate-rich, and intermediate borate-phosphate glasses were evaluated using adipose stem cells (ASCs), a cell population known for their therapeutic abilities. BPBGs were investigated on their ability to modify the pH of cell culture, ions released during degradation, and changes in ASC functions, including viability, migration, angiogenic ability, differentiation, and protein secretions. The intermediate borate-to-phosphate BPBGs created a physiologically neutral pH in cell culture media after 24 hours. The slightly alkaline borate-free BPBG promoted ASC migration while the highly alkaline borate-rich BPBGs showed to increase the angiogenic ability of ASCs. Together, these

results show that BPBG can be used safely in cell culture studies and can be customized for specific biomedical applications.

1. INTRODUCTION

Bioactive glasses (BGs) are a class of oxide-based ceramics first invented by Larry Hench in the late 1960s[1]. BGs have gained interest due to their bioactivity, biocompatibility, ability to bond to hard and soft tissues, and potential to stimulate tissue regeneration[2–5]. They have a versatile nature to be manufactured into different shapes and sizes such as powders, fibers, and scaffolds[6, 7]. Consequently, several BG families have emerged with different compositions, one of which is borate BGs (BBGs). When compared to the traditional silicate BG, BBGs showed lower chemical durability which increased their degradation rate[8–10], enhanced cell proliferation and differentiation in vitro[11], and tissue infiltration in vivo[12]. Remarkably, BBGs have been shown to help in healing chronic wounds and stimulating angiogenesis[13–16]. However, BBGs quickly release borate ions creating a basic pH environment[17, 18]. This increase in pH has been shown to be toxic to cells under static conditions in vitro[15, 19]. A recent study demonstrated that preconditioning BGs with cell culture medium will prevent the cytotoxic effects of the BG[20]. However, preconditioning is still unclear in terms of how different pretreating periods can affect the cell viability and characteristics. Furthermore, prolonged preconditioning times are not ideal in clinical or in laboratory settings.

As the blood and most of the interstitial fluids in the human body have a normal pH level of 7.35-7.45 which is considered physiological pH neutral range, it is important

to maintain this normal pH range when developing a new biomaterial[21].

Borophosphate glasses have been shown to dissolve congruently which impacts the pH of the solution. Another way to control the local pH of BG is to add phosphate to the glass composition[7, 17, 22]. Phosphate based bioactive glasses (PBGs) have increased interest because degradation rates can be controlled, ion release can be customized, and the glass can influence the local pH[23–26]. A previous study showed that increasing the phosphate content in the BBG can balance the basic borate ions and reduce the local pH without the need of pretreating the glass prior to use[27]. However, the usage of PBGs in the clinic was potentially limited due to the high temperature preparation requirements and their tendency to crystallize after thermal treatment[28]. Adding phosphate to BBGs could control the local pH conditions, which would be beneficial for many applications, including cell culture.

A series of novel borophosphate bioactive glasses (BPBG) were investigated on adipose stem cells (ASCs). ASCs are therapeutic cells with increased clinical interests due to their ease of isolation, differentiation capacity, immunomodulatory effects, and angiogenic abilities[29–31]. Currently, it is believed that the therapeutic effect of ASCs largely results from their secretome, which are proteins secreted into the extracellular space[32–38]. The secretome of any cell is often overlooked when evaluating biomaterials. However, as this is a very important mechanism in tissue regeneration, this study evaluates for the first time the effects of novel BPBGs on the ASC secretome.

2. MATERIALS AND METHODS

2.1. GLASS PREPARATION

Glasses of the compositional space $16\text{Na}_2\text{O}-24\text{CaO}-\text{XB}_2\text{O}_3-(60-\text{X})\text{P}_2\text{O}_5$ (mol %) system are listed in Table 1. Batch materials were calcined at 300°C for at least 4 hours, and then melted in platinum crucibles from $1000-1150^\circ\text{C}$, depending on the composition. Melts were quenched in graphite molds after one hour and were stirred on the half hour during melting with a platinum stir rod. Samples were annealed at 350°C for one hour then allowed to cool to room temperature. Glasses were confirmed to be fully amorphous by x-ray diffraction (XRD), using a PANalytical X'Pert Multipurpose diffractometer utilizing a Cu K- α source and a PIXcel Detector. Glasses were ground into $75-150\mu\text{m}$ particles and stored in a vacuum desiccator until use.

Table 1. Bioactive glass compositions.

Glass Designation	Na_2O	CaO	B_2O_3	P_2O_5
X0	16	24	-	60
X40	16	24	40	20
X60	16	24	60	-

2.2. CELL CULTURE

2.2.1. Adipose Stem Cells. ASCs were prepared by thawing frozen vials of approximately 1×10^6 cells (Obatala Sciences, LLC, New Orleans, LA) into 150cm^2

culture plates (Nunc, Rochester, NY) in 20ml complete culture media (CCM) consisting of alpha minimum essential media (α -MEM; Sigma; St. Louis, MO), 10% fetal bovine serum (FBS; VWR, Dixon, CA), 1% 100x L-glutamine (Sigma), and 1% 100x antibiotic/antimycotic (Sigma). After 24 hours incubation at 37°C humidified and 5% CO₂, media was removed and the adherent, viable cells were washed twice with phosphate buffer solution (PBS; Sigma) and harvested using 0.25% trypsin/1mM Ethylenediaminetetraacetic acid (EDTA; Sigma). ASCs then were plated at 100 cells/cm² in CCM. The media was changed every 3–4 days and sub-confluent cells ($\leq 70\%$ confluent) from three separate donors between passages 2-6 were used for all experiments.

2.2.2. Dermal Microvascular Endothelial Cells. Human dermal microvascular endothelial cells (HMVEC-d, pooled donors) were obtained from Lonza (Walkersville, MA). HMVECs were grown under normal conditions in Endothelial Cell Basal Medium-2 (Lonza), and the media was changed every 3-4 days.

2.3. GLASS CHARACTERIZATION

Approximately 2.5mg/ml of X0, X40, or X60 glass was dissolved in CCM, added to cell culture, and incubated under normal static conditions for 5 hours or 24 hours. Media was then collected, and the pH of each glass composition was measured. At the same timepoints, media was diluted with 1% HNO₃ to obtain solutions with ion concentrations in the 1-20 ppm range. Ions release rates were measured using Inductively Coupled Plasma – Optical Emission Spectroscopy (ICP-OES) on an Avio 200

Spectrometer (PerkinElmer; Waltham, MA, USA). CCM with no glass was used as a control. Samples were run in triplicate and averages are reported.

2.4. CELL VIABILITY

ASCs were plated in 8-chambered slides (LabTek; ThermoFisher; Rochester, NY) and grown until 70% confluence under normal static conditions. Approximately 2.5mg/mL of X0, X40 or X60 glass dissolved in CCM was added to the cells for 24 or 72 hours. After incubation at 37°C humidified 5% CO₂, chambers were gently washed 3-4 times in pre-warmed PBS and stained with live/dead stain (Fisher Scientific, Pittsburg, PA). Micrographs were taken with 10x objective on a Nikon A1R-HD/Ti2 E inverted confocal microscope (Melville, NY) and quantified by Fiji software (Madison, Wisconsin).

2.5. DIFFERENTIATION

ASCs were cultured in 6 well plates at 37°C humidified 5% CO₂ until 100% confluent in CCM. A solution of 2.5mg/ml X0, X40 or X60 glass dissolved in CCM was added to the wells and incubated for 24 hours under static conditions. Media was aspirated, wells were gently washed twice with PBS, and differentiation media was added. Adipogenic induction media (Lonza; Walkersville, MD) consisted of 1mM Dexamethasone, 0.5mM methyl-isobutyl xanthine, 10mg/mL insulin, 100mM indomethacin, and 10% FBS in DMEM (4.5 g/ L glucose). Osteogenic induction media (Lonza) consisted of 50mM ascorbate-2-phosphate, 10mM b-glycerol phosphate, and 1028M dexamethasone. Media was changed every 3-4 days for 14 days. Cells were washed gently with PBS and fixed in 10% formalin for 1 hour at room temperature. Cells

were stained with 0.5% Oil Red O to visualize fat droplets or with 40mM Alizarin Red (pH 4.1) to measure calcium deposition. Differentiation was imaged with an inverted microscope (Leica DMi1; Heerbrugg, Switzerland). Data was quantified by Fiji software (Madison, Wisconsin).

2.6. MIGRATION

Cell migration assays were performed in a 96-well transwell with 8mm pore membrane inserts (BD Biosciences, Bedford, MA). To evaluate if ASCs were attracted to BPBG, 5.0×10^4 ASCs were suspended in serum-free (SF) media and were added to the top of the transwell inserts. Approximately 2.5mg/ml X0, X40 or X60 glass were suspended in CCM and were added to the bottom of the transwells. After 5 hours of incubation at 37°C, 5% CO₂, the transwell insert was removed and gently placed into trypsin/EDTA (Figure. 1A). Cells that had migrated to the bottom of the insert were stained with CyQuant and quantified using a fluorescent microplate reader (Fluostar Omega; BMG Labtech, Cary, NC).

In order to evaluate if BPBG could increase the angiogenic ability of ASCs, ASCs were treated with 2.5mg/ml of X0, X40, or X60 glass in CCM for 24 hours. Media was then collected, filtered to remove any remaining glass, and placed in the lower chamber of a transwell. Around 2×10^4 HMVEC-d were added to the top of the inserts and incubated for 5 hours. HMVEC-d that migrated to the bottom of the inserts were stained with CyQuant and read on a plate reader (Figure. 1B). Each experiment was performed in triplicate.

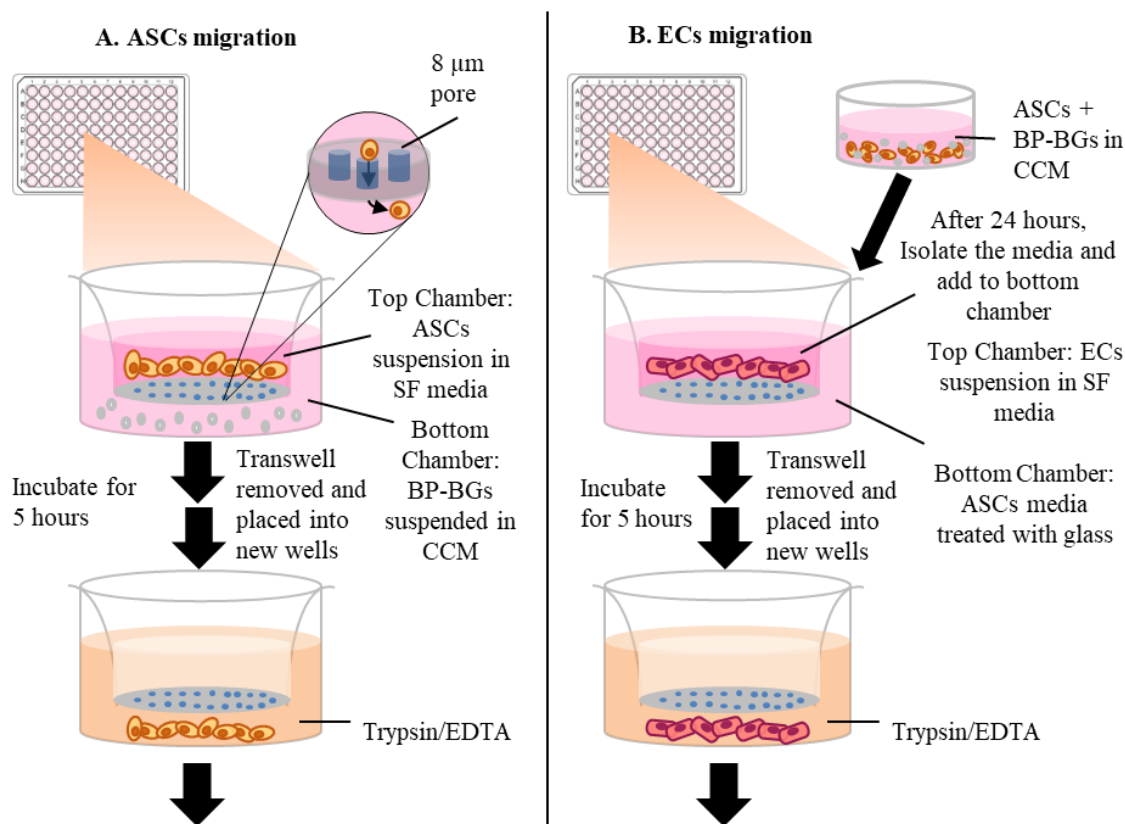


Figure 1. Schematic of the experimental setup for migration assays. (A) ASCs suspended in serum-free media were added to the top of 8mm transwell inserts. Glass solutions at 2.5mg/ml were added to the bottom of the transwells. After 5 hours, cells that had migrated to the bottom were measured by CyQuant. (B) ASCs were grown under standard conditions until 70% confluent. Glass was added to ASCs at 2.5mg/ml for 24 hours. The glass-treated conditioned media was then added to the bottom of a transwell. ECs were added to the top of 8mm transwell inserts and incubated for 5 hours. ECs that migrated to the bottom of the inserts were measured by CyQuant.

2.7. CYTOKINE ARRAY

Subconfluent ASCs were incubated with 2.5mg/ml of X0, X40, X60, or CCM. After 24 hours of incubation, 200 μl of conditioned media was collected, filtered to remove any remaining glass, and analyzed using the Human Cytokine Quantibody Array 4000 (RayBiotech, Norcross, GA) following the manufacturer's instructions. Cytokine concentrations data was sorted on Microsoft Excel spreadsheets based on the concentration hierarchy. A log base 2 of the ratio of the significant protein concentrations

datasets compared to the control was calculated and used in designing the hierarchical clustered heatmaps. These experiments were performed in duplicates on pooled conditioned media from three ASC donors.

2.8. STATISTICS

Each experiment was performed in triplicate with a minimum of three separate ASC donors. All values are presented as means \pm standard deviation (SD). The statistical differences among two or more groups were determined by ANOVA, followed by post-hoc Tukey versus the control groups.

3. RESULTS

3.1. GLASS PROPERTIES

BPBG was added to ASCs under normal culture conditions, and the pH and ions released were measured (Table 2). The X0 glass, which is acidic in water (data not shown), created a physiologically neutral pH of 7.36 in cell culture at 5 hours and further increased to pH 7.57, creating a slightly alkaline environment at 24 hours. On the other hand, borate rich X60 glass increased the alkalinity to pH 7.78 at 5 hours and maintained a similar pH until 24 hours. The intermediate boron to phosphate X40 glass retained a physiologically pH neutral environment at both 5 and 24 hours. For all glasses, the pH change was less when cells were present, showing that cells even under static condition have a buffering potential.

Alongside the pH changes, the ions released from each glass composition varied according to the boron to phosphate ratios. At 5 hours, X40 glass released 40% more

phosphorus than X0, however, by 24 hours, X0 released 10% more phosphorus than X40. The calcium release from X0 at 5 hours was insignificant compared to the cell culture without glass, while X40 was 20% higher than control and X60 was 62% higher than control. Boron release for X40 increased 42% between 5 and 24 hours, while boron release for X60 only increased by 17%. It is interesting to note that at 24 hours, X0 glass released more ions (Ca and P) than X40, which shows the faster degradation of X0 than X40 glass. Furthermore, X40 showed a higher rate of boron release while slow-release rates of calcium and phosphorus ions between the 5- and 24-hour time points. The slow release of calcium and phosphorus in the X40 glass may be due to the formation of a brushite reaction layer. As more glass dissolved, it left behind a fully reacted particle and a solid precipitate.

Table 2. pH change and ion release in CCM with or without cells.

Sample	Time (hours)	Cells present	pH	Ions Released (ppm)		
				P	B	Ca
CCM	0	-	7.42	35.74±0.98	ND	66.54±1.58
		+	7.44	-	-	-
	5	-	7.42	-	-	-
		+	7.44	34.80±1.45	ND	65.82±2.68
	24	-	7.44	-	-	-
X0	0	-	7.95	80.48±2.16	ND	78.57±1.09
		+	7.94	-	-	-

Table 2. pH change and ion release in CCM with or without cells (cont.).

X0	5	-	7.39	79.47±0.60	ND	76.25±0.52
		+	7.36	72.04±0.47	ND	68.84±2.67
	24	-	7.81	237.62±2.92	ND	113.40±0.29
		+	7.57	197.03±5.91	ND	101.28±1.64
X40	0	-	7.92	160.98±3.20	211.12±7.73	72.23±1.11
		+	7.89	–	–	–
	5	-	7.38	113.72±3.07	109.49±0.40	83.34±1.55
		+	7.33	121.06±3.61	126.10±1.46	82.36±1.37
	24	-	7.50	150.27±0.88	179.79±1.88	68.24±0.66
		+	7.47	176.01±4.24	217.40±1.06	73.26±1.11
X60	0	-	8.31	29.44±0.42	88.84±1.15	109.52±1.08
		+	8.18	–	–	–
	5	-	7.83	23.56±0.57	351.90±8.23	215.86±4.55
		+	7.78	23.27±0.30	249.43±8.00	173.16±3.79
	24	-	7.92	25.62±0.59	482.47±21.85	256.79±12.31
		+	7.75	24.96±0.18	301.26±6.03	201.43±5.03

3.2. HIGH CONCENTRATION OF BPBGs REDUCED ASCS VIABILITY AT 72 HOURS

According to ISO norm, a decrease in cell viability by 30% indicates a biomaterial is toxic and not biocompatible[39]. To evaluate the cytotoxicity effect of BPBGs on ASCs, low and high concentrations (2.5 and 10mg/ml, respectively) of three

glass compositions were directly added to ASCs under normal static conditions (Figure 2). At 24 hours, all glass compositions, at both low and high concentrations, were viable. Interestingly, the phosphate-rich X0 glass had the lowest viability with both concentrations, despite having a more neutral pH than the X60 glass (7.57 vs 7.75, respectively). The X0 glass did have 7.8 times more phosphorus released than the X60, suggesting that cell viability is dependent on pH, as well as ion concentration.

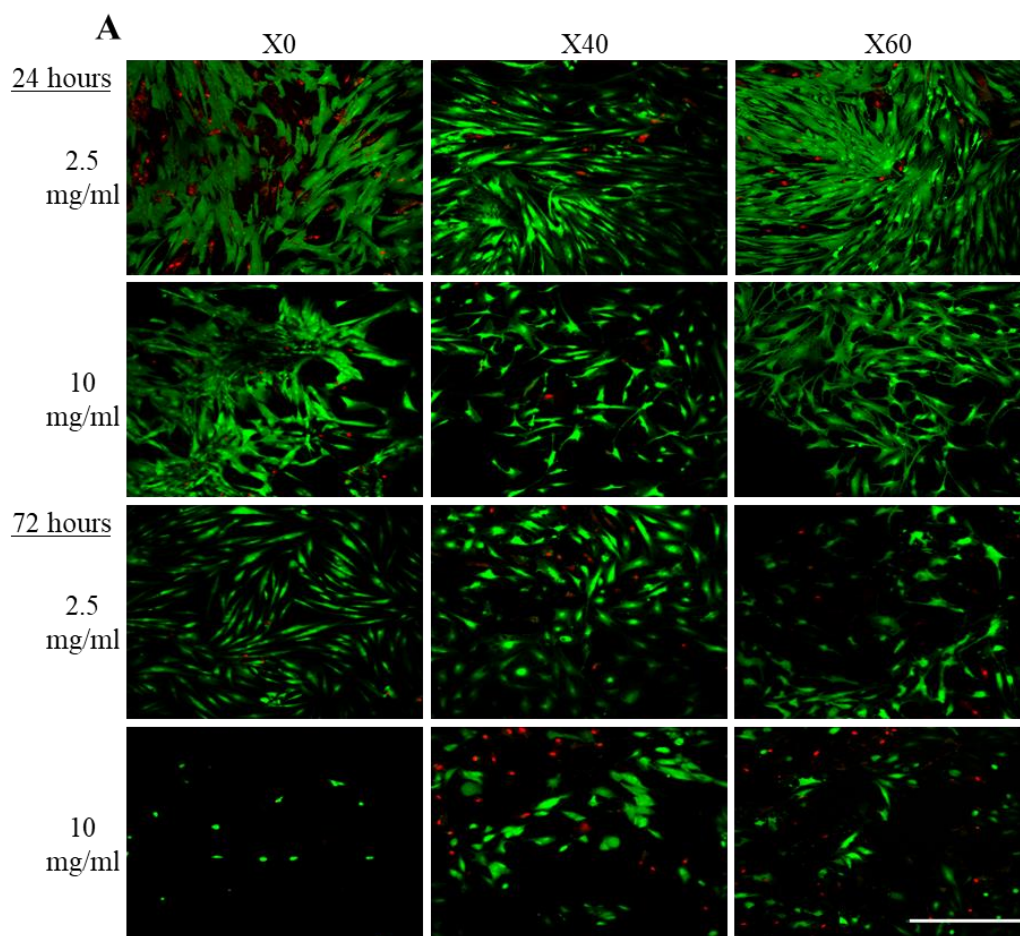


Figure 2. A high concentration of BPBGs reduced ASCs viability at 72 hours under static conditions. Subconfluent ASCs were treated with low or high concentrations of BPBG. (A) Live/dead stain showed ASC viability at 24 and 72 hours. Scale bar = 500 μ m. (B) Viability was quantified with three donors examined in triplicate. Error bars indicate SD (n=9); * $p \leq 0.01$, and ** $p < 0.05$.

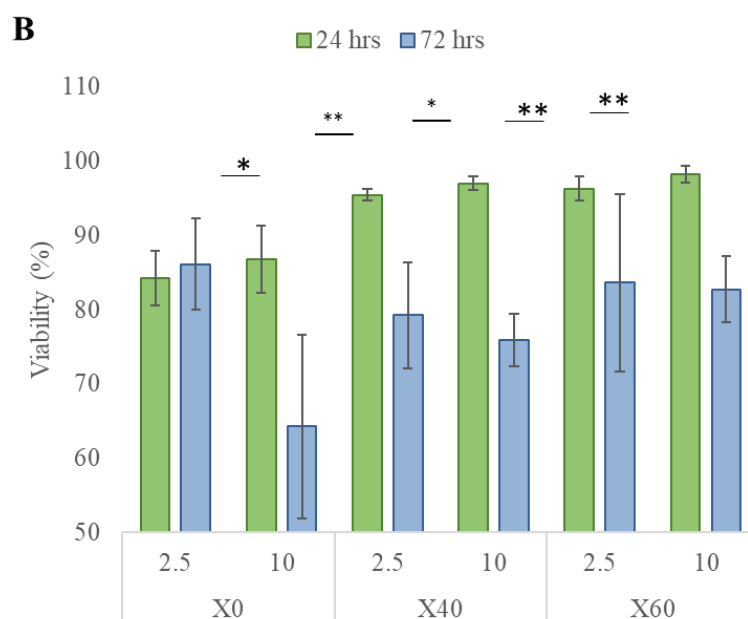


Figure 2. A high concentration of BPBGs reduced ASCs viability at 72 hours under static conditions. Subconfluent ASCs were treated with low or high concentrations of BPBG. (A) Live/dead stain showed ASC viability at 24 and 72 hours. Scale bar = 500 μ m. (B) Viability was quantified with three donors examined in triplicate. Error bars indicate SD (n=9); * $p \leq 0.01$, and ** $p < 0.5$ (cont.).

Only one composition, the phosphorus-rich X0 glass, was considered non-viable, and that was using a high concentration for 72 hours. Interestingly, a low concentration of the same glass maintained its viability while all other glass compositions and concentrations decreased at that timepoint.

3.3. BPBGs AFFECTS ASCS DIFFERENTIATION

In the presence of low concentration BPBGs, ASCs were evaluated for their differentiation ability into adipogenic and osteogenic lineages. ASCs were grown to 100% confluency and were incubated with X0, X40, or X60 glasses under normal, static conditions for 24 hours. ASCs were then grown for 14 days in adipogenic or osteogenic media. Interestingly, X60 glass reduced adipogenic differentiation, while X0 glass

inhibited osteogenic differentiation (Figure 3). Furthermore, X0 inhibited osteogenesis in all three donors tested, while there was a donor variation with all other differentiation assays.

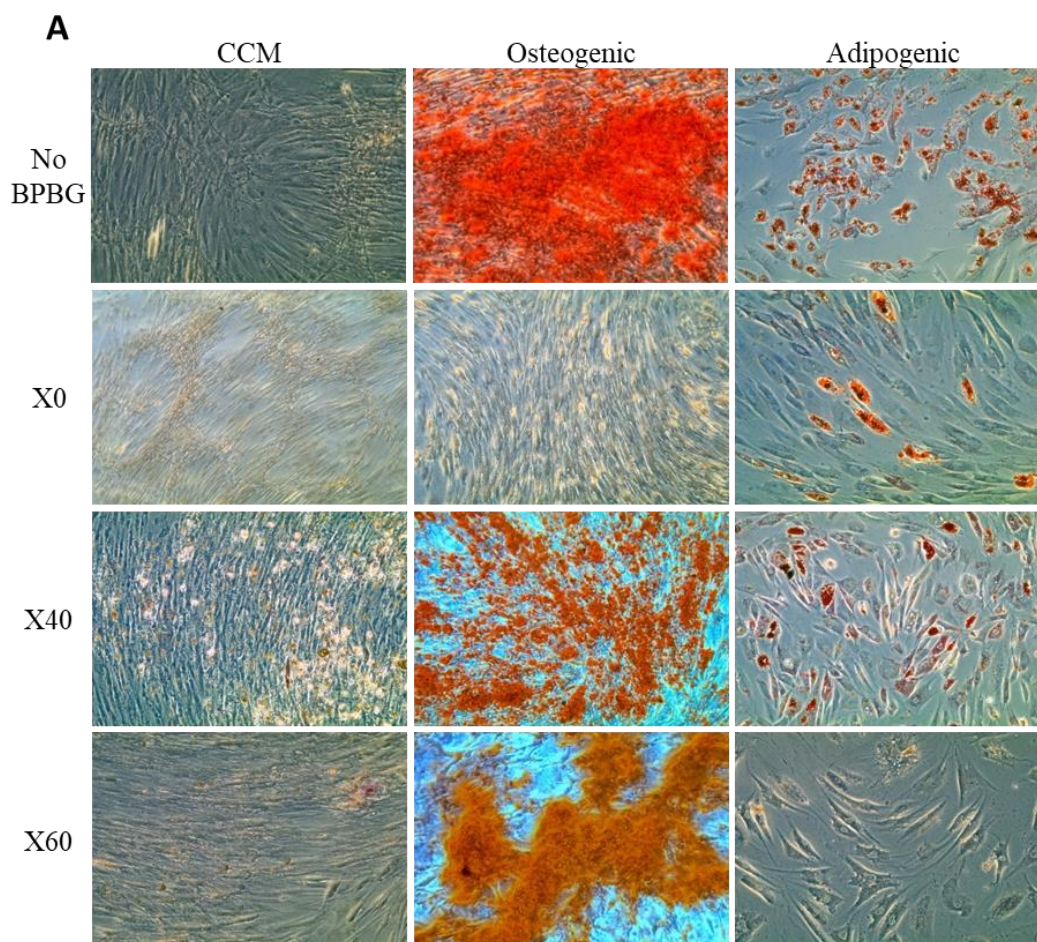


Figure 3. BPBGs influence ASC differentiation. ASCs were induced to differentiate in the absence or presence of BPBG. (A) Representative micrographs of 3 ASC donors are shown. Osteogenic (B) and adipogenic (D) differentiation quantified using Fiji software. Mean \pm SEM; $^{\wedge}$ $p < 0.05$ compared to no glass control; * $p < 0.05$ compared to X0; $\#$ $p < 0.05$ compared to X40. Donor differences with ability of glass to stimulate osteogenesis (C) and adipogenesis (E). Mean \pm SEM; $^{\wedge}$ $p < 0.05$ compared to D1; * $p < 0.05$ compared to D2; $\#$ $p < 0.05$ compared to D3.

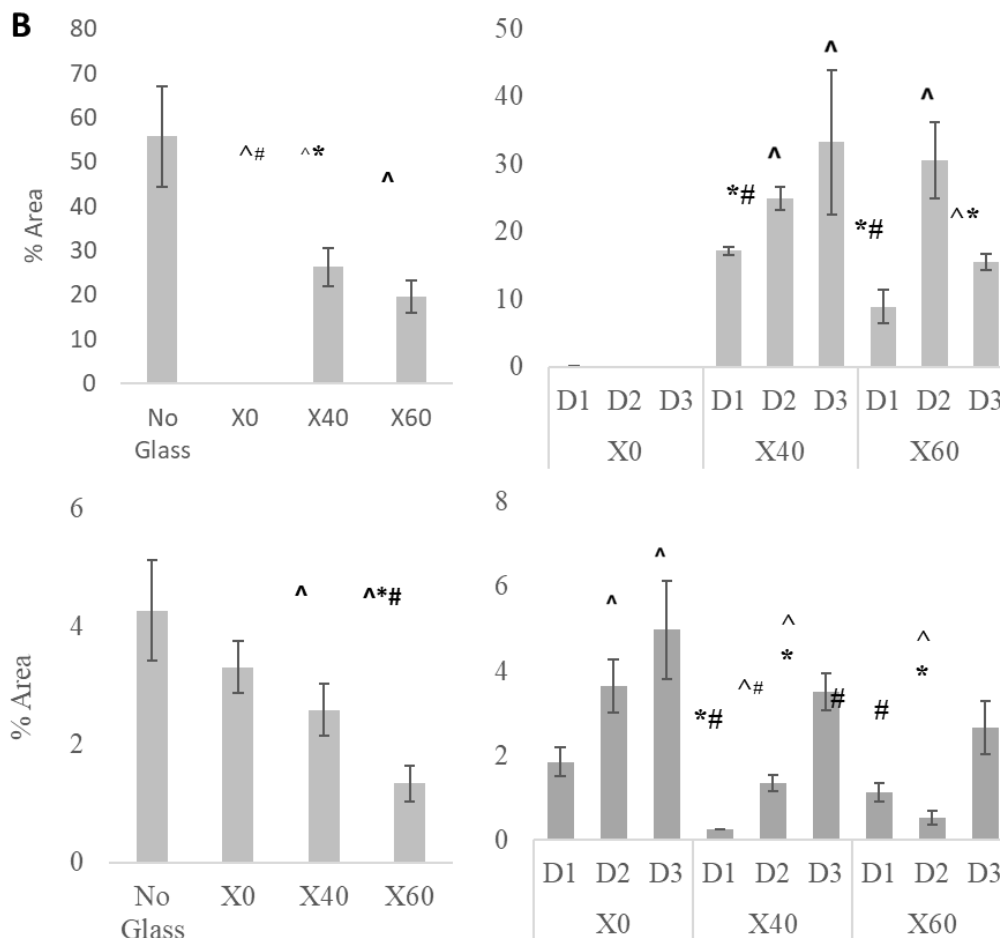


Figure 3. BPBGs influence ASC differentiation. ASCs were induced to differentiate in the absence or presence of BPBG. (A) Representative micrographs of 3 ASC donors are shown. Osteogenic (B) and adipogenic (D) differentiation quantified using Fiji software. Mean \pm SEM; ^ $p < 0.05$ compared to no glass control; * $p < 0.05$ compared to X0; # $p < 0.05$ compared to X40. Donor differences with ability of glass to stimulate osteogenesis (C) and adipogenesis (E). Mean \pm SEM; ^ $p < 0.05$ compared to D1; * $p < 0.05$ compared to D2; # $p < 0.05$ compared to D3 (cont.).

3.4. PH-NEUTRAL BPBGs ATTRACT ASCS WHILE ASCS TREATED WITH BASIC BPBGs ATTRACT ECS

Adipose stem cells possess an inherent ability to migrate to sites of injuries and secrete various chemokines, cytokines, and growth factors that enable them to mediate the regeneration process[40–43]. To test whether different compositions of BPBGs affected migration of ASCs, a 5-hour transwell migration assay was used. Glasses X0 and

X40 increased ASC migration, while X60 had no statistical effect (Figure 4A). ASCs are also angiogenic, partially due to their ability to attract endothelial cells (ECs)[35]. To test if BPBG could affect the ability of ASCs to attract ECs, sub-confluent ASCs were treated with BPBG for 24 hours. The resulting conditioned media was used as an attractant for EC migration. Interestingly, only X60 increased the ASCs' ability to attract ECs (Figure 4B).

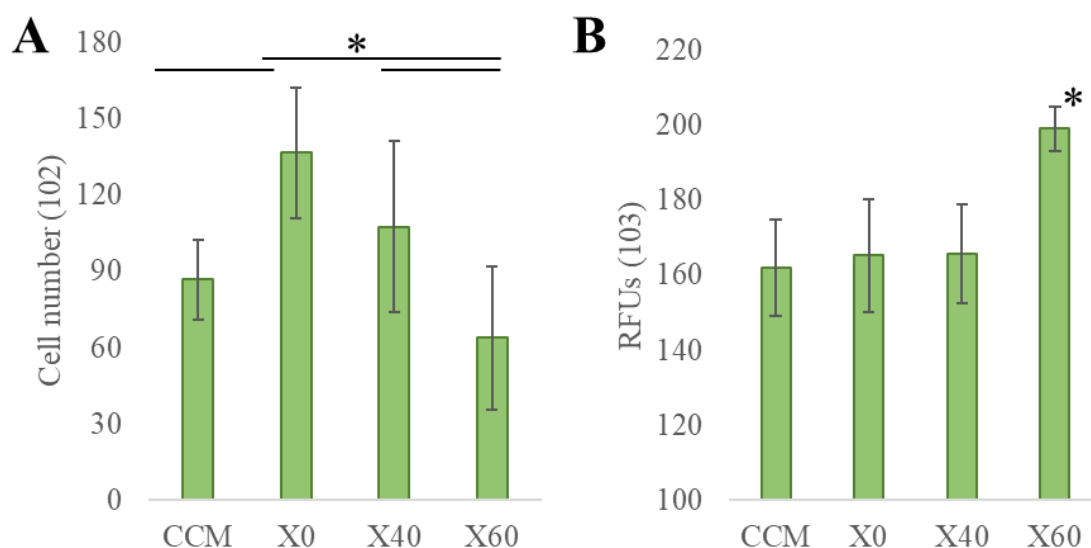


Figure 4. BPBGs affect cell migration. (A) Migration was examined by a transwell assay. ASCs were loaded onto the top inserts, while 2.5mg/ml of glass was added to the bottom. After 5 hours incubation, migrated cells were measured by CyQuant. (B) ASCs Figure 4. BPBGs affect cell migration (cont.). were treated with glass for 24 hours under standard conditions. The resulting conditioned media was put in the bottom of a transwell with ECs added to the top. After 5 hours of incubation, migrated cells were measured by CyQuant. In both assays, three separate ASC donors were examined in triplicate. Error bars indicated SD (n=9); *p-value ≤ 0.05 .

3.5. BPBG ALTERS ASC SECRETOME

To determine if BPBGs influenced the ASC secretome, a quantitative sandwich-based ELISA array was performed. After conditioning ASCs with a low concentration of

BPBG for 24 hours, the conditioned media was examined for 200 secreted proteins, including cytokines, growth factors, proteases, soluble receptors, and other proteins. Of those, 183 proteins were detectable in sufficient expression levels, with only 154 proteins differentially expressed between BPBG treatment groups and the control.

Of the 55 proteins that were differentially secreted regardless of glass treatment, 5 proteins were secreted in all three BPBG treatments while not being secreted at all under normal conditions (Figure 5A), 26 proteins increased their expression irrespective of glass treatment (Figure 5C), 20 proteins decreased with all three glass treatments (Figure 5D), and the secretion of 4 proteins were completely hampered (Figure 5B) regardless of glass treatment. There were 22 proteins that were differentially secreted with boron concentration: 2 decreased while 20 increased (Figure 6, Table 2). Figure 7 shows the unique secretion pattern for each glass composition represented in hierarchal clustering heatmaps.

4. DISCUSSION

Because alkaline glasses are toxic to cells and tissues, they are often pre-reacted before use in cell culture. Even pH-neutral BPBGs have been pre-reacted to maintain high ASC viability for 14 days[44]. This makes cell culture, and potential clinical applications of BGs, complicated. Furthermore, in order to understand the role of BGs in the clinic, it is important to evaluate them in direct contact with cells.

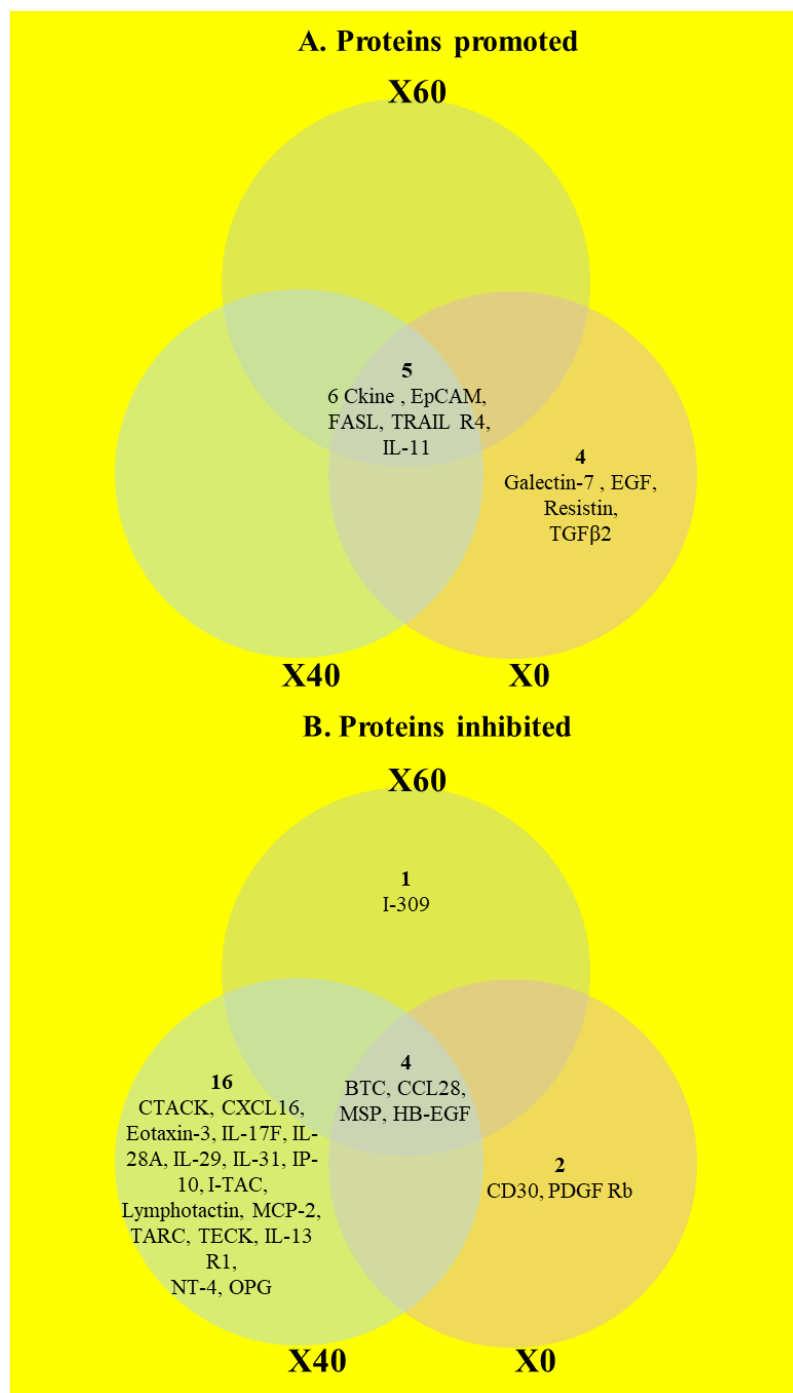


Figure 5. Effect of BPBGs on the ASCs secretory profile. Subconfluent ASCs were treated with 2.5mg/ml of BPBG for 24 hours. Media was then collected and analyzed for secreted proteins. ASC protein secretion was promoted (A), inhibited (B), increased (C), or decreased (D) with glass treatment. All three glass compositions increased the secretion of 26 proteins (C) while promoting the secretion of 5 additional proteins that ASCs did not secrete under normal conditions (A). All three BPBGs decreased the secretion of 20 proteins (D) while the secretion of 4 additional proteins was completely inhibited (B).

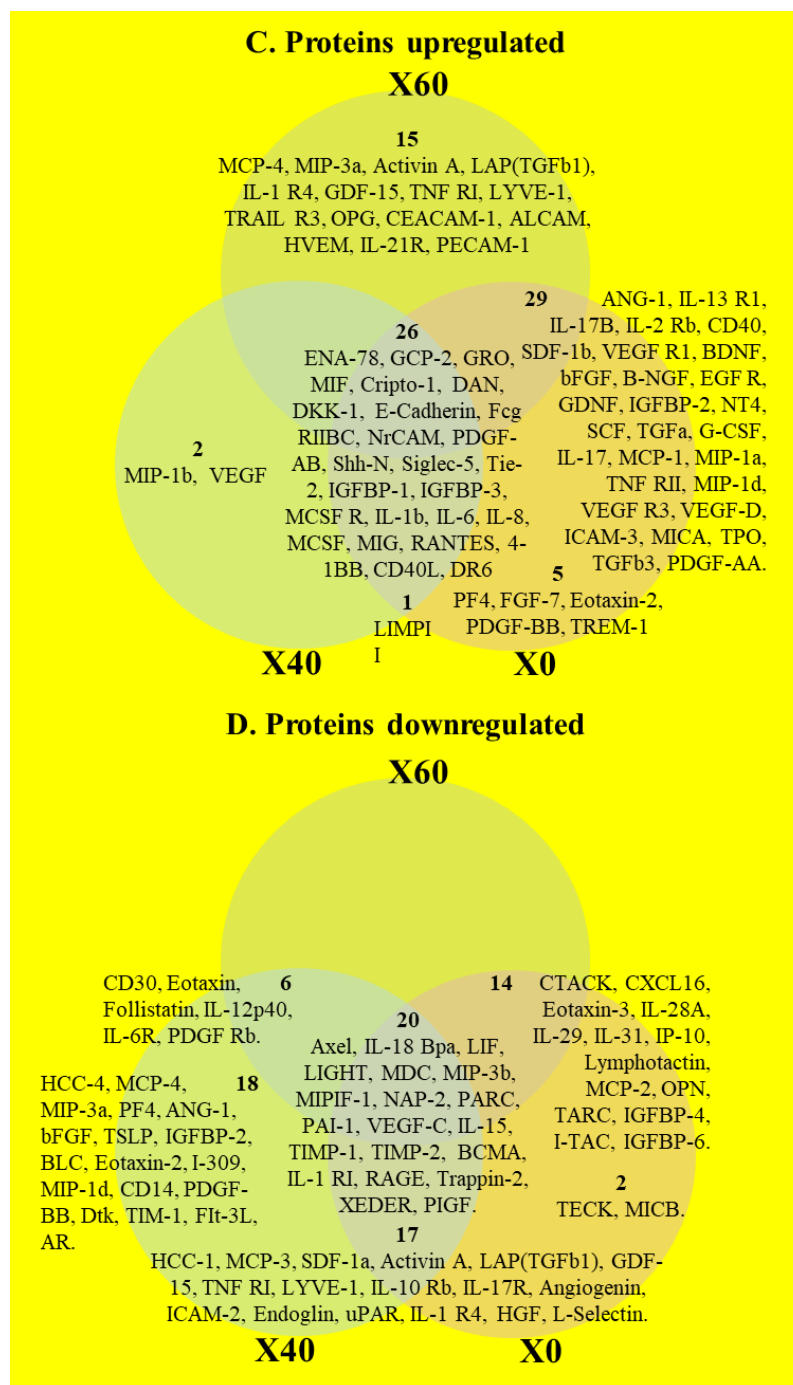


Figure 5. Effect of BPBGs on the ASCs secretory profile. Subconfluent ASCs were treated with 2.5mg/ml of BPBG for 24 hours. Media was then collected and analyzed for secreted proteins. ASC protein secretion was promoted (A), inhibited (B), increased (C), or decreased (D) with glass treatment. All three glass compositions increased the secretion of 26 proteins (C) while promoting the secretion of 5 additional proteins that ASCs did not secrete under normal conditions (A). All three BPBGs decreased the secretion of 20 proteins (D) while the secretion of 4 additional proteins was completely inhibited (B) (cont.).

The low concentration of the phosphate-rich X0 glass-maintained viability over the course of 72 hours better than the glasses with less phosphate, however, the high concentration of the same glass was considered non-viable at the same timepoint. This correlates with other studies showing that increasing extracellular levels of inorganic phosphate promotes cell growth and proliferation, while further increasing the concentration (above 16mM) triggered cell death by activating both intrinsic and extrinsic apoptotic pathway[45].

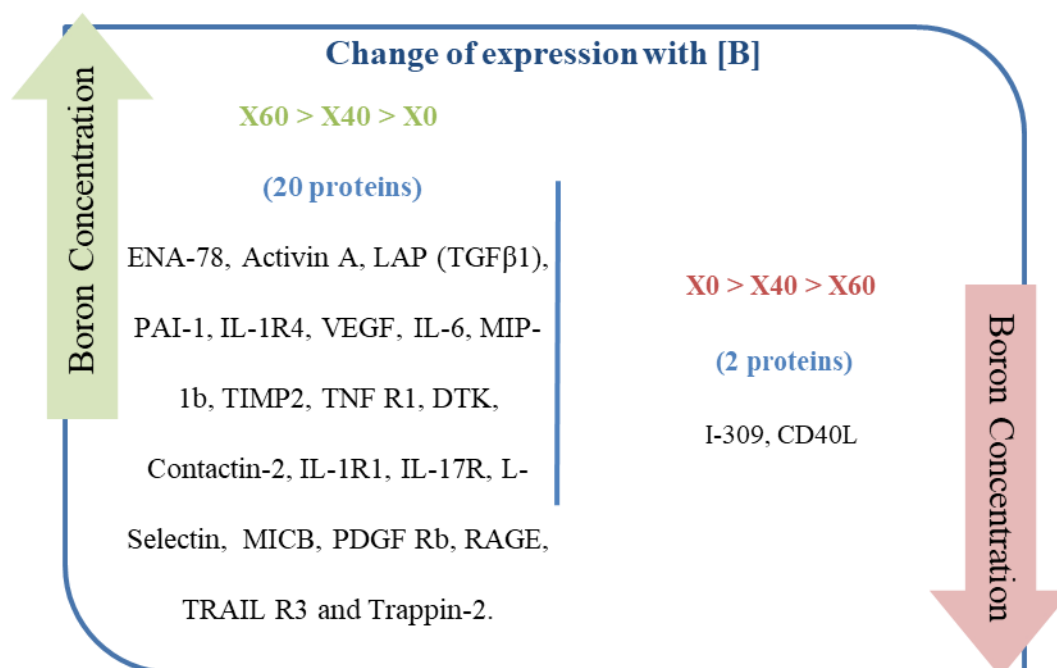


Figure 6. Boron concentration influenced ASC secretome. There were 20 proteins that increased and 2 that decreased with increasing boron in BPBG compositions.

Our results show that ASCs act as buffers, making the extracellular environment more acidic when in the presence of BGs. Though little is known about the ability of ASCs to regulate extracellular pH, it is understood that cells can maintain a narrow range

(7.1-7.2) of intracellular pH through the actions of membrane proton pumps and transporters, which are controlled by intra-cytoplasmic pH sensors[46]. These sensors have the ability to recognize and induce cellular responses to maintain the intracellular pH, often at the expense of acidifying the extracellular pH. In turn, this extracellular acidification impacts G-protein coupled receptors.

Table 3. Protein secretion levels, presented in pg/ml and mean±SD. Yellow represents the highest expression.

	CCM	X0	X40	X60
ENA-78	5.72 ± 0.58	16.91 ± 0.94	34.72 ± 18.34	66.43 ± 19.25
Activin A	280.68 ± 3.43	43.34 ± 4.66	112.34 ± 40.94	725.43 ± 86.71
LAP (TGFβ1)	32.84 ± 3.69	21.13 ± 1.78	27.32 ± 2.82	39.70 ± 1.17
TNF RI	201.07 ± 8.25	185.55 ± 14.80	188.68 ± 14.05	289.75 ± 0.51
TRAIL R3	22.90 ± 7.87	19.34 ± 1.15	22.52 ± 2.56	35.79 ± 0.92
IL-1 R4	68.35 ± 53.92	2.01 ± 2.84	8.30 ± 11.74	158.44 ± 43.02
VEGF	92.27 ± 2.51	94.50 ± 3.18	137.60 ± 14.54	294.71 ± 7.60
IL-6	2701.45 ± 26.20	3118.31 ± 41.64	3865.87 ± 254.17	4109.95 ± 226.75
MIP-1b	68.36 ± 13.41	70.92 ± 4.68	92.55 ± 2.58	96.42 ± 2.91
TIMP-2	12795.45 ± 1190.17	6473.49 ± 1026.09	7645.48 ± 155.76	8481.24 ± 400.92
PAI-1	4466.23 ± 255.95	3381.66 ± 472.87	3408.96 ± 451.51	3876.75 ± 261.23
Dtk	45.79 ± 10.57	29.92 ± 40.39	37.39 ± 6.93	43.84 ± 12.14

Table 3. Protein secretion levels, presented in pg/ml and mean±SD. Yellow represents the highest expression (cont.).

Contactin-2	54.06 ± 25.45	34.79 ± 23.03	39.99 ± 15.39	41.34 ± 11.09
IL-1 RI	9.29 ± 0.58	1.51 ± 0.18	2.36 ± 0.29	8.00 ± 1.02
IL-17R	32.17 ± 0.49	14.40 ± 18.02	17.93 ± 1.26	30.14 ± 5.68
L-Selectin	149.13 ± 58.12	4.48 ± 6.85	10.85 ± 12.99	144.18 ± 23.18
MICB	356.25 ± 61.86	241.29 ± 140.60	322.14 ± 82.21	339.68 ± 24.50
PDGF Rb	441.62 ± 174.57	0.00	70.73 ± 99.85	149.87 ± 193.95
RAGE	7.73 ± 1.51	2.63 ± 2.20	3.02 ± 2.71	5.72 ± 1.28
Trappin-2	15.20 ± 1.92	3.47 ± 0.47	8.47 ± 2.55	11.78 ± 0.54
	Control	X0	X40	X60
I-309	1.77 ± 0.57	1.98 ± 0.00	0.05 ± 0.07	0.00
CD40L	15.91 ± 13.60	37.10 ± 13.53	36.48 ± 0.87	32.77 ± 10.19

There is evidence that expression of proton-sensing GPCRs can regulate migration and invasion of cells. Which may explain why X0 increased ASC migration the most. On the other hand, elevated levels of extracellular inorganic phosphate have been shown to induce epithelial-mesenchymal transition through ERK1/2 signaling, promoting cell migration and invasiveness during development, cancer metastasis, wound healing, and fibrosis[45]. The exact mechanism for the increased migration, extracellular pH or increased extracellular phosphate, needs to be explored to maximize the use of the X0 glass.

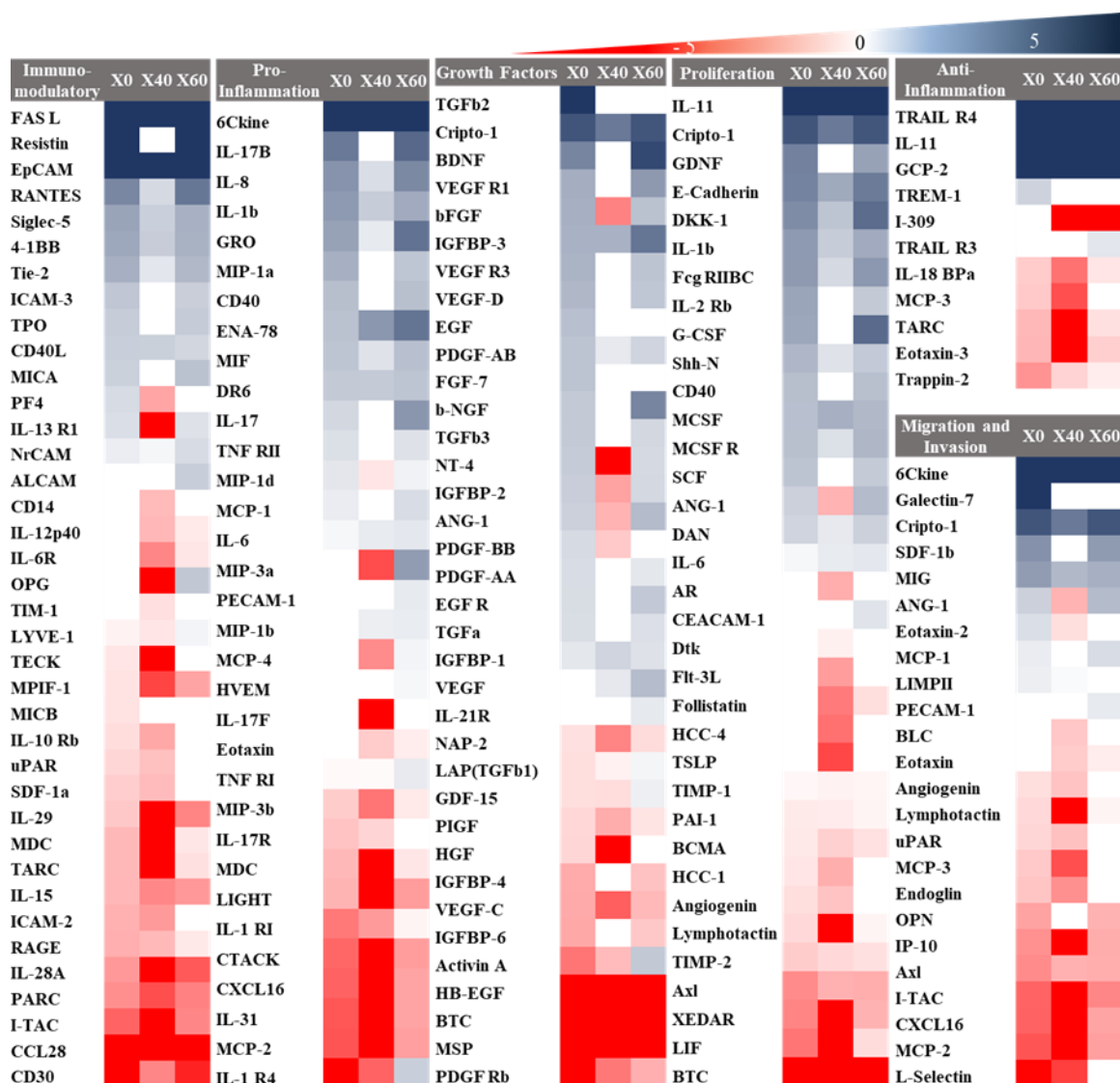


Figure 7. Representative hierarchal heatmap clustering the proteins based on function. All proteins presented are significant from the control ($p < 0.5$). Log₂(FC) is used in which (-5 to 5) is the range and any value above 5 represented as dark blue while any value below - 5 represented as dark red color while the white color represents all the proteins that are not significant. FC represents the fold change between the samples treated with glass in relation to the control.

ASCs demonstrated increased migration to X0 as it degraded over 5 hours.

Because X0 and X40 both exhibited similar pH neutral effects with cells at this timepoint, it suggests that the migration difference is due to the ions present and not the

pH. Consequently, it is worth noting that X0 released the lowest amount of calcium ions at this timepoint. Calcium has long been known as a crucial regulator and mediator in cell migration[47–49]. Indeed, previous research shows calcium has an optimal range to promote BMSC migration[50]. The X40 and X60 glasses may be releasing too much calcium to effectively stimulate downstream genes of G-protein coupled receptor (GPCR) signaling pathways, which is an early response to calcium-based ceramics[51]. Consequently, calcium sensing receptor (CaSR), a receptor belonging to the GPCR family and modulates the chemotactic response of MSCs in response to extracellular calcium, may be stimulated by X0 glass and not X40 or X60 glasses.

BMSCs, with similar properties to ASCs, are known to migrate during the initial stages of wound healing. During this inflammatory phase, the pH of the damaged area decreases to an acidic state[52]. The pre-treatment of BMSCs with an acidic (pH 6.8) environment enhances the stemness of stem cell markers (oct 4, nanog)[52]. Though it's reported that this ability decreases BMSCs migration ability, the X0 glass may be able to provide an acidic pH for stem cell markers while also providing calcium for cellular migration.

BBG has been previously reported to be angiogenic[14, 53, 54]. In our study, we showed that after 24 hours, only the boron-rich X60 glass increased the angiogenic ability of ASCs by attracting endothelial cells, as well as increased secreted angiogenic, such as VEGF, ANG-1, b-NGF, IGFBP-3, TGFb3 and bFGF. This agrees with other studies that have shown the impact of boron in BBG on promoting angiogenesis[14, 27, 54–56]. The phosphate-rich X0 glass completely inhibited osteogenesis in all three ASC donors. The adipogenic ability was also reduced from controls, though not at significant levels. This

again correlates with the notion that pre-treating MSCs with an acidic environment enhances the stemness of MSCs, thus resulting in a lack of differentiation ability[52]. The borate-rich X60 glass, on the other hand, reduced adipogenic differentiation. This coincides with previous work showing boron prevented lipid deposition, suppressed adipogenesis transcriptional programming, while still maintaining cell viability[13].

Most literature on bioactive glass, including BPBG, focuses on cell viability, proliferation, or differentiation of ASCs[16, 44, 57–59]. However, there is little reported on the effect of BG on the ASCs secretome. ASCs have a broad secretory profile of different growth factors, cytokines, and other proteins which impact the body's response to injuries, healing, and tissue regeneration. These secreted proteins all work to keep the body in homeostasis[34, 37]. In this study, we showed for the first time that BPBGs can alter the ASCs secretome.

Our study showed that, regardless of the glass composition, the expression of 6-Ckine, EpCAM, FasL, TRAIL R4, and IL-4 were promoted, while they were not secreted without any of the glass treatments. Each of these biomolecules are worth looking into, as BGs may be able to be used as a cell treatment to increase the efficacy of the cells. For example, IL-4 overexpression in BMSCs polarized macrophages from an inflammatory M1 macrophage into a tissue regenerative M2 phenotype[60]. Evaluating these molecules will allow biomaterial designers to cater their materials for different applications.

The concentration of boron affected the ability of ASCs to secrete 22 proteins: two decreased with increased boron while 20 increased, which included many pro-inflammatory (IL-1, IL-6, IL17, etc.) and angiogenic (VEGF, L-Selectin, TIMP-2, etc.) proteins. As boron has been shown to be anti-inflammatory in other applications, it is

worth looking into how the controlled release of boron ions, in different pH ranges, may have different control over cells[61]. On the other hand, ASCs treated with the pH-neutral X40 glass increased the secretion of anti-proliferation and anti-migration proteins which may be more related to the high phosphorus release[7, 15, 62].

5. CONCLUSION

Phosphate-rich glasses create acidic environments, borate-rich glasses create basic environments, and the intermediate compositions can retain pH neutral environments. We, for the first time, evaluated BPBGs on the secretome of ASCs, which provides some insight as to how to customize BPBG for specific biomedical applications. At a low concentration, each of these glasses can be used safely in cell culture studies without having to pretreat the glass. This opens the doors for further investigating the impact of BG directly on cells in vitro.

REFERENCES

- Hench LL. The story of Bioglass®. *Journal of Materials Science: Materials in Medicine*. 2006;17(11):967–978. doi:10.1007/s10856-006-0432-z
- Baino F, Fiorilli S, Vitale-Brovarone C. Bioactive glass-based materials with hierarchical porosity for medical applications: Review of recent advances. *Acta Biomaterialia*. 2016;42:18–32. doi:10.1016/j.actbio.2016.06.033
- Kaur G, Pandey O p., Singh K, Homa D, Scott B, Pickrell G. A review of bioactive glasses: Their structure, properties, fabrication and apatite formation. *Journal of Biomedical Materials Research Part A*. 2014;102(1):254–274. doi:10.1002/jbm.a.34690

- Pajares-Chamorro N, Chatzistavrou X. Bioactive Glass Nanoparticles for Tissue Regeneration. *ACS omega*. 2020;5(22):12716–12726. doi:10.1021/acsomega.0c00180
- Rahaman MN, Day DE, Sonny Bal B, Fu Q, Jung SB, Bonewald LF, Tomsia AP. Bioactive glass in tissue engineering. *Acta Biomaterialia*. 2011;7(6):2355–2373. doi:10.1016/j.actbio.2011.03.016
- Jones JR. Review of bioactive glass: From Hench to hybrids. *Acta Biomaterialia*. 2013;9(1):4457–4486. doi:10.1016/j.actbio.2012.08.023
- Mehrabi T, Mesgar AS, Mohammadi Z. Bioactive Glasses: A Promising Therapeutic Ion Release Strategy for Enhancing Wound Healing. *ACS biomaterials science & engineering*. 2020;6(10):5399–5430. doi:10.1021/acsbomaterials.0c00528
- Fu Q, Rahaman MN, Fu H, Liu X. Silicate, borosilicate, and borate bioactive glass scaffolds with controllable degradation rate for bone tissue engineering applications. I. Preparation and in vitro degradation. *Journal of Biomedical Materials Research Part A*. 2010;95A(1):164–171. doi:10.1002/jbm.a.32824
- Huang W, Day DE, Kittiratanapiboon K, Rahaman MN. Kinetics and mechanisms of the conversion of silicate (45S5), borate, and borosilicate glasses to hydroxyapatite in dilute phosphate solutions. *Journal of Materials Science. Materials in Medicine*. 2006;17(7):583–596. doi:10.1007/s10856-006-9220-z
- Yao A, Wang D, Huang W, Fu Q, Rahaman MN, Day DE. In Vitro Bioactive Characteristics of Borate-Based Glasses with Controllable Degradation Behavior. *Journal of the American Ceramic Society*. 2007;90(1):303–306. doi:10.1111/j.1551-2916.2006.01358.x
- Fu H, Fu Q, Zhou N, Huang W, Rahaman MN, Wang D, Liu X. In vitro evaluation of borate-based bioactive glass scaffolds prepared by a polymer foam replication method. *Materials Science and Engineering: C*. 2009;29(7):2275–2281. doi:10.1016/j.msec.2009.05.013
- Zhang J, Guan J, Zhang C, Wang H, Huang W, Guo S, Niu X, Xie Z, Wang Y. Bioactive borate glass promotes the repair of radius segmental bone defects by enhancing the osteogenic differentiation of BMSCs. *Biomedical Materials*. 2015;10(6):065011. doi:10.1088/1748-6041/10/6/065011
- Apdik H, Doğan A, Demirci S, Aydın S, Şahin F. Dose-dependent Effect of Boric Acid on Myogenic Differentiation of Human Adipose-derived Stem Cells (hADSCs). *Biological Trace Element Research*. 2015;165(2):123–130. doi:10.1007/s12011-015-0253-3

- Balasubramanian P, Hupa L, Jokic B, Detsch R, Grünewald A, Boccaccini AR. Angiogenic potential of boron-containing bioactive glasses: in vitro study. *Journal of Materials Science*. 2017;52(15):8785–8792. doi:10.1007/s10853-016-0563-7
- Kargozar S, Baino F, Hamzehlou S, Hill RG, Mozafari M. Bioactive Glasses: Sprouting Angiogenesis in Tissue Engineering. *Trends in Biotechnology*. 2018;36(4):430–444. doi:10.1016/j.tibtech.2017.12.003
- Thyparambil NJ, Gutgesell LC, Bromet BA, Flowers LE, Greaney S, Day DE, Semon JA. Bioactive borate glass triggers phenotypic changes in adipose stem cells. *Journal of Materials Science: Materials in Medicine*. 2020;31(4):35. doi:10.1007/s10856-020-06366-w
- Hoppe A, Güldal NS, Boccaccini AR. A review of the biological response to ionic dissolution products from bioactive glasses and glass-ceramics. *Biomaterials*. 2011;32(11):2757–2774. doi:10.1016/j.biomaterials.2011.01.004
- Jones JR, Sepulveda P, Hench LL. Dose-dependent behavior of bioactive glass dissolution. *Journal of Biomedical Materials Research*. 2001;58(6):720–726. doi:10.1002/jbm.10053
- Qazi TH, Hafeez S, Schmidt J, Duda GN, Boccaccini AR, Lippens E. Comparison of the effects of 45S5 and 1393 bioactive glass microparticles on hMSC behavior. *Journal of Biomedical Materials Research Part A*. 2017;105(10):2772–2782. doi:10.1002/jbm.a.36131
- Hohenbild F, Arango-Ospina M, Moghaddam A, Boccaccini AR, Westhauser F. Preconditioning of Bioactive Glasses before Introduction to Static Cell Culture: What Is Really Necessary? *Methods and Protocols*. 2020;3(2):38. doi:10.3390/mps3020038
- Kellum JA. Determinants of blood pH in health and disease. *Critical Care (London, England)*. 2000;4(1):6–14. doi:10.1186/cc644
- Carta D, Qiu D, Guerry P, Ahmed I, Abou Neel EA, Knowles JC, Smith ME, Newport RJ. The effect of composition on the structure of sodium borophosphate glasses. *Journal of Non-Crystalline Solids*. 2008;354(31):3671–3677. doi:10.1016/j.jnoncrysol.2008.04.009
- Ahmed I, Lewis M, Olsen I, Knowles JC. Phosphate glasses for tissue engineering: Part 1. Processing and characterisation of a ternary-based P₂O₅-CaO-Na₂O glass system. *Biomaterials*. 2004;25(3):491–499. doi:10.1016/s0142-9612(03)00546-5
- Ahmed I, Lewis M, Olsen I, Knowles JC. Phosphate glasses for tissue engineering: Part 2. Processing and characterisation of a ternary-based P₂O₅-CaO-Na₂O glass fibre system. *Biomaterials*. 2004;25(3):501–507. doi:10.1016/s0142-9612(03)00547-7

- Mneimne M, Hill RG, Bushby AJ, Brauer DS. High phosphate content significantly increases apatite formation of fluoride-containing bioactive glasses. *Acta Biomaterialia*. 2011;7(4):1827–1834. doi:10.1016/j.actbio.2010.11.037
- Saranti A, Koutselas I, Karakassides MA. Bioactive glasses in the system CaO–B₂O₃–P₂O₅: Preparation, structural study and in vitro evaluation. *Journal of Non-Crystalline Solids*. 2006;352(5):390–398. doi:10.1016/j.jnoncrysol.2006.01.042
- Li K, Lu X, Razanau I, Wu X, Hu T, Liu S, Xie Y, Huang L, Zheng X. The enhanced angiogenic responses to ionic dissolution products from a boron-incorporated calcium silicate coating. *Materials Science & Engineering. C, Materials for Biological Applications*. 2019;101:513–520. doi:10.1016/j.msec.2019.04.009
- Massera J, Shpotyuk Y, Sabatier F, Jouan T, Boussard-Plédel C, Roiland C, Bureau B, Petit L, Boetti NG, Milanese D, et al. Processing and characterization of novel borophosphate glasses and fibers for medical applications. *Journal of Non-Crystalline Solids*. 2015;425:52–60. doi:10.1016/j.jnoncrysol.2015.05.028
- De Francesco F, Ricci G, D'Andrea F, Nicoletti GF, Ferraro GA. Human Adipose Stem Cells: From Bench to Bedside. *Tissue Engineering. Part B, Reviews*. 2015;21(6):572–584. doi:10.1089/ten.TEB.2014.0608
- Dykstra JA, Facile T, Patrick RJ, Francis KR, Milanovich S, Weimer JM, Kota DJ. Concise Review: Fat and Furious: Harnessing the Full Potential of Adipose-Derived Stromal Vascular Fraction. *Stem Cells Translational Medicine*. 2017;6(4):1096–1108. doi:10.1002/sctm.16-0337
- Gadelkarim M, Abushouk AI, Ghanem E, Hamaad AM, Saad AM, Abdel-Daim MM. Adipose-derived stem cells: Effectiveness and advances in delivery in diabetic wound healing. *Biomedicine & Pharmacotherapy = Biomedecine & Pharmacotherapie*. 2018;107:625–633. doi:10.1016/j.biopha.2018.08.013
- Bacakova L, Zarubova J, Travnickova M, Musilkova J, Pajorova J, Slepicka P, Kasalkova NS, Svorcik V, Kolska Z, Motarjemi H, et al. Stem cells: their source, potency and use in regenerative therapies with focus on adipose-derived stem cells - a review. *Biotechnology Advances*. 2018;36(4):1111–1126. doi:10.1016/j.biotechadv.2018.03.011
- Blaber SP, Webster RA, Hill CJ, Breen EJ, Kuah D, Vesey G, Herbert BR. Analysis of in vitro secretion profiles from adipose-derived cell populations. *Journal of Translational Medicine*. 2012;10:172. doi:10.1186/1479-5876-10-172
- Salgado AJBOG, Reis RLG, Sousa NJC, Gimble JM. Adipose tissue derived stem cells secretome: soluble factors and their roles in regenerative medicine. *Current Stem Cell Research & Therapy*. 2010;5(2):103–110. doi:10.2174/157488810791268564

- Kilroy GE, Foster SJ, Wu X, Ruiz J, Sherwood S, Heifetz A, Ludlow JW, Stricker DM, Potiny S, Green P, et al. Cytokine profile of human adipose-derived stem cells: expression of angiogenic, hematopoietic, and pro-inflammatory factors. *Journal of Cellular Physiology*. 2007;212(3):702–709. doi:10.1002/jcp.21068
- L PK, Kandoi S, Misra R, S V, K R, Verma RS. The mesenchymal stem cell secretome: A new paradigm towards cell-free therapeutic mode in regenerative medicine. *Cytokine & Growth Factor Reviews*. 2019;46:1–9. doi:10.1016/j.cytogfr.2019.04.002
- Lombardi F, Palumbo P, Augello FR, Cifone MG, Cinque B, Giuliani M. Secretome of Adipose Tissue-Derived Stem Cells (ASCs) as a Novel Trend in Chronic Non-Healing Wounds: An Overview of Experimental In Vitro and In Vivo Studies and Methodological Variables. *International Journal of Molecular Sciences*. 2019;20(15):3721. doi:10.3390/ijms20153721
- Mussano F, Genova T, Corsalini M, Schierano G, Pettini F, Di Venere D, Carossa S. Cytokine, Chemokine, and Growth Factor Profile Characterization of Undifferentiated and Osteoinduced Human Adipose-Derived Stem Cells. *Stem Cells International*. 2017;2017:6202783. doi:10.1155/2017/6202783
- ISO Technical Committee ISO/TC 194, Biological evaluation of medical devices. ISO 10993-5:2009(en), Biological evaluation of medical devices — Part 5: Tests for in vitro cytotoxicity. 2009. <https://www.iso.org/obp/ui/#iso:std:iso:10993:-5:ed-3:v1:en>
- Fu X, Liu G, Halim A, Ju Y, Luo Q, Song AG. Mesenchymal Stem Cell Migration and Tissue Repair. *Cells*. 2019;8(8):784. doi:10.3390/cells8080784
- Liu M, Lei H, Dong P, Fu X, Yang Z, Yang Y, Ma J, Liu X, Cao Y, Xiao R. Adipose-Derived Mesenchymal Stem Cells from the Elderly Exhibit Decreased Migration and Differentiation Abilities with Senescent Properties. *Cell Transplantation*. 2017;26(9):1505–1519. doi:10.1177/0963689717721221
- de Lucas B, Pérez LM, Gálvez BG. Importance and regulation of adult stem cell migration. *Journal of Cellular and Molecular Medicine*. 2018;22(2):746–754. doi:10.1111/jcmm.13422
- Baek SJ, Kang SK, Ra JC. In vitro migration capacity of human adipose tissue-derived mesenchymal stem cells reflects their expression of receptors for chemokines and growth factors. *Experimental & Molecular Medicine*. 2011;43(10):596–603. doi:10.3858/emm.2011.43.10.069
- Mishra A, Ojansivu M, Autio R, Vanhatupa S, Miettinen S, Massera J. In-vitro dissolution characteristics and human adipose stem cell response to novel borophosphate glasses. *Journal of Biomedical Materials Research Part A*. 2019;107(9):2099–2114. doi:10.1002/jbm.a.36722

- He P, Mann-Collura O, Fling J, Edara N, Hetz R, Razzaque MS. High phosphate actively induces cytotoxicity by rewiring pro-survival and pro-apoptotic signaling networks in HEK293 and HeLa cells. *FASEB journal: official publication of the Federation of American Societies for Experimental Biology*. 2021;35(1):e20997. doi:10.1096/fj.202000799RR
- Damaghi M, Wojtkowiak JW, Gillies RJ. pH sensing and regulation in cancer. *Frontiers in Physiology*. 2013;4:370. doi:10.3389/fphys.2013.00370
- Howe AK. Cross-talk between calcium and protein kinase A in the regulation of cell migration. *Current Opinion in Cell Biology*. 2011;23(5):554–561. doi:10.1016/j.ceb.2011.05.006
- Prevarskaya N, Skryma R, Shuba Y. Calcium in tumour metastasis: new roles for known actors. *Nature Reviews. Cancer*. 2011;11(8):609–618. doi:10.1038/nrc3105
- Ridley AJ, Schwartz MA, Burridge K, Firtel RA, Ginsberg MH, Borisy G, Parsons JT, Horwitz AR. Cell migration: integrating signals from front to back. *Science (New York, N.Y.)*. 2003;302(5651):1704–1709. doi:10.1126/science.1092053
- Aquino-Martínez R, Angelo AP, Pujol FV. Calcium-containing scaffolds induce bone regeneration by regulating mesenchymal stem cell differentiation and migration. *Stem Cell Research & Therapy*. 2017;8(1):265. doi:10.1186/s13287-017-0713-0
- Barradas AMC, Monticone V, Hulsman M, Danoux C, Fernandes H, Tahmasebi Birgani Z, Barrère-de Groot F, Yuan H, Reinders M, Habibovic P, et al. Molecular mechanisms of biomaterial-driven osteogenic differentiation in human mesenchymal stromal cells. *Integrative Biology: Quantitative Biosciences from Nano to Macro*. 2013;5(7):920–931. doi:10.1039/c3ib40027a
- Hazehara-Kunitomo Y, Hara ES, Ono M, Aung KT, Komi K, Pham HT, Akiyama K, Okada M, Oohashi T, Matsumoto T, et al. Acidic Pre-Conditioning Enhances the Stem Cell Phenotype of Human Bone Marrow Stem/Progenitor Cells. *International Journal of Molecular Sciences*. 2019;20(5):1097. doi:10.3390/ijms20051097
- Benderdour M, Hess K, Dzondo-Gadet M, Nabet P, Belleville F, Dousset B. Boron modulates extracellular matrix and TNF alpha synthesis in human fibroblasts. *Biochemical and Biophysical Research Communications*. 1998;246(3):746–751. doi:10.1006/bbrc.1998.8688
- Durand LAH, Góngora A, López JMP, Boccaccini AR, Zago MP, Baldi A, Gorustovich A. In vitro endothelial cell response to ionic dissolution products from boron-doped bioactive glass in the SiO₂–CaO–P₂O₅–Na₂O system. *Journal of Materials Chemistry B*. 2014;2(43):7620–7630. doi:10.1039/C4TB01043D

- Durand LAH, Vargas GE, Romero NM, Vera-Mesones R, Porto-López JM, Boccaccini AR, Zago MP, Baldi A, Gorustovich A. Angiogenic effects of ionic dissolution products released from a boron-doped 45S5 bioactive glass. *Journal of Materials Chemistry. B*. 2015;3(6):1142–1148. doi:10.1039/c4tb01840k
- Lin Y, Brown RF, Jung SB, Day DE. Angiogenic effects of borate glass microfibers in a rodent model. *Journal of Biomedical Materials Research Part A*. 2014;102(12):4491–4499. doi:10.1002/jbm.a.35120
- Ojansivu M, Hyväri L, Kellomäki M, Hupa L, Vanhatupa S, Miettinen S. Bioactive glass induced osteogenic differentiation of human adipose stem cells is dependent on cell attachment mechanism and mitogen-activated protein kinases. *European Cells & Materials*. 2018;35:54–72. doi:10.22203/eCM.v035a05
- Ojansivu M, Mishra A, Vanhatupa S, Juntunen M, Larionova A, Massera J, Miettinen S. The effect of S53P4-based borosilicate glasses and glass dissolution products on the osteogenic commitment of human adipose stem cells. *PloS One*. 2018;13(8):e0202740. doi:10.1371/journal.pone.0202740
- Vuornos K, Ojansivu M, Koivisto JT, Häkkänen H, Belay B, Montonen T, Huhtala H, Kääriäinen M, Hupa L, Kellomäki M, et al. Bioactive glass ions induce efficient osteogenic differentiation of human adipose stem cells encapsulated in gellan gum and collagen type I hydrogels. *Materials Science & Engineering. C, Materials for Biological Applications*. 2019;99:905–918. doi:10.1016/j.msec.2019.02.035
- Ueno M, Lo C-W, Barati D, Conrad B, Lin T, Kohno Y, Utsunomiya T, Zhang N, Maruyama M, Rhee C, et al. Interleukin-4 overexpressing mesenchymal stem cells within gelatin-based microribbon hydrogels enhance bone healing in a murine long bone critical-size defect model. *Journal of Biomedical Materials Research. Part A*. 2020;108(11):2240–2250. doi:10.1002/jbm.a.36982
- Zheng K, Fan Y, Torre E, Balasubramanian P, Taccardi N, Cassinelli C, Morra M, Iviglia G, Boccaccini AR. Incorporation of Boron in Mesoporous Bioactive Glass Nanoparticles Reduces Inflammatory Response and Delays Osteogenic Differentiation. *Particle & Particle Systems Characterization*. 2020;37(7):2000054. doi:10.1002/ppsc.202000054
- Rahmati M, Mozafari M. Selective Contribution of Bioactive Glasses to Molecular and Cellular Pathways. *ACS biomaterials science & engineering*. 2020;6(1):4–20. doi:10.1021/acsbomaterials.8b01078

III. FUNCTIONAL HYDROGEL BIOINK MODIFIED WITH BOROPHOSPHATE GLASSES

Bradley A. Bromet^a, Krishna Kolan^b, Rebekah L. Blatt^c, Richard K. Brow^c, Julie A. Semon^a

^a Department of Biological Sciences, Missouri University of Science and Technology, Rolla, MO, USA

^b Department of Mechanical Engineering, Missouri University of Science and Technology, Rolla, MO, USA

^c Department of Material Science and Engineering, Missouri University of Science and Technology, Rolla, MO, USA

ABSTRACT

In summary, we have developed a bioink system that can be used to print scaffolds for biomedical applications. The ink has rheological properties suitable for extrusion-based printing techniques and adipose stem cells infused in the ink remain viable seven days after printing. The ink consists of a mixture of alginate hydrogels, which provides the structural integrity of the printed scaffolds, and gelatin hydrogels, which supports cell proliferation. Borophosphate glass particles are added to the hydrogel mixture where they release Ca-ions that control the viscoelastic properties of the gel before and after printing. Glasses, like X40, that release Ca-ions without creating local alkaline conditions promote significantly better ASC viability than the more basic glasses. It is anticipated that these “pH neutral” glasses could be doped with other ions that promote specific responses from the stem cells or surrounding tissues when such scaffolds are implanted in animals.

Keywords: bioactive glass, bioprinting, borophosphate, adipose stem cells, MSCs.

1. INTRODUCTION

Three-dimensional (3D) printing techniques are used to produce bio-engineered structures for biomedical applications. The materials used to print these scaffolds, the bioinks, should possess rheological properties that allow efficient printing of structures that maintain desired forms and functions. The bioinks should be made from non-toxic materials that can be resorbed by the body and that support the proliferation of stem cells added to the inks to promote tissue regeneration.

Alginate-based hydrogels have been used with extrusion techniques to print 3D structures[1]. Alginate has the requisite non-toxicity and bio-compatibility properties required for biomedical applications and these hydrogels have the rheological properties for efficient printing. To maintain the structural integrity of printed structures, alginate gels must be cross-linked with divalent ions, like calcium. In addition, alginate hydrogels do not support cell proliferation and so they are mixed with hydrogels that have arginine-glycine-aspartate (RGD) peptides and amide groups such as gelatin, fibrin, etc. to produce a mixed hydrogel base ink that support cell proliferation and can then be infused with stem cells intended to regenerate desired tissue[1]. The desired rheological properties required to print Alg-Gel bioinks are typically achieved by ionic solvents which can also affect the viability of encapsulated stem cells added to the bioinks to promote tissue regeneration[2].

Bioactive glasses, including the borate-based 13-93B3, have been shown to promote wound healing, although the mechanism for soft-tissue regeneration is not well-understood[3]. Conventional borate and silicate bio-active glasses create local alkaline conditions when they react in aqueous solutions[4]. The “pH shock” associated with the rapid release of alkali ions creates conditions that are often detrimental to cell proliferation[5], particularly under static in vitro conditions, although cell proliferation is enhanced under dynamic in vitro conditions[6]. Bioactive silicate glass particles (1wt%) have been added to Alg-Gel bioinks infused with osteogenic cells and were found to reduce cell viability compared to bioinks without the bioactive glass[7]. Recently, 13-93B3 glass particles were added to Alg-Gel bioink systems and infused with adipose stem cells (ASCs) before printing, but again, cell viability was reduced compared with bioinks that contained no glass[8].

2. METHODS

2.1. GLASS PREPARATION

Glasses with the nominal molar composition $16\text{Na}_2\text{O}-24\text{CaO}-\text{XB}_2\text{O}_3-(60-\text{X})\text{P}_2\text{O}_5$ (mol%) were produced, where $X = 0, 20, 40,$ and 60 (Table 1). The borate bioactive glass 1393-B3 (B3)[9], with the nominal composition $6\text{Na}_2\text{O}, 12\text{K}_2\text{O}, 5\text{MgO}, 20\text{CaO}, 4\text{P}_2\text{O}_5,$ $53\text{B}_2\text{O}_2$ (wt%), was also produced. Reagent grade batch materials were calcined at 300°C for at least 4 hours and then melted for an hour in platinum crucibles at $1000-1150^\circ\text{C}$, depending on composition. Melts were stirred on the half hour with a platinum rod, then quenched in graphite molds. Samples were annealed at 350°C for one hour then allowed

to cool to room temperature and stored in a vacuum desiccator until use. Glasses were analyzed by x-ray diffraction, using a PANalytical X'Pert Multipurpose diffractometer with a Cu K- α source and a PIXcel detector, and all compositions were found to be amorphous.

Table 1. Bioactive glass compositions. Nominal compositions in mol% of the glasses used in this study.

Bioactive Glass	SiO ₂	Na ₂ O	K ₂ O	MgO	CaO	P ₂ O ₅	B ₂ O ₃
13-93B3	0	6.0	12.0	5.0	20.0	4.0	53.0
X0	0	16	0	0	24	60	0
X20	0	16	0	0	24	40	20
X40	0	16	0	0	24	20	40
X60	0	16	0	0	24	0	60

2.2. HYDROGEL PREPARATION

Gelatin (Type B, Sigma-Aldrich, St. Louis, MO, USA), alginate (Sigma-Aldrich, St. Louis, MO, USA), and bioactive glass powders were UV sterilized for 5 min before gel preparation. Gelatin in 3wt/vol% (0.3g in 10mL) was dissolved in Dulbecco's Modified Eagle Medium (DMEM) (Gibco, ThermoFisher Scientific, MA, USA) in a glass beaker at ~40°C while being magnetically stirred at 200RPM. Upon gelatin dissolution, glass, (10wt% of hydrogel material) was added to the gelatin solution and stirred to obtain uniform suspension of glass particles. Sodium alginate was added to the solution and mixed overnight to prepare the gelatin-alginate hydrogel. The hydrogel was

transferred to 3mL Loctite® Henkel syringe barrel, centrifuged to remove air pockets, and attached with 25G (100 μ m) tips (SmoothFlow Tapered, Nordson EFD, Westlake, OH, USA) for fabrication.

2.3. CHEMICAL TESTING

Glass particles (75-150 microns) in the amount of 150 ± 1 mg was sealed in nylon mesh bags with 45 μ m openings, then immersed in 50ml of either deionized water or cell culture media contained in high density polyethylene centrifuge tubes in a shaker bath at 37°C. The bags were removed after 24 hours, dried and weighed, and the solution pH was measured. Glass dissolution and ion concentrations in the dissolution solutions were analyzed using Inductively Coupled Plasma – Optical Emission Spectroscopy (ICP-OES), using a Perkin-Elmer Avio 200. These pH and ion concentration measurements were done in triplicate and the average values are reported with their respective standard deviations.

2.4. MECHANICAL TESTING

For rheological characterization, hydrogels were prepared in DI water with gelatin (3 w/v %), alginate (3 w/v %), AG (6 w/v %), and with addition of borophosphate glasses in varying concentrations. AG hydrogels with and without glass were tested for viscosity using a Kinexus rheometer (Malvern Panalytical, Westborough, MA, USA) with a parallel plate set-up. A gap of 0.5mm was set between plates and measurements were conducted at room temperature. Hydrogels were subjected to increasing shear rates from 0.01 to 1000 s⁻¹. A fresh scoop of gel was loaded each time to test viscosity, recovery, yield strength, etc. Data points below 0.01 s⁻¹ shear rate were not reported because of the

instability at low shear rates. Although one set of data is reported for each gel type, measurements were repeated to confirm the validity of the data.

2.5. MICROSTRUCTURE OBSERVATION

A cross section of the hydrogel was observed using scanning electron microscopy (SEM). Samples were extruded by 10ml syringe on a microslip with a size around 2mm diameter and 1cm in length. Samples were imaged post extrusion, post -20C, post freeze dry, and post SEM by a digital single-lens reflex camera (DSLR) (Nikon D5500 with an AF-S DX Micro NIKKOR 40mm f/2.8G lens, Nikon Inc, USA) Dorsal and lateral images were taken of four samples per group. For environmental SEM preparation, samples were put in a -20C freezer for 24hrs after printing / crosslinking, then put in a FreeZone 2.5 Liter -50C Benchtop Freeze Dryers (Labconco, Kansas City, MO) for 24hrs. After warming to room temperature, samples were taken to the Advanced Materials Characterization Laboratory (MS&T, Rolla, MO) and broken in half (LN₂ was used to help break AlgGel crosslinked sample) and a PrismaE SEM (Thermo Fisher Scientific Inc.) was used to analyze the interior cross section of each sample.

2.6. CELL CULTURE

ASCs were prepared by thawing frozen vials of approximately 1×10^6 cells (Obatala Sciences, LLC, New Orleans, LA) into 150cm² culture plates (Nunc, Rochester, NY) in 20ml complete culture media (CCM) consisting of alpha minimum essential media (α -MEM; Sigma; St. Louis, MO), 10% fetal bovine serum (FBS; VWR, Dixon, CA), 1% 100x L-glutamine (Sigma), and 1% 100x antibiotic/antimycotic (Sigma). After 24 hours incubation at 37°C humidified and 5% CO₂, media was removed and the

adherent, viable cells were washed twice with phosphate buffer solution (PBS; Sigma) and harvested using 0.25% trypsin/1mM Ethylenediaminetetraacetic acid (EDTA; Sigma). ASCs then were plated at 100 cells/cm² in CCM. The media was changed every 3–4 days and sub-confluent cells ($\leq 70\%$ confluent) from three separate donors between passages 2-6 were used for all experiments.

2.7. SCAFFOLD FABRICATION

ASCs were added to the hydrogel ink after alginate had finished mixing. 4×10^6 ASCs pellet was re-suspended in 0.2mL CCM and pipetted into AG hydrogel and magnetically stirred for no more than 3 min to obtain a uniform cell distribution and a final ASC concentration of 1×10^6 cells per 1mL of bioink. The bioink is then transferred to the 3ml syringes and made ready for bioprinting. A custom-modified tabletop cartesian 3D printer to include syringes connected through digital syringe dispenser (Loctite®, Rocky Hill, CT, USA) was used to fabricate scaffolds. Scaffold dimensions were set to 15mm length, 15mm width and ~ 1mm thick (6 layers) and printed with 0-90° filament orientation in alternate layers. Customized software was written for g-code generation and syringe dispenser control. Sterile practices were followed for scaffold fabrication with ASCs, bioink syringes were maintained at room temperature, and the scaffolds were bioprinted in less than an hour inside the laminar flow hood.

2.8. CELL VIABILITY

Cell viability was evaluated using a Live/Dead kit (ThermoFisher Scientific Inc., USA), according to the manufacturer's protocol. Scaffolds were washed with PBS and soaked in 1mL of prepared reagent (Calcein AM to stain live cells green and Ethidium

homodimer-1 to stain dead cells red) for 30min at room temperature. Micrographs were taken with 10x objective on a Nikon A1R-HD Eclipse Ti2 inverted confocal microscope (Nikon Instruments Inc., USA). Three scaffolds were examined per experimental group and images were taken covering an area of 6x6mm² of the full scaffold thickness. A Z-step thickness of 40µm was used during image acquisition. One maximum intensity projection image of multiple Z-step images was used for quantification. Cell viability was calculated as $[\text{live cells} / (\text{live cells} + \text{dead cells})] \times 100\%$. Live/Dead images were quantified using Fiji ImageJ software.

2.9. STATISTICAL ANALYSIS

5 samples in each set were used for rheology tests and three samples in each set were used for cell viability quantification. The results were reported as average \pm standard deviation. Minitab® software was used to analyze the difference in means of different groups using One-way ANOVA. The means were considered significantly different if the P-value is less than 0.05.

3. RESULTS

3.1. PH CHANGE, GLASS DISSOLUTION, AND ION RELEASE

Figure 1 shows the effect of borophosphate glasses effect on solution pH in DI water. There is a clear trend as phosphate rich glasses, X20 & X0, produce more acidic solutions and borate rich glasses, X40 & X60 produce more basic solutions (although X40 is more pH-neutral than basic. This corresponds to the dissolution rate at which Ca²⁺ is released from the glasses (X20 < X0 < X40 < X60). The pH change in

surrounding media of varying wt% of hydrogel with BPBGs at 1 and 7 days is displayed in Figure 2. Gels with lower concentrations of glass with a higher amount of phosphate stayed around the same acidic pH values in the buffered SBF (~6) through day 7.

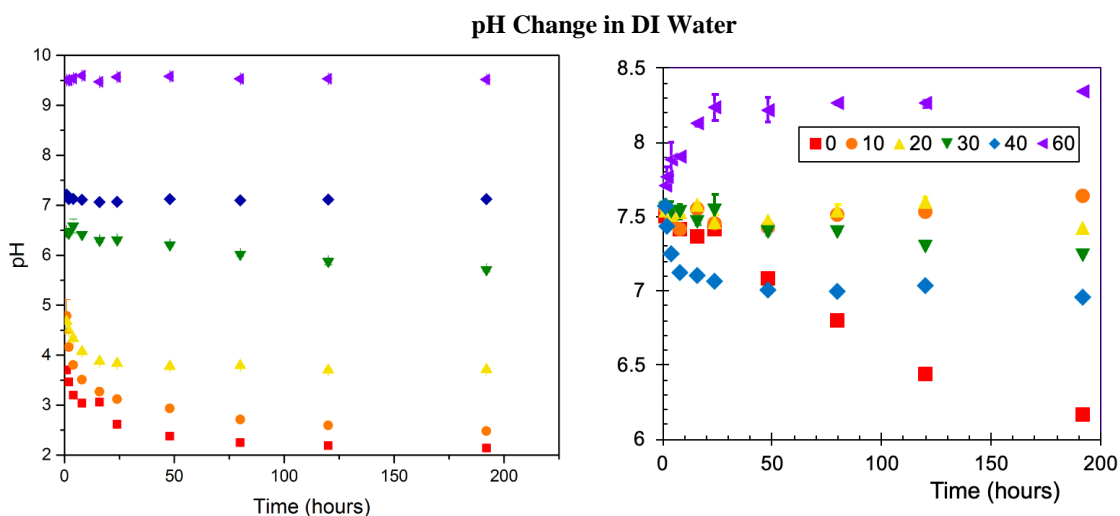


Figure 1. pH shifts for borophosphate glasses dissolved in water after more than 8 days. The boron content in borophosphate glass series is varied to control the dissolution rate of glasses and thereby pH.

However, the trend is disrupted at 10wt% where X0 has the lowest pH values measured and continues to decrease at Day 7 while X20's pH increases over time. X40 continued to stay pH-neutral, even though it had a higher borate content, which is consistent with prior research. The pH increase is significant for the basic borate glass (X60 glass) at 2wt%. Any pH approaching 8 is too basic for cells and will have a negative effect on cell viability. Gels with 10wt% X60 glass proved too difficult to print with as X60 dissolves too fast and did not produce a uniform gel needed for printing (which is why X60 is not included).

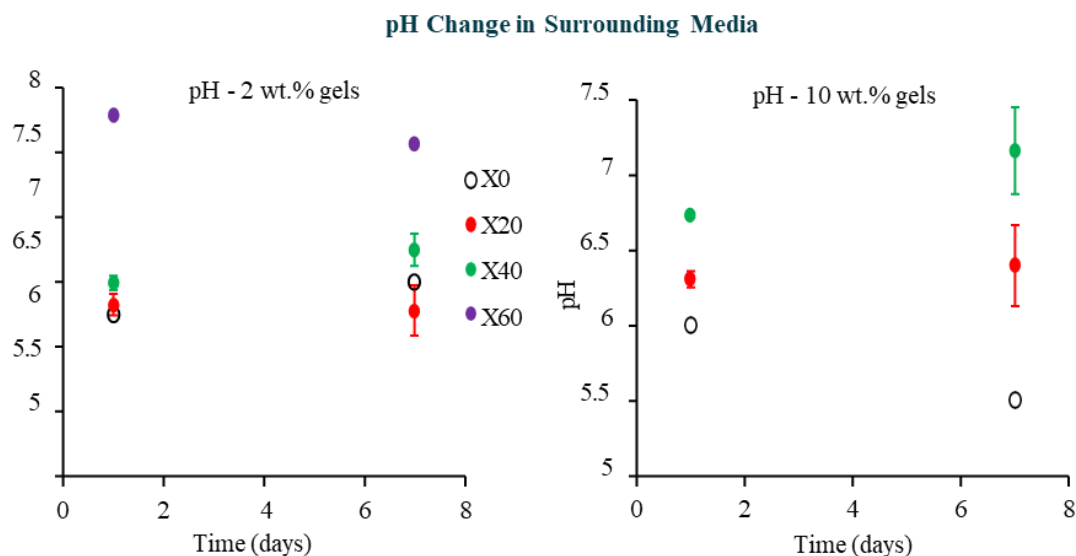


Figure 2. pH change of gels with differing wt% glass in SBF at 1 and 7 days. The dissolution trend is followed in at low concentrations, but not at higher glass wt% where X0 has the lowest pH for both time points.

The ion release rates of Na, Ca, B, and P at days 1 and 7 days (Figure 3) for the hydrogel doped with X20, X40, and X60 and compared to 13-93B3 at concentrations of 1.25, 2.5, 5, and 10wt% show most of the glass groups and concentrations follow the trend of increased release of each ion over time. Only X40, which follows that trend for 1.25 and 2.5wt%, but at 5 and 10wt% suddenly has a decrease in release for each ion. X40 also has a larger difference between day 1 and 7 samples for Na and Ca, especially at 2.5wt% there the largest change of about ~40ppm for Na. 13-93B3 releases the most Ca overall for any glass concentration but does not have a large change between time points. X20 does not have much of a difference in ion release between 1 and 7 days for each concentration due to its slow-release dissolution rate. While X60 behaves like 13-93B3 at lower concentrations, but 5 and 10wt% leases less Ca and more Na.

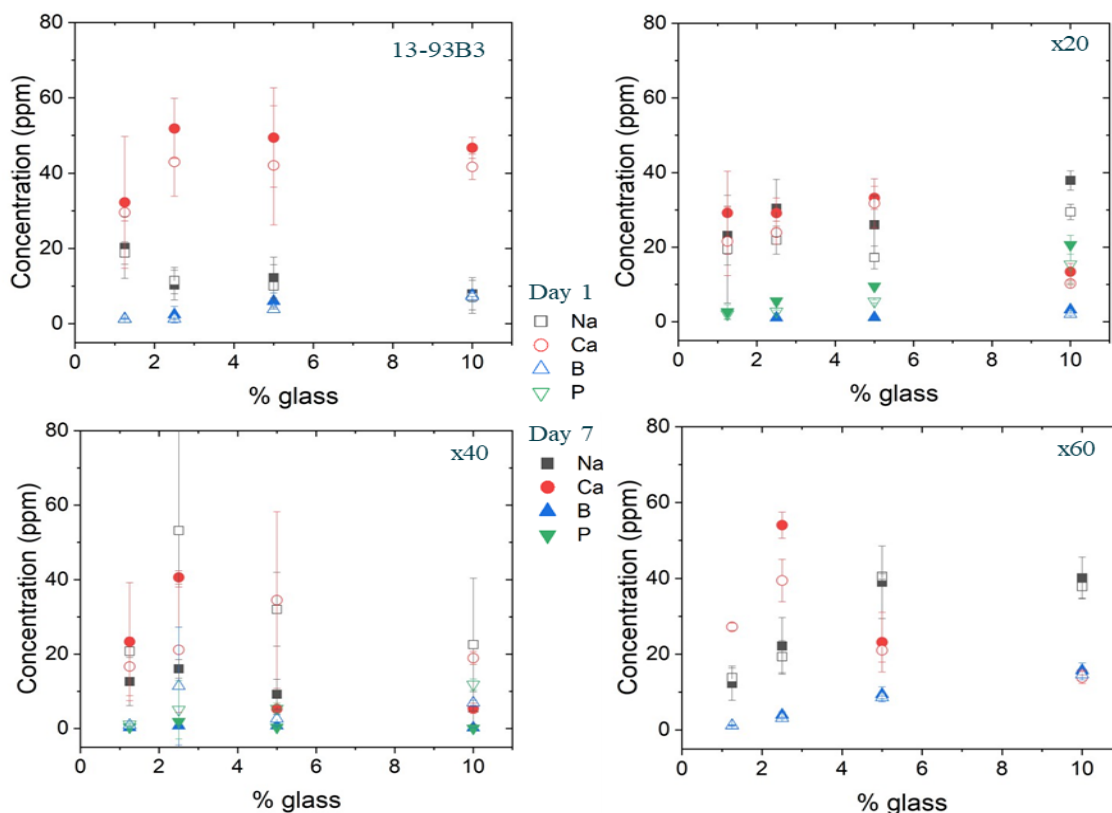


Figure 3. Ion release rates for the major elements that compose each glass type. The release rates are detected in doped gels at 1 and 7 days at concentrations of 1.25, 2.5, 5, and 10wt%. Most glasses follow a trend of increased ion release from day 1 to day 7.

For the dissolution rates of the gel by itself or with the X series glasses by release of Ca and P in 2 and 10wt% gels at days 1 and 7 (Figure 4), in the group with no glass, there is an upward trend in Ca release from 1 to 7 days at both concentrations. This could be due to alginate dissolving and/or gelatin being released from the samples. For the rest of the glasses, XO has the highest release of Ca and P in every scenario, which is different from what is expected, and another surprising discovery is that there is an upward trend for over time in 10wt% gels for all glasses (except X60, which does not contain any P). The dissolution trend of $X20 < X0 < X40 < X60$ mostly behaves as expected, where the fast-reacting glasses have higher a decrease between Days 1 and Day

7, since these glasses release more ions quicker compared to X20 which has a slower release profile. Our earlier research has shown that in SBF, X20 dissolves about 30 times slower than X0, which dissolves about 10 times slower than X40, and X40 dissolves about half as fast as X60 [Bromet, et al., 2022 (edits submitted)].

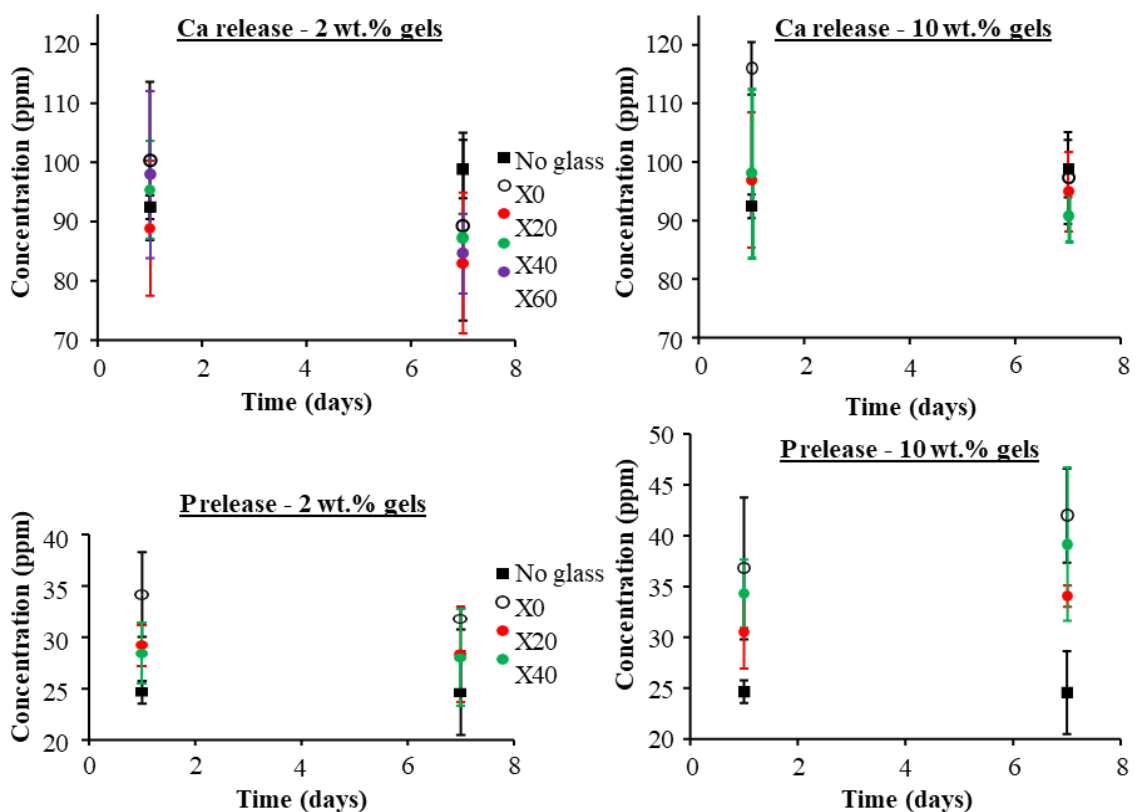


Figure 4. Glass dissolution rates for borophosphate glasses with Ca and P ion release profile at 1 and 7 days.

An additional benefit of alginate cross-linking by the controlled release of Ca-ions from the borophosphate glasses was the reduced rate at which gelatin was released from the printed scaffolds (data not shown). The gelatin-fractions from undoped scaffolds dissolved in a matter of hours in water, whereas little gelatin was released from hydrogels

doped with 5 and 10wt% X40 samples. The gelatin-fractions from undoped scaffolds dissolved in a matter of hours in water, whereas little gelatin was released from hydrogels doped with 5 and 10wt% X40 samples.

3.2. VISCOELASTIC BEHAVIOR OF BOROPHOSPHATE GLASSES

An ideal bioink should demonstrate two properties to guarantee high shape fidelity and printing accuracy: 1) the ability to exhibit a shear-thinning behavior upon the application of a deforming force (Figure 5); and 2) the ability to exhibit a rapid increase in viscosity after the removal of a force (Figure 6)[10]. In water and in SBF the dissolution rates of these new glasses increase in the order X20<X0<X40<X60. In Figure 5, when 10wt% glass particles were added to an Alg-Gel mixture, the viscosity of this composite gel increased in the same order, from about 25Pa.s (shear rate of 1 s^{-1}) for the X20 glass to 2000Pa.s for the X60 glass. Clearly, increasing the rate at which Ca-ions are released to the hydrogel increased the extent of cross-linking of the alginate, and so increased the viscosity of the gel. Similar behavior was noted for the addition of 13-93B3 to an Alg-Gel bioink[8], and the addition of bioactive silicate glass particles to Alg-Gel[7].

Figure 6 indicates that the hydrogels doped with borophosphate glass particles possess the shear-thinning viscoelastic properties desired for printing- low viscosity under the high shear-rates associated with printing, then high viscosity when the shearing conditions were removed. This means that structures that are printed under the high-shear rate conditions are retained. A key parameter is the time required for the high viscosity to recover after shearing.

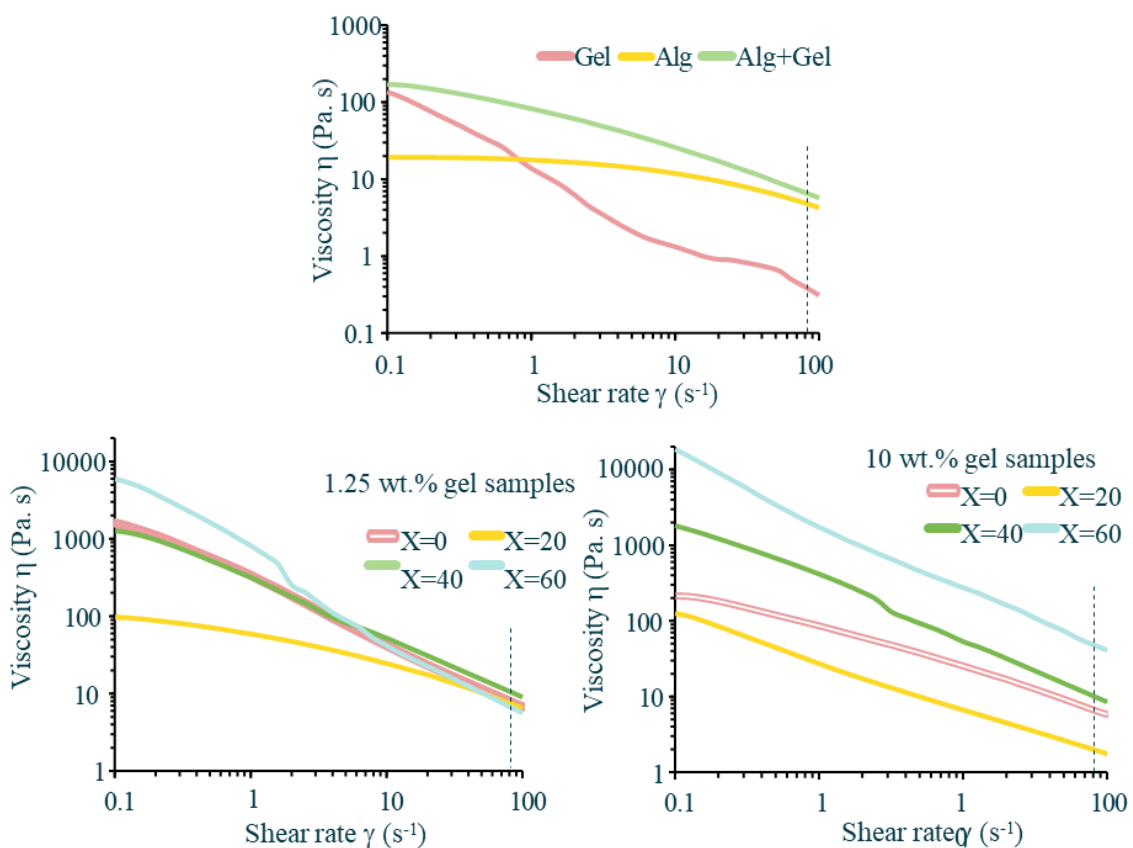


Figure 5. Shear rate dependence of alginate-gelatin hydrogels doped with and without BPBG particles. The flow behavior of the hydrogel + glass, where viscosity is a function of shear rate. This is important because it shows how gel behaves for printing purposes, as the air pressure needed, and the tips (25GA) used have a shear rate around 80 (indicated by the dotted line).

Long recovery times mean that after printing, a structure will continue to flow, losing resolution and integrity. In Figure 6, gels doped with X0 and X20 glasses behaved like undoped gels; their long recovery times (60 and 90 seconds, respectively) made it difficult to build 3D structures with the desired resolution (Figure 5, left and middle). The viscosities of gels doped with X40 and X60 glasses, on the other hand, recovered almost immediately after shearing, and so could be used to print structures with better resolution (Figure 5, right).

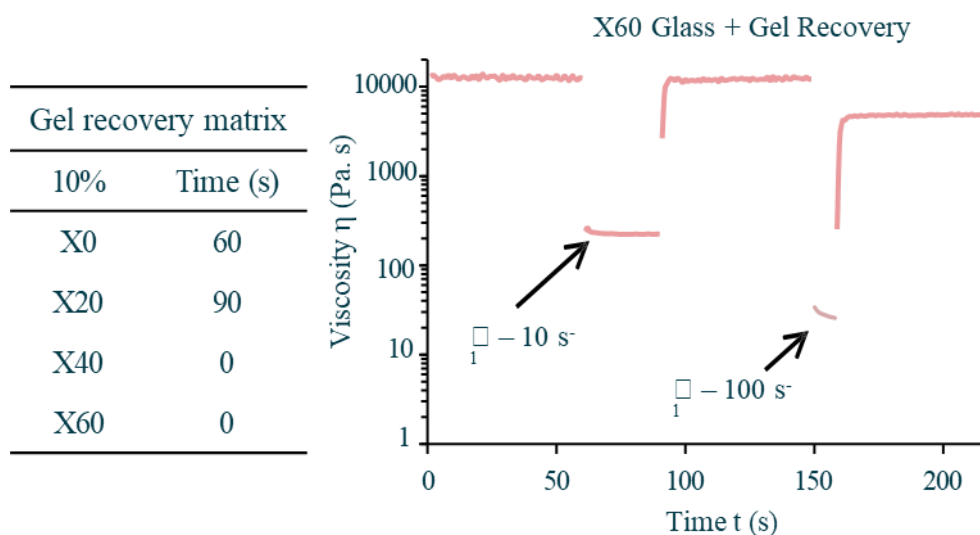


Figure 6. Hydrogel recovery with borophosphate glasses. Recovery time is directly related to glass dissolution rate and likely Ca^{2+} ion release. Gels made with X60 glass and 10% X40 glass had “zero” recovery time. Recovery is related to how filament behaves after printing, X40 & X60 make an instant filament, while X20 & take much longer to recover, 60 and 90 secs respectively.

Other rheological methods that have bioprinting implications are oscillatory tests which characterize the viscoelastic features of hydrogel inks. In Figure 7, the viscous modulus (G'') and the elastic modulus (G') are determined, where G'' is used to describe how the ink passes through a tip and G' is linked to precision during printing and the shape fidelity post printing[11]. The different graphs indicate that only gelatin shows viscoelastic behavior until about 200 shear strain, while alginate and AlgGel samples only exhibit viscous behavior over the shear strain range. Even though gelatin is viscoelastic, the pressure needed is extremely low compared to the other two groups, this results in an inability to retain filament shape post print. Elastic properties are able to influence the extrusion pressure of our hydrogel ink and is co-determined by G' and G'' [11].

Figure 8 shows the elastic or viscous behavior of the hydrogel with the different BPBGs. Only X40 and X60 displayed viscoelastic behavior, where X40 has elastic characteristics until about 200 shear strain and X60 over 300 shear strain, while X20 and X0 displayed viscous behavior comparable to alginate and alginate gelatin gels respectively. These results also correspond to the glass dissolution rate of the borophosphate glasses. Although viscosity, which is usually considered the primary physicochemical parameter that affects print quality, itself does not reflect how complex the behavior of hydrogels is during the 3D printing process[12].

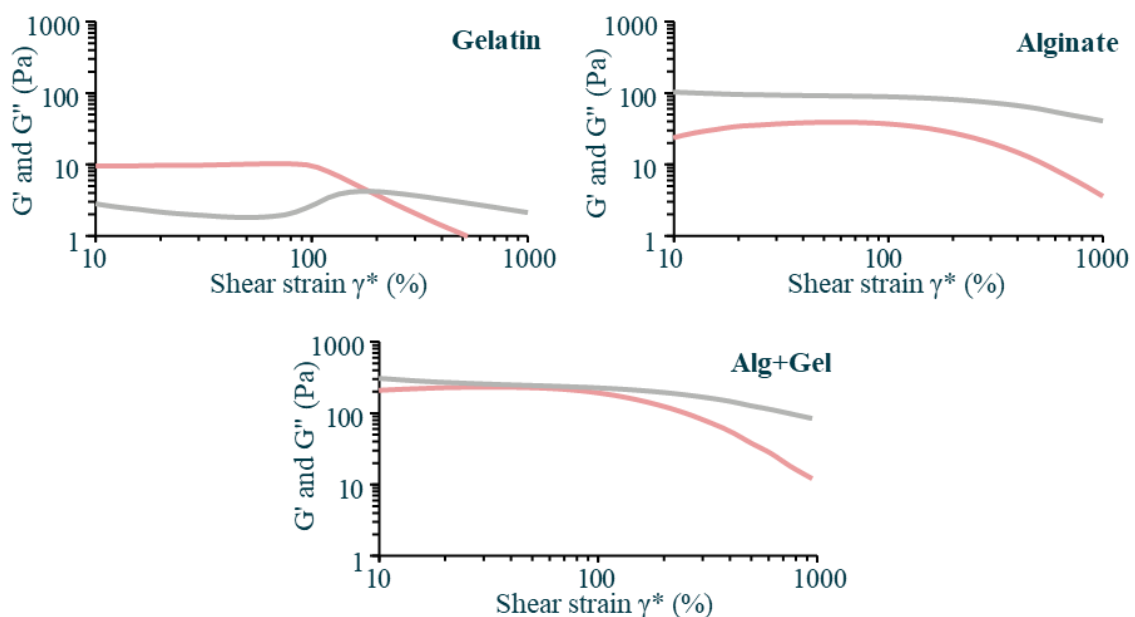


Figure 7. Elastic & viscous modulus of the different components of the hydrogel. The ratio of G' (red) and G'' (grey) represent the different behaviors, which are: elastic ($G' > G''$), viscous ($G'' > G'$), and viscoelastic is when elastic behavior transitions to viscous.

Only Gelatin has viscoelastic behavior while Alginate and Alg-Gel show viscous behavior over shear strain range.

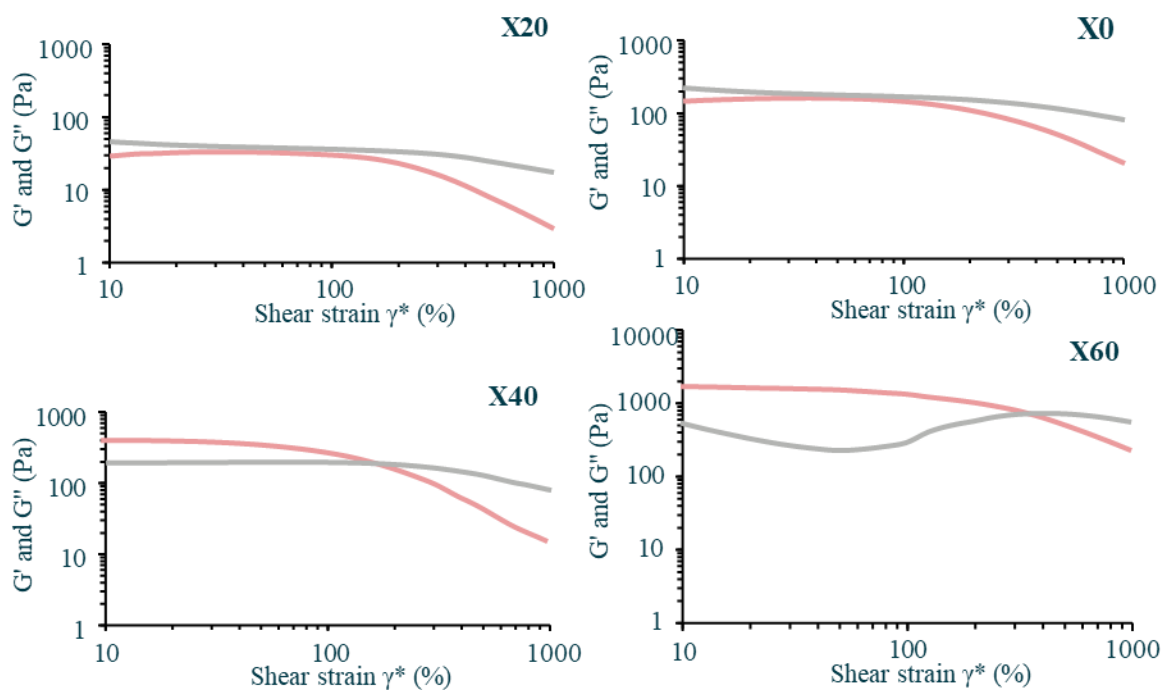


Figure 8. Elastic & viscous modulus of the different glass compositions. Both X40 and X60 exhibit viscoelastic behavior, meanwhile X0 and X20 behave like the base hydrogel and only show viscous behavior.

3.3. COMPARISON OF X40 AND CROSSLINKING ON HYDROGEL MICROSTRUCTURE

To look at the microstructure of the base hydrogel plus X40 glass, the samples were put in a -20C freezer for 24hours and then Freeze dried at -50C for another 24 hours and then imaged by SEM. During the SEM preparation, we decided to see how the different glass affected the hydrogel shape during the process. In Figure 9, close-view photographs were taken to compare post mixing to post freeze dried shape. Both groups with X40 were able to retain their shape under the pressure of the vacuum during freeze drying, while both groups without glass collapsed.

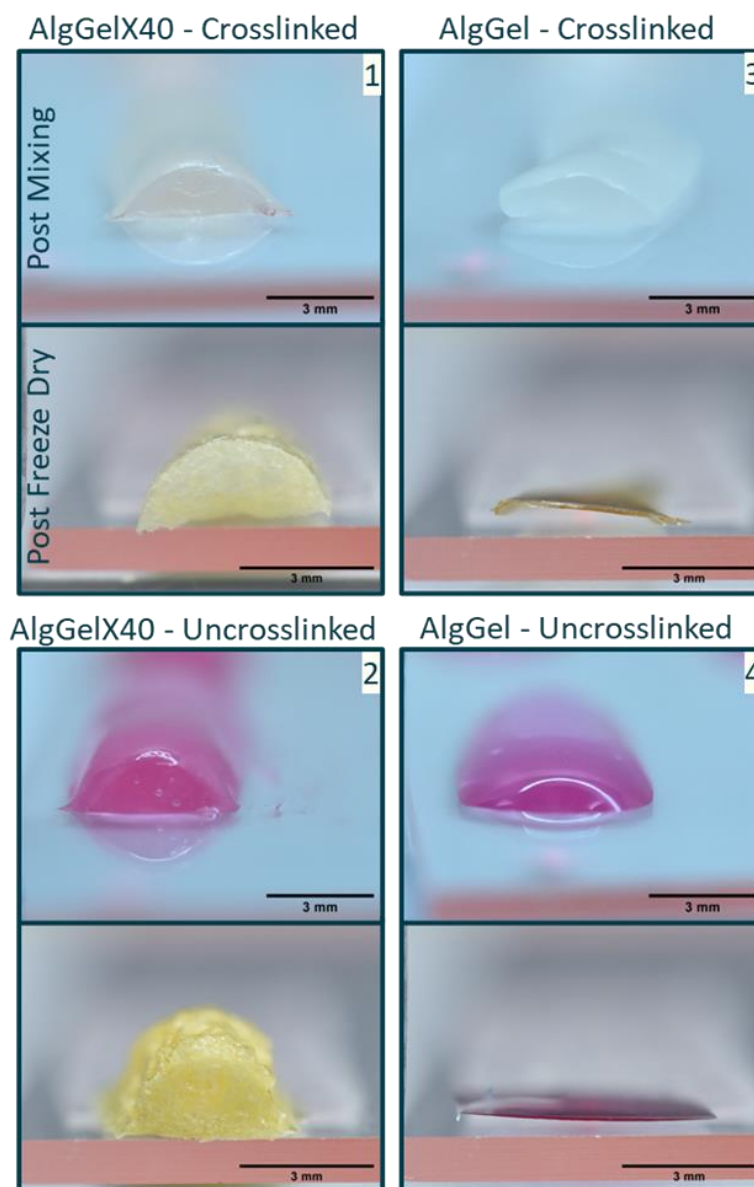


Figure 9. Internal cross section of hydrogels with and without crosslinker or X40 glass. Close-view photographs were taken either post mixing / crosslinking and compared to post freeze-dried samples. The addition of glass is clearly seen to allow samples 1 and 2 to keep their shape, while samples 3 and 4 lost their shape.

SEM images of the hydrogel with and without X40 or crosslinked by CaCl_2 , shown in Figure 10, indicate that glass influences the microstructure of the hydrogel during freeze drying. Only AlgGel samples with X40 (1 & 2) still retained their shape

after freeze drying and had a microstructure with cells, but only sample 1 that was crosslinked had any visible pores. Meanwhile samples 3 & 4, which did not contain glass, collapsed with no visible microstructure, which is a little surprising for AlgGel crosslinked by CaCl_2 .

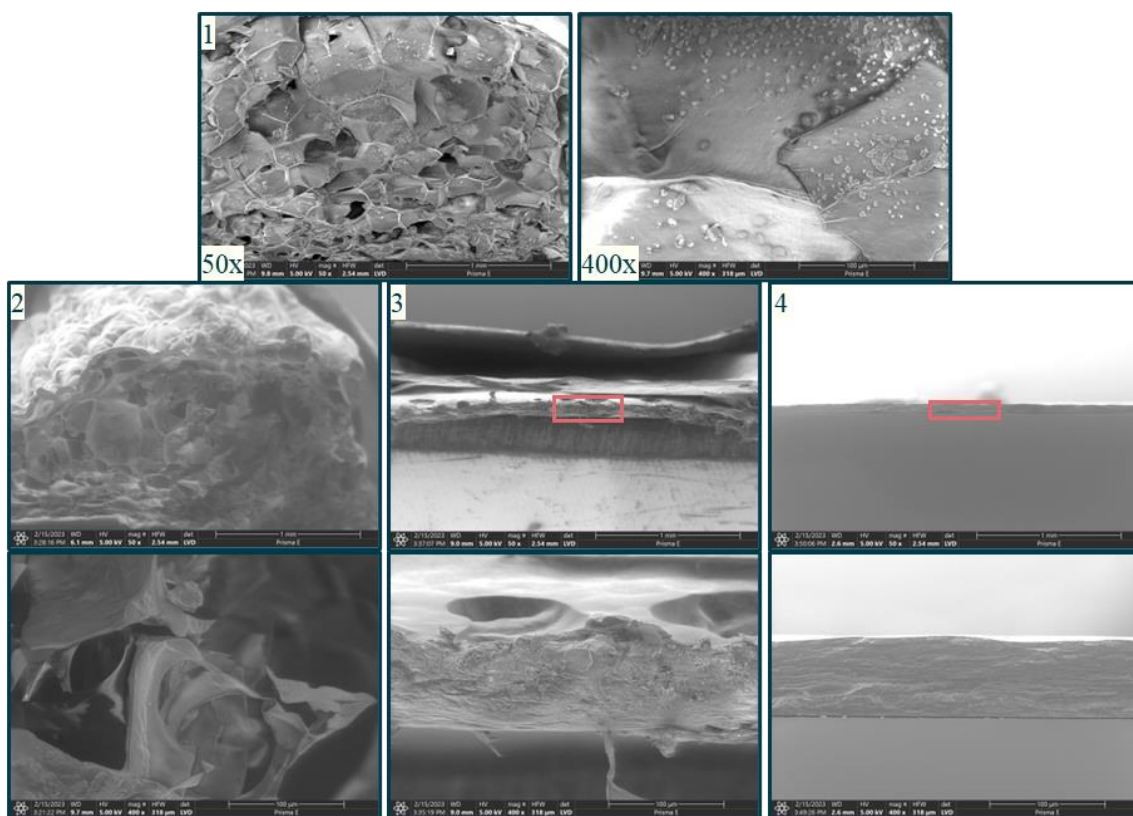


Figure 10. Microstructure of alginate-gelatin \pm X40 with and without crosslinker by Environmental SEM at 50x and 400x magnification. Only crosslinked AlgGel + X40 is seen to have any real microstructure or pores. Both crosslinked (1) and uncrosslinked (2) AlgGel + X40 have retained their structure while both AlgGel samples (3 and 4) did not. The pink rectangle indicates the sample in 50x magnification.

3.4. CELL VIABILITY WITH BIOINK AND GLASS

Scaffold fabricated with hydrogel containing BPBGs were printed to observe the printability of each glass type in Figure 11. X40 and X60 displayed good printability as

seen by square pores and mostly constant filament size. The printability of X20 on the other hand was poor in comparison. The ink did not retain its shape post print and caused the pores to become unregular circles and there is no clear filament see. This corresponds to the results from the rheology tests where X40 and X60 and instant gel recovery and higher viscosity during shear stress. The dwell time for each scaffold was adjusted based on the gel recovery.

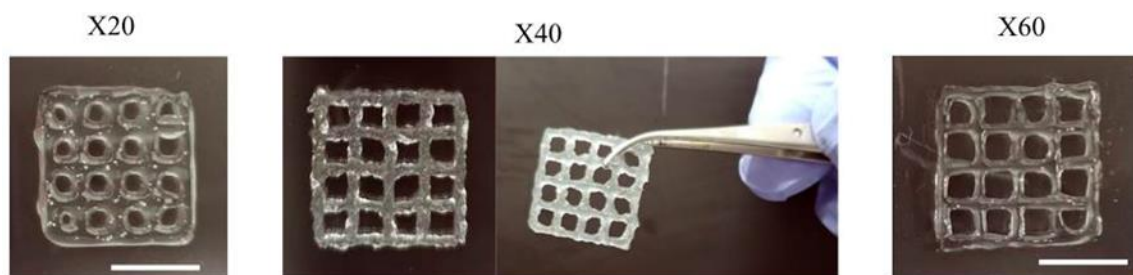


Figure 11. Scaffold fabrication using borophosphate glasses. Grid scaffolds printed from hydrogels doped with X20 glass particles (left), X40 glass particles (middle), and X60 glass particles (right). Gels modified with X40 and X60 provided good printability, while gels with X0 and X20 glasses behaved like base hydrogel.

Gels doped with 10wt% of these new borophosphate glasses were infused with ASCs and cell populations were determined, using a live-dead assay, immediately after printing, then after one and seven days. Figure 12 shows the live and dead cells in representative gel samples doped with 10wt% X0, X20, X40 and X60 glasses. Here, a greater percentage of dead cells (bottom row) were observed in gels doped with X20 and X60 glasses, whereas few dead cells were found with the gel samples prepared with X40 glass.

The quantitative cell viability analyses are summarized in Figure 13. Over 80% of the ASCs in gels doped with acidic (X0, X20) and pH neutral (X40) glasses remained

viable after printing, whereas only 60% of the ASCs remained viable in gels doped with alkaline (X60) glass. After seven days, over 90% of the cells remained viable in gels doped with X0 and X40. This compared favorably with the undoped gels, where 75% of the cells were viable after seven days and the X60 glasses, where only 65% of the cells remained viable.

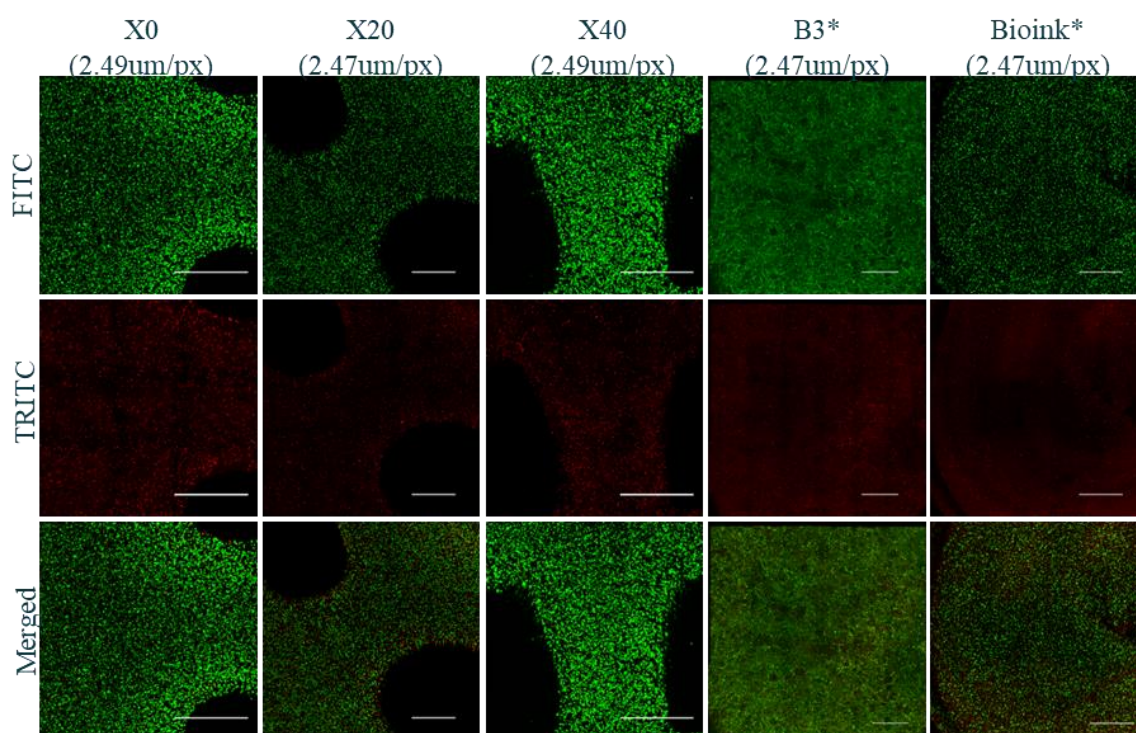


Figure 12. Cell viability after 7 days in static culture for scaffolds printed with hydrogels doped with different borophosphate glasses. Green dots represent live cells and red dots represent dead cells. Images in the Top and middle rows are separated into green (live cells) and red channel (dead cells) images showing only that color of cells. Color images in the bottom row show both live and dead cells.

It is worth noting that cell viability with several of the 10wt% borophosphate glasses after seven days was statistically greater than for the undoped Alg-Gel system, indicating that the glasses indeed promoted cell viability. Our results for the alkaline X60

glasses are consistent with those reported in the literature; viz., as little as 1wt% loading of an alkaline bioactive silicate glass was reported to be sufficient to reduce cell viability in an Alg-Gel bioink[7], as did 2.5wt% of the alkaline bioactive borate glass 13-93B3[8].

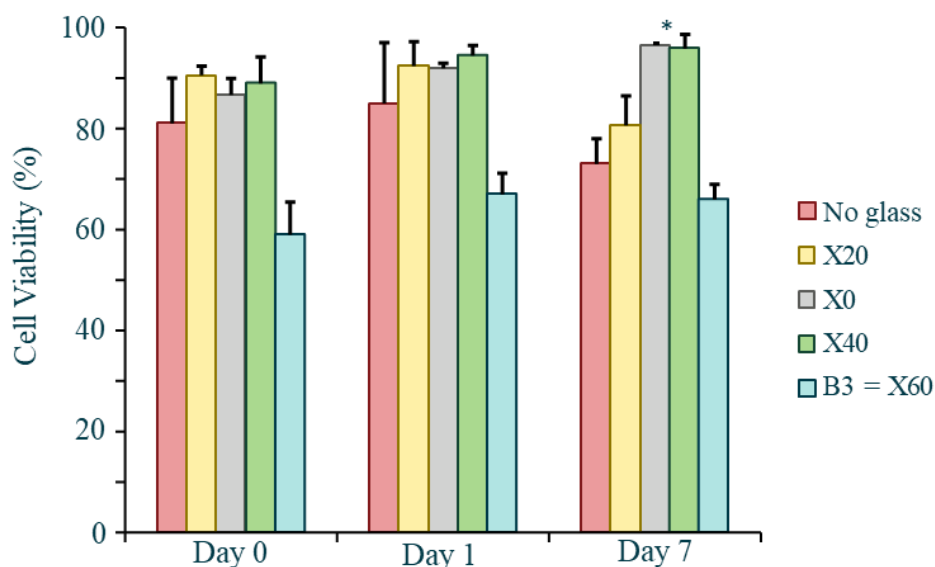


Figure 13. Cell viability measurements for scaffolds printed with undoped hydrogels and hydrogels doped with borophosphate glasses. Measurements were taken immediately after printing, then one and seven days after printing. The fast release of boron ions proved toxic to cells, while pH neutral X40 glass provided an excellent environment for cells because of its controlled ion release. X0 also provided a good environment despite its low pH.

4. DISCUSSION

The incorporation of pH neutral glass particles into an Alg-Gel system creates a novel bioink, one in which the borophosphate glass particles release desired ionic species that stimulate desired cellular responses and that control the bioink viscosity to optimize printing. Alginate normally needs to be pre crosslinked, in-situ cross-linked or

crosslinked immediately after 3D printing. The advantage of our formulations is that the borophosphate glass particles do not induce the “pH shock” effect that has been shown to be detrimental to cell viability in other bioink formulations.

This novel functional pH neutral bioink can be used to fabricate human tissue scaffolds and has the potential in the clinic to repair and replace damaged or diseased tissue. It also has the potential to be used by many researchers in the ever-growing field of human organoid development, which creates novel and improved models of human tissues and organs for drug development, disease modeling, and basic cellular and molecular studies. By using our novel bioink to fabricate human tissues, this invention would be of interest to clinicians and scientists who study cancer, immunology, aging, diabetes, regenerative medicine, as well as many other fields.

REFERENCES

- You F, Eames BF, Chen X. Application of Extrusion-Based Hydrogel Bioprinting for Cartilage Tissue Engineering. *Int J Mol Sci*. 2017 Jul;18(7):1597.
- Li Z, Huang S, Liu Y, Yao B, Hu T, Shi H, et al. Tuning Alginate-Gelatin Bioink Properties by Varying Solvent and Their Impact on Stem Cell Behavior. *Sci Rep*. 2018 May 22;8(1):8020.
- Zhao S, Li L, Wang H, Zhang Y, Cheng X, Zhou N, et al. Wound dressings composed of copper-doped borate bioactive glass microfibers stimulate angiogenesis and heal full-thickness skin defects in a rodent model. *Biomaterials*. 2015 Jun 1;53:379–91.
- Fu Q, Rahaman MN, Fu H, Liu X. Silicate, borosilicate, and borate bioactive glass scaffolds with controllable degradation rate for bone tissue engineering applications. I. Preparation and in vitro degradation. *J Biomed Mater Res A*. 2010;95A(1):164–71.

- Cirraldo FE, Boccardi E, Melli V, Westhauser F, Boccaccini AR. Tackling bioactive glass excessive in vitro bioreactivity: Preconditioning approaches for cell culture tests. *Acta Biomater.* 2018 Jul 15;75:3–10.
- Yang Q, Chen S, Shi H, Xiao H, Ma Y. In vitro study of improved wound-healing effect of bioactive borate-based glass nano-/micro-fibers. *Mater Sci Eng C.* 2015 Oct 1;55:105–17.
- Ojansivu M, Rashad A, Ahlinder A, Massera J, Mishra A, Syverud K, et al. Wood-based nanocellulose and bioactive glass modified gelatin–alginate bioinks for 3D bioprinting of bone cells. *Biofabrication.* 2019 Apr;11(3):035010.
- Kolan KCR, Semon JA, Bromet B, Day DE, Leu MC. Bioprinting with human stem cells-laden alginate-gelatin bioink and bioactive glass for tissue engineering. *Int J Bioprinting* [Internet]. 2019 Jul 8 [cited 2020 May 29];5(2.2). Available from: <http://ijb.whoice.com/index.php/int-j-bioprinting/article/view/204>
- Liu X, Rahaman MN, Day DE. Conversion of melt-derived microfibrinous borate (13-93B3) and silicate (45S5) bioactive glass in a simulated body fluid. *J Mater Sci Mater Med.* 2013 Mar 1;24(3):583–95.
- Amorim PA, d'Ávila MA, Anand R, Moldenaers P, Van Puyvelde P, Bloemen V. Insights on shear rheology of inks for extrusion-based 3D bioprinting. *Bioprinting.* 2021 Jun 1;22:e00129.
- Bom S, Ribeiro R, Ribeiro HM, Santos C, Marto J. On the progress of hydrogel-based 3D printing: Correlating rheological properties with printing behaviour. *Int J Pharm.* 2022 Mar 5;615:121506.
- Gao T, Gillispie GJ, Copus JS, PR AK, Seol YJ, Atala A, et al. Optimization of gelatin–alginate composite bioink printability using rheological parameters: a systematic approach. *Biofabrication.* 2018 Jun;10(3):034106.

IV. DEVELOPMENT OF NOVEL BIOINK FOR SIZABLE ORGANOIDS VIA INNER GELATION

Bradley A. Bromet^a, Nathaniel P. Blackwell^a, Rebekah L. Blatt^b, Emily Pesselato^a, Drew Gildehaus^a, Richard K. Brow^b, Julie A. Semon^a

^a Department of Biological Sciences, Missouri University of Science and Technology, Rolla, MO, USA

^b Department of Material Science and Engineering, Missouri University of Science and Technology, Rolla, MO, USA

ABSTRACT

Together, the use of 3D cell cultures such as organoids along with better stem cell models allow for a more natural representation of cell behavior and responses that mimic natural tissues. 2D models can not accurately demonstrate natural cell behavior and animal models have species-specific differences that make interpreting and translating results into human tissues difficult. These 3D models can demonstrate how stem cell interactions in tissue constructs that more closely resemble the human microenvironment. This knowledge may also help to end any controversy in published studies from differing results due to the use of traditional models in research. Our novel bioink developed for non-traditional-sized organoids by using internal gelation. By using alginate and fibrin to create a vascularized organoid with adipose stem cells and endothelial cells and crosslinked with calcium carbonate, we can create models larger than ten millimeters squared that do not have the negative aspects from the more common methods of

crosslinking alginate. This can then be translated and applied to further invent technologies to aid in disease modeling, target identification and validation, drug discovery, drug screening and efficacy for other diseases.

1. INTRODUCTION

There is a need in preclinical studies for an improved human-like research model. The other standard method is 2D cultures, where cells do not have the same behavior as in vivo compared to a 3D tissue. The absence of the 3D environment can lead to misleading and unpredictable data that does not translate to in vivo studies[1]. The other traditional method for preclinical testing is animal models, which are the gold standard for in vivo studies and are a major reason why many drugs that pass preclinical trials fail in the clinical stage. Animal studies are not always physiologically relevant, can be expensive, and time consuming[2]. The incapability issues between animals and humans can be overcome by using human organoids as a better predictive model for drug screening and patient outcomes. There is a need for a middle ground that is physiologically relevant, but also cost-effective and easily reproducible. Another reason is the uncontroversial understanding of ASCs characteristics would help with developing new therapies for treatment. Part of the discrepancy in results may be due to how ASCs transform when taken from the body and grow under static, 2D conditions.

This issue could be solved using novel 3D tissue models. Culturing cells in dynamic, 3D conditions can be used to answer some of the contradictions in the clinic and to help in understanding how cells interact and behave in their natural environments.

These biomimetic tissue models better emulate the complex environment and functionality of human systems. Organoids, can fill that need as they are more able to mimic natural tissues that form complex organs. Organoids or 3D tissues are cultures of multiple cell types in an extracellular matrix-like gel, containing growth factors that can be precisely organized in natural arrangements. These organoids are models that can simulate in vivo microenvironments while being high-throughput, precisely organized biological structures in vitro[3]. Advantages include highly ordered regulation of environmental clues, low cost and short time of development, manipulation of multiple parameters, and the ability to be used in a wide range of analysis[4]. The major innovation of this study is the creation of a novel bioink for a 3D tissue model that more closely resembles the human hypodermis tissue, which allows for natural cell behavior and interactions. Human organoids are better predictive models for patient outcome and drug efficacy. Recently, organoids have been used successfully for drug screening and disease modeling. Human organoids are limited, however, due to the difficulties of incorporating vasculature, which we have overcome via bioprinting with our novel bioink.

The overarching hypothesis of this study is that human ASCs cultured in a 3D vascularized tissue using a novel bioink with internal crosslinking leads to a more realistic representation of cellular behavior and functions found in tissues compared to traditional 2D or animal models. We will show why clinical results aren't as promising as expected since the conditions in each preclinical and clinical test environment are vastly different and a more realistic human model is needed for preclinical trials. Organoids fabricated using our bioink can then be used as model systems to study disease states and

developmental biology. The following report details the development of the novel bioink using alginate and fibrin for bioprinting.

2. MATERIALS AND METHODS

2.1. FABRICATION OF HYDROGEL INKS

2.1.1. Fabrication of Alginate-Gelatin Hydrogel. Gelatin from bovine skin (Type B, Sigma-Aldrich, St. Louis, MO, USA) in 3wt/vol.% (0.03 g/1mL) was dissolved in DMEM/high glucose with phenol red (Hyclone, GE Healthcare Life Sciences, UT, USA). The parafilm covered glass beaker was maintained at ~40°C while being magnetically stirred @ ~200RPM. Upon gelatin dissolution, Sodium Alginate (Alg) (Alginic acid sodium salt from brown algae, medium viscosity, Sigma) in 3wt/vol.% (0.03g/1mL) was added to the solution and covered while mixed for at least 6 hours at 40°C and 60RPM to prepare the gelatin-alginate hydrogel. The AlgGel mix was then transferred to a 3mL syringe barrel, centrifuged for 30 secs at 1000RPM, then attached with 25G (100µm internal diameter) (Smooth Flow Tapered, Nordson EFD, OH, USA) tips before printing. The gelatin and alginate powders and any crosslinking agents (covered in section 1.1.3.) were UV sterilized for 10 min before gel preparation[5,6].

2.1.2. Fabrication of Alginate-Fibrinogen Hydrogel. 15, 30, 45 or 60mM CaCO₃ (BioXtra, Sigma) and 6-aminocaproic acid (ACA) [Sigma] was dissolved in DMEM (1X) without phenol red (Gibco, ThermoFisher Scientific, MA, USA). The parafilm covered glass beaker was maintained at ~40°C and magnetically stirred @ ~200RPM for 10 mins. After 10 mins, sodium alginate in 3wt/vol.% (0.03g/1mL) was

added to the solution and mixed for at least 6 hours @ 40°C and 60RPM. Fibrinogen from bovine plasma [Type I-S, 65-85% protein ($\geq 75\%$ clottable), Sigma] in 10mg/ml is laid on top of Alg solution and allowed to equilibrate in an incubator for 45 mins. The AlgFib solution is then mixed for 5 mins @ 40°C and 60RPM and allowed to rest in incubator for 15mins (fibrinogen will cause the hydrogel mix to clot/flocculate instead of gel if mixed/disturbed too vigorously). 30, 60, 90, or 120mM GDL (Sigma) is then added to the beaker, covered, and mixed for 5mins at 40°C and 60RPM (this step would be starting time of internal gelation). The AlgFib mix was then transferred to a 3mL syringe barrel, centrifuged for 30 secs at 1000RPM, then attached with 25G tips (Smooth Flow Tapered) before printing. The alginate, fibrinogen and all other solid reagents were UV sterilized for 10 mins prior fabrication.

2.1.3. Crosslinking of Hydrogels. Crosslinking of alginate in AlgGel hydrogels was done both externally (0.1M CaCl₂ (Sigma) + PBS (Sigma) solution, 0.22 μ m sterile filtered) and internally (30mM CaCO₃/60GDL). CaCl₂ solution was immediately applied post-print and samples were kept in the solution for either 10 mins or 1 hour. For external crosslinking, CaCO₃ and GDL are added as explained in 1.1.2. External vs internal crosslinking for AlgGel were compared to each other in 15x15mm by 6-layer samples and imaged at different time points. In AlgFib gels, alginate was only internally crosslinked by the same protocol as AlgGel gels, only 15, 45, and 60mM CaCO₃ was used in addition to 30mM. After printing, samples are to be further crosslinked by thrombin (from bovine plasma, Sigma) plus PBS and MTG (Moo Gloo™ RM formula, Modernist Pantry LLC, ME, USA) plus PBS. Printed samples kept in the thrombin

solution for one hour, then washed three times with PBS and then kept in MTG solution for one more hour and washed three times with PBS.

2.2. SCAFFOLD FABRICATION

A custom-modified tabletop cartesian 3D printer to include syringes connected through digital syringe dispenser (Loctite®, Rocky Hill, CT, USA) was used to fabricate scaffolds. The 3D printer and printing schema are illustrated in Figures 1(A) and 1(B) and the 3D printer is shown in Figure 1(C). Scaffold dimensions were set to 15mm length, 15mm width and ~ 1mm thick (6 layers) and printed with 0-90° filament orientation in alternate layers. Customized software was written for g-code generation and syringe dispenser control. Sterile practices were followed for scaffold fabrication with ASCs, bioink syringes were maintained at room temperature, and the scaffolds were printed inside the laminar flow hood[6].

2.3. ALGINATE-FIBRINOGEN HYDROGEL CHARACTERIZATION

Fourier Transform Infrared Spectroscopy (FTIR) was used to ensure that the hydrogel was uniformly mixed by comparing characterizing the presence of specific chemical groups in the materials. Samples were taken from the top, middle, and bottom layer of the AlgFib hydrogel once. Samples were analyzed by FTIR using Transmittance Mode. FTIR spectra were obtained in the range of 4000 to 500 wavenumber (cm^{-1}) during 1814 scans with a 4cm^{-1} resolution (Bruker Invenio R). The FTIR results of the different layers were graphed using excel with .1 absorbance unit offsets between bottom and middle layers and middle and top layer results. The FTIR spectra were normalized, and major vibration bands were associated with chemical groups.

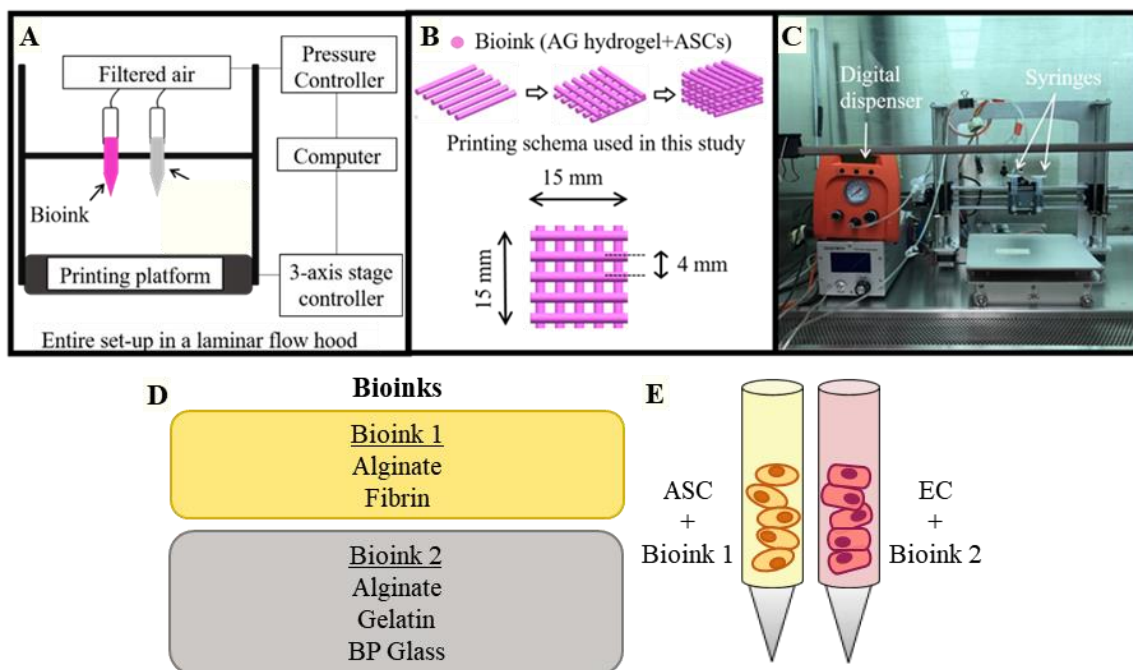


Figure 1. Extrusion-based 3D printing and components of the bioinks. (a) printer schematic used in this study, (b) the printing process and scaffold dimensions, and (c) bioprinter in the laminar flow hood with a syringe dispenser. (d) components of the two bioinks used in organoid fabrication and (e) are the cells that are used with each ink. Bioink 2 is based on previous research, while bioink 1 is a continuation of that research with modifications.

Printability was tested in multiple ways, by individual filament uniformity and printing shape fidelity[7,8]. In filament uniformity, ink was deposited in 1cm long lines every minute in a 15cm culture dish, starting at 15 minutes from initiation of internal gelation for 80 total filaments. Gel time was determined by the second non-uniform filament in a row, while print window equaled gel time minus the first filaments that were not under-gelled (fat and spread-out filaments). For shape fidelity, scaffolds of 10 x10mm² by 3 layers were printed every 15 minutes until 3 hours (after starting from 15 minutes gel initiation). Each sample was then imaged using a DSLR.

2.4. BOROPHOSPHATE BIOACTIVE GLASSES

Glasses with the nominal molar composition $16\text{Na}_2\text{O}-24\text{CaO}-\text{XB}_2\text{O}_3-(60-\text{X})\text{P}_2\text{O}_5$ (mol%) were produced, where $X = 0, 20,$ and 40 as seen in Table 1. Reagent grade batch materials were calcined at 300°C for at least 4 hours and then melted for an hour in platinum crucibles at $1000-1150^\circ\text{C}$, depending on composition. Melts were stirred on the half hour with a platinum rod, then quenched in graphite molds. Samples were annealed at 350°C for one hour then allowed to cool to room temperature and stored in a vacuum desiccator until use.

Table 1. Bioactive glass compositions. Nominal compositions in mol% of the glasses used in this study.

Bioactive Glass	SiO₂	Na₂O	K₂O	MgO	CaO	P₂O₅	B₂O₃
X0	0	16	0	0	24	60	0
X20	0	16	0	0	24	40	20
X40	0	16	0	0	24	20	40

Glasses were analyzed by x-ray diffraction, using a PANalytical X'Pert Multipurpose diffractometer with a Cu K- α source and a PIXcel detector, and all compositions were found to be amorphous. Bioactive glass (10wt% X40) was added to the alginate-fibrinogen solution before the alginate step, after the alginate was added, and with GDL right before printing. It didn't matter when X40 10wt%, the ink was not extrudable due to clotting.

3. RESULTS

3.1. EXTERNAL VS INTERNAL CROSSLINKING

An external crosslinker (0.1M CaCl₂ + PBS solution) (Figure 2A) was compared to internal crosslinker (30mM CaCO₃ / 60mM GDL) (Figure 2B) in the alginate-gelatin hydrogel in 15x15mm by 6-layer constructs. For external crosslinking, calcium chloride was immediately applied post-print and samples were kept in the CaCl₂ solution for either 10 minutes or 1 hour, was unable to fully crosslink the hydrogels even after 1 hour (Figure 2A and Figure 3A, B).

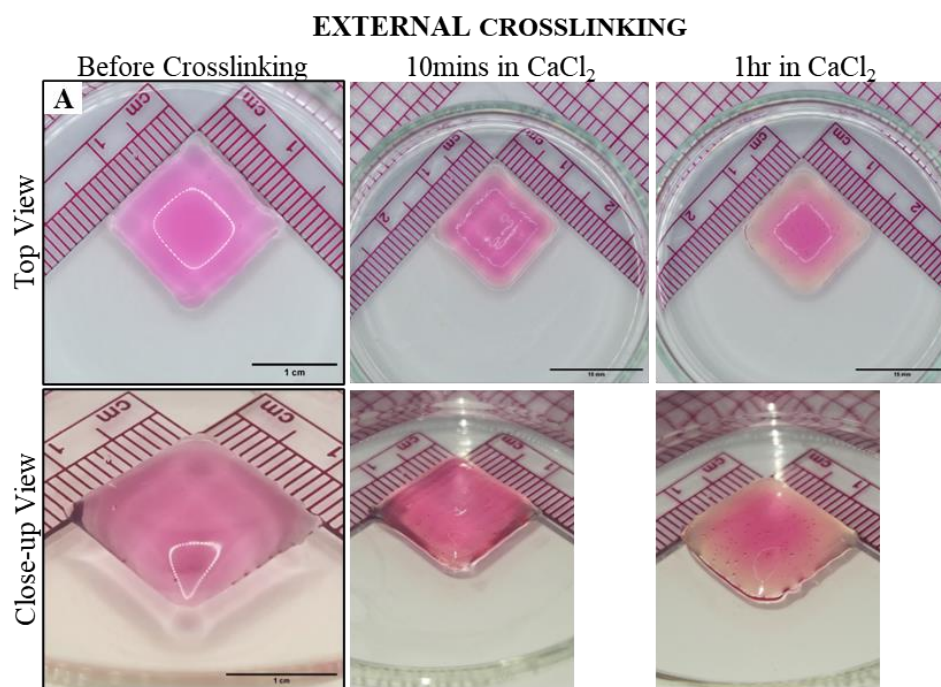


Figure 2. External vs internal crosslinking of alginate in alginate-gelatin hydrogel. External (A)(CaCl₂) crosslinking of organoids compared to internal (B) (GDL initiates CaCO₃ to crosslink of alginate). CaCl₂ is insufficient for crosslinking of constructs/organoids (10x10mm by 6 layers), since CaCl₂ took too long to crosslink samples in static conditions (> 1 hour). In the AlgGel protocol previously developed by co-authors, 10mins was sufficient time to crosslink 12x12x1mm³(5).

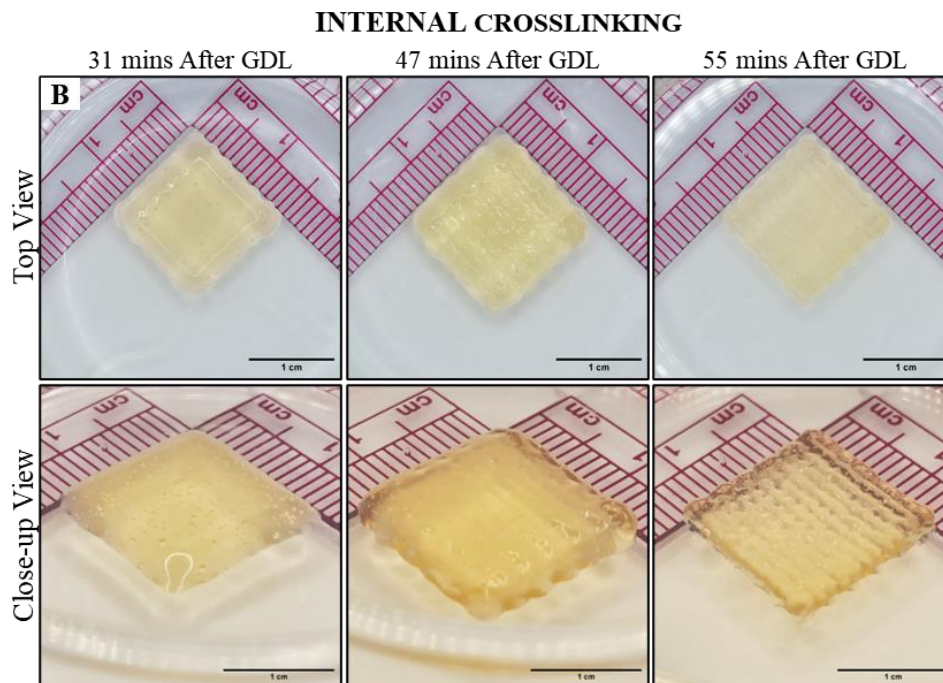


Figure 2. External vs internal crosslinking of alginate in alginate-gelatin hydrogel. External (A)(CaCl₂) crosslinking of organoids compared to internal (B) (GDL initiates CaCO₃ to crosslink of alginate). CaCl₂ is insufficient for crosslinking of constructs/organoids (10x10mm by 6 layers), since CaCl₂ took too long to crosslink samples in static conditions (> 1 hour). In the AlgGel protocol previously developed by co-authors, 10mins was sufficient time to crosslink 12x12x1mm³(5) (cont.).

In the lateral view of the hydrogel, liquid is still visible in the uncrosslinked section (Figure 2B). For internal crosslinking, calcium carbonate was introduced during the gelatin addition step (Figure 2B, Figure 3B). These hydrogel samples were printed after 20-30 minutes of initial crosslinking with CaCO₃, and subsequent gels were printed at average print times of 26, 32, 43, and 50 mins. The internally cross-linked hydrogels were consistently gelled throughout. Four samples per both groups were printed and images.

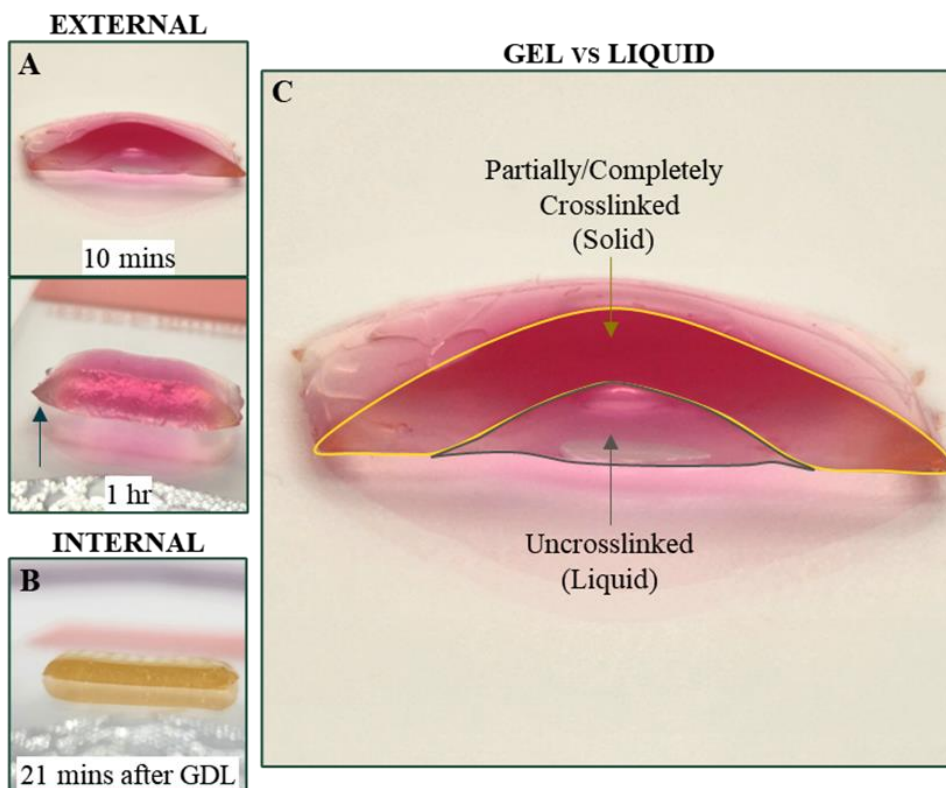


Figure 3. Lateral cross section of external vs. internal crosslinked samples. CaCl₂ (A) at both time points are not completely gelled, while CaCO₃ (B) is consistently gelled throughout. This phenomenon can clearly be seen in Gel Vs Liquid image (C) of 10mins CaCl₂ where there is an uncrosslinked section that is still liquid. The black arrow points to uneven gelling due to external crosslinking.

3.2. FTIR CONFIRMATION FOR UNIFORM MIX OF ALGINATE-FIBRINOGEN HYDROGEL

To determine uniform mixing of the internally crosslinked alginate-fibrinogen hydrogel, we took samples from the top, middle, and bottom layers to run on FTIR (Figure 4). FTIR confirmed that there was uniform mixing throughout the AlgFib hydrogel, even though there were two areas of the graph with any difference between the three layers (Figure 4A). Area #1 (Figure 4B) was within sufficient margin (< .005 absorbance units at its largest difference) of each other to confirm sufficient mixing,

because any time there is a negative dip below the starting point (-0.045), as in Area #2 (Figure 4C), it is due to variation in background gases, most likely CO₂[9], during the tests.

The peaks that correspond to each component of the gel were identified to confirm that they are consistent with literature (Figure 4A). The large broad peak at 3300cm⁻¹ is attributed to alginate and stretching vibration of -OH groups but is usually found at 3430cm⁻¹ and has shifted mostly likely because of a C-H groups from fibrinogen interacting with alginate. The other characteristic bands for alginate include peaks at 1636cm⁻¹ and 1412cm⁻¹ from asymmetric and symmetric COO⁻ stretching vibrations of carboxylate salt groups which have shifted, 1632cm⁻¹ and 1418cm⁻¹ respectively, due to ionic bonds with a Ca²⁺ crosslinker (CaCO₃). The small peak at 1032cm⁻¹ is from C=O stretching of alcohol groups[10–13]. Fibrinogen is also associated with 1632 peak, which is where amide I and stretching vibrations of C=O group, and peptides and amino acids from fibrinogen are in this range 1800 to 1000cm⁻¹[14–17]. Only one sample for each layer was run using the FTIR.

3.3. COMPARISON OF VARYING CONCENTRATIONS OF INTERNAL CROSSLINKER IN BIOINK FOR PRINTABILITY

To find the best concentration of internal crosslinker for alginate in AlgFib in terms of the printability, specifically printing window and gel time of the ink. Figure 5 compares filament uniformity between 30, 45, and 60mM of internal crosslinker. Starting from the blue arrow, individual filaments were printed every minute for 80 minutes. For 30mM, the gel time is 76 minutes total (61 mins filament test + 15 mins gelation start), and the printing window would be about 55 minutes (76mins total gel time - 20 mins from gelation start).

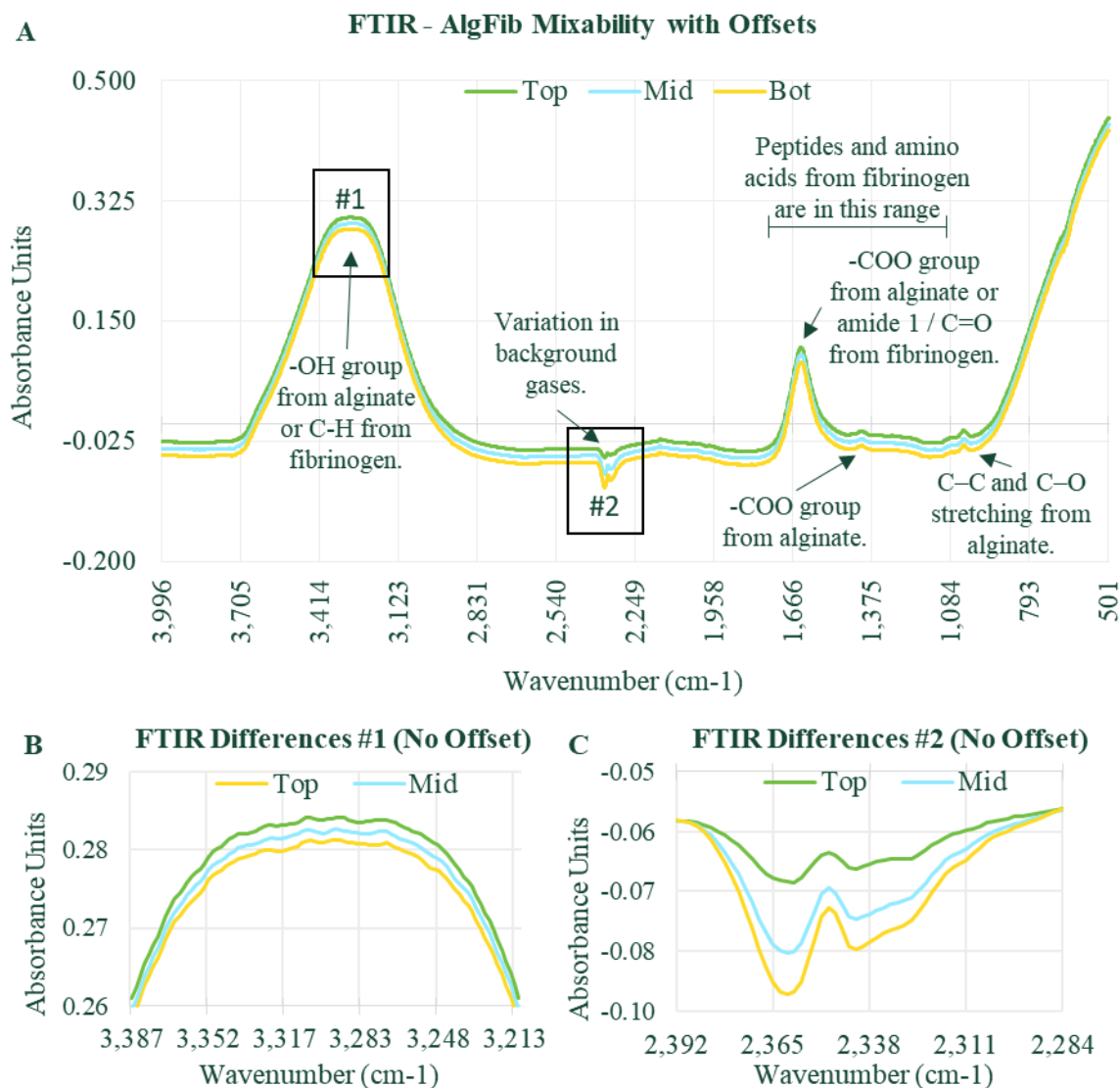


Figure 4. FTIR confirmation of uniform mix for alginate-fibrinogen hydrogel. Three different samples from the top, middle, and bottom layer were run on a FTIR to detect any difference between layers and to confirm uniform mixing throughout gel (A). Peaks associated with the components of the hydrogel were also identified. Only 2 areas had any differences between layers (B) and (C) without an offset.

The printability times for 45 and 60mM sharply decreases compared with 30mM. The gel times and printing window of 45 is 50 mins and 30mins, while 60mM is 35mins is less than 20 mins. 60mM does not have enough of a window to print multiple organoids of the size that we want. Another test to determine printability is printing shape

fidelity, where fidelity, gel time, and printing window can be determined. Figure 6 compares 15, 30, and 45mM (10x10mm, 3 layers) samples at different time points. Where every 15mins, a sample is printed, starting from 15mins after gelation start. 15mM was used instead of 60mM because of the results from the prior test. From the figure, 15mM is under-gelled until the third time point, but does become over-gelled within the test parameters (3 hours, images taken but not included). While 30mM also shows under-gelling until 60 mins (45mins +15 start of gelation) and then over gelling occurs starting by 75 mins and by 90 mins.

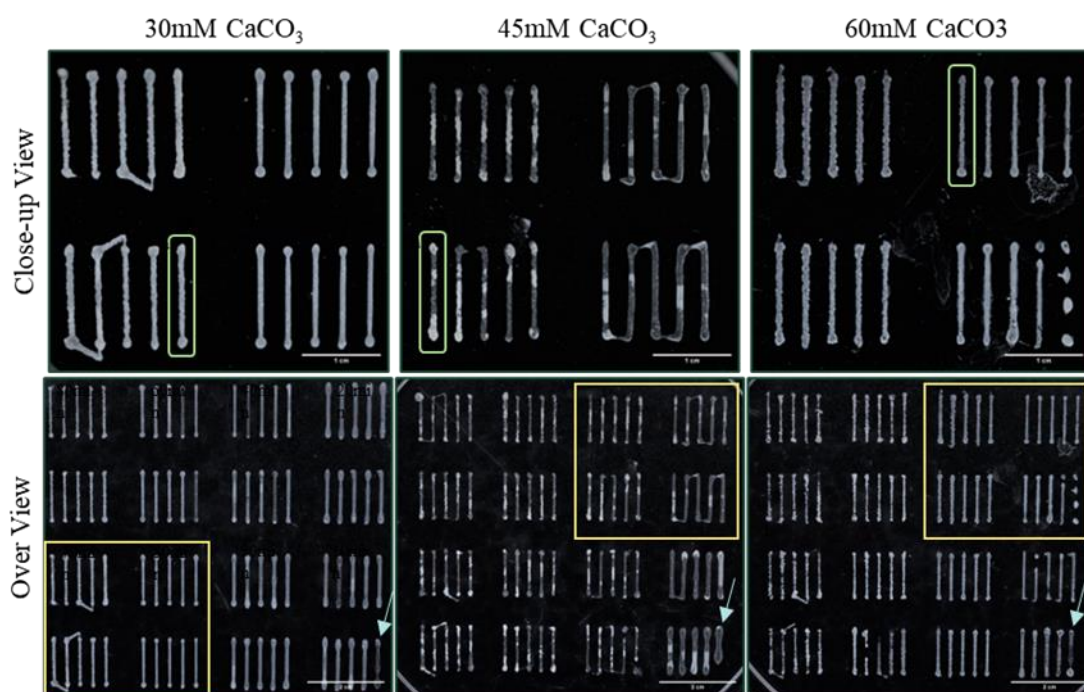


Figure 5. Printability of differing CaCO_3 concentrations in alginate-fibrinogen hydrogel ink. Individual filaments were printed every minute to determine gel time and print window, with 30, 45, and 60mM internal crosslinker. 60mM demonstrated that there would not be enough time to print multiple consistent organoids. The Blue arrows point to the starting filament, the yellow boxes correspond to the samples in the close-up view, and the green box indicates where the printed filaments no longer become consistent and have started to gel.

While 45mM did not have any good prints and it is difficult to determine any clear results from those images, except for maybe over-gelling occurred at 45 mins. The 30mM sample at 60mins is a perfect example of what was supposed to be printed, it was unfortunate that there was so much variation in printing during the test. Further testing would have narrowed the testing to a print every 5 mins, but we were only able to obtain data for 45mM.

4. DISCUSSION

In summary, we have developed a bioink system that can be used to print more realistic sized organoids for biomedical applications. The ink has rheological properties suitable for extrusion-based printing techniques and adipose stem cells infused in the ink remain viable seven days after printing. The ink consists of a mixture of alginate hydrogels, which provides the structural integrity of the printed scaffolds, and fibrin hydrogels, which supports cell proliferation and is a ready component of human extracellular matrix.

We demonstrated that using calcium carbonate and GDL for internal crosslinking produced better results than external crosslinking by calcium chloride in a $10 \times 10 \times 1 \text{mm}^3$ construct, since external crosslinking was unable to fully crosslink samples within a reasonable amount of time. FTIR was used to confirm that the protocol we developed for this novel bioink had uniform mixing and finally 30mM CaCO_3 was demonstrated to be the optimal concentration for bioprinting regarding printability.

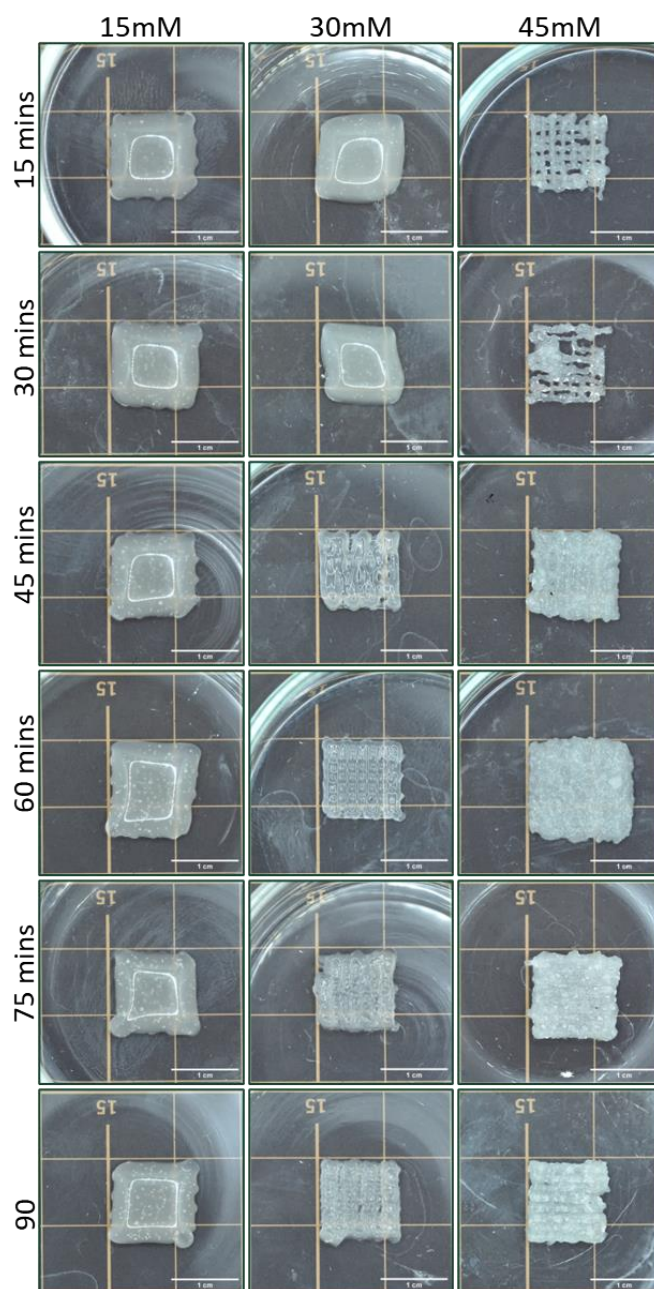


Figure 6. Comparison between varying concentrations of internal crosslinking in alginate-fibrinogen samples at multiple time points. The 15, 30, and 45mM samples (10x10mm, 3 layers) at 10 time points starting from 15 mins to 3 hours. 15mM did not gel within the 3hrs of testing, while 30mM gelled around 75mins and 45 at about 45 mins.

Borophosphate glass particles can then be added to the hydrogel mixture where they release Ca-ions that control the viscoelastic properties of the gel before and after

printing. Glasses, like X40, that release Ca-ions without creating local alkaline conditions promote significantly better ASC viability than the more basic glasses and X20- which has a much slower release profile, which allows it to be used with fibrin without clotting. It is anticipated that these “pH neutral” glasses could be doped with other ions that promote specific responses from the stem cells to create tissue models for different disease states.

REFERENCES

- Edmondson R, Broglie JJ, Adcock AF, Yang L. Three-Dimensional Cell Culture Systems and Their Applications in Drug Discovery and Cell-Based Biosensors. *ASSAY Drug Dev Technol.* 2014 May 1;12(4):207–18.
- Bray LJ, Binner M, Körner Y, Bonin M von, Bornhäuser M, Werner C. A three-dimensional ex vivo tri-culture model mimics cell-cell interactions between acute myeloid leukemia and the vascular niche. *Haematologica.* 2017 Jul 1;102(7):1215–26.
- Sun W, Starly B, Daly AC, Burdick JA, Groll J, Skeldon G, et al. The bioprinting roadmap. *Biofabrication.* 2020 Feb;12(2):022002.
- Park J, Wetzel I, Dréau D, Cho H. 3D Miniaturization of Human Organs for Drug Discovery. *Adv Healthc Mater.* 2018;7(2):1700551.
- Kolan KCR, Semon JA, Bromet B, Day DE, Leu MC. Bioprinting with human stem cells-laden alginate-gelatin bioink and bioactive glass for tissue engineering. *Int J Bioprinting [Internet].* 2019 Jul 8 [cited 2020 May 29];5(2.2). Available from: <http://ijb.whioce.com/index.php/int-j-bioprinting/article/view/204>
- Kolan KCR, Semon JA, Bindbeutel AT, Day DE, Leu MC. Bioprinting with bioactive glass loaded polylactic acid composite and human adipose stem cells. *Bioprinting.* 2020 Jun 1;18:e00075.
- Bom S, Ribeiro R, Ribeiro HM, Santos C, Marto J. On the progress of hydrogel-based 3D printing: Correlating rheological properties with printing behaviour. *Int J Pharm.* 2022 Mar 5;615:121506.

- Amorim PA, d'Ávila MA, Anand R, Moldenaers P, Van Puyvelde P, Bloemen V. Insights on shear rheology of inks for extrusion-based 3D bioprinting. *Bioprinting*. 2021 Jun 1;22:e00129.
- Smith BC. *Fundamentals of Fourier Transform Infrared Spectroscopy*. 2nd ed. Boca Raton: CRC Press; 2011. 207 p.
- Allaboun H, Fares MM, Abu Al-Rub FA. Removal of Uranium and Associated Contaminants from Aqueous Solutions Using Functional Carbon Nanotubes-Sodium Alginate Conjugates. *Minerals*. 2016 Mar;6(1):9.
- Kusuktham B, Prasertgul J, Srinun P. Morphology and Property of Calcium Silicate Encapsulated with Alginate Beads. *Silicon*. 2014 Jul;6(3):191–7.
- Remaggi G, Catanzano O, Quaglia F, Elviri L. Alginate Self-Crosslinking Ink for 3D Extrusion-Based Cryoprinting and Application for Epirubicin-HCl Delivery on MCF-7 Cells. *Molecules*. 2022 Jan;27(3):882.
- Soleimanpour M, Mirhaji SS, Jafari S, Derakhshankhah H, Mamashli F, Nedaei H, et al. Designing a new alginate-fibrinogen biomaterial composite hydrogel for wound healing. *Sci Rep*. 2022 May 4;12(1):7213.
- Montalbano G, Toumpaniari S, Popov A, Duan P, Chen J, Dalgarno K, et al. Synthesis of bioinspired collagen/alginate/fibrin based hydrogels for soft tissue engineering. *Mater Sci Eng C*. 2018 Oct 1;91:236–46.
- Xie HG, Zheng JN, Li XX, Liu XD, Zhu J, Wang F, et al. Effect of Surface Morphology and Charge on the Amount and Conformation of Fibrinogen Adsorbed onto Alginate/Chitosan Microcapsules. *Langmuir*. 2010 Apr 20;26(8):5587–94.
- Schwinté P, Voegel JC, Picart C, Haikel Y, Schaaf P, Szalontai B. Stabilizing Effects of Various Polyelectrolyte Multilayer Films on the Structure of Adsorbed/Embedded Fibrinogen Molecules: An ATR–FTIR Study. *J Phys Chem B*. 2001 Nov 1;105(47):11906–16.
- Gila-Vilchez C, Mañas-Torres MC, García-García ÓD, Escribano-Huesca A, Rodríguez-Arco L, Carriel V, et al. Biocompatible Short-Peptides Fibrin Co-assembled Hydrogels. *ACS Appl Polym Mater*. 2023 Feb 21;acsapm.2c02164.

SECTION

2. CONCLUSIONS AND FUTURE DIRECTIONS

The results in thesis indicate that by varying the phosphate-to-borate ratio in these Na-Ca-borophosphate glasses, local pH conditions can be tuned from acidic to basic. The incorporation of these pH neutral glass particles into an alginate-gelatin system creates a novel bioink, one in which the borophosphate glass particles release desired ionic species that stimulate desired cellular responses and that control the bioink viscosity to optimize printing. The cell viability and rheological results together demonstrate the potential benefits of adding borophosphate glasses to alginate-gelatin hydrogel system in bioprinting applications. Of the borophosphate glasses, X40 provided the best results for angiogenic potential and with culturing of ASCs due to its pH-neutral behavior and relatively fast degradation rate. The replacement of gelatin with fibrin and internal gelation further allows for this novel bioink to be used for 3D tissue models, like organoids. These organoids could then be a part of microphysiological systems in more dynamic and biomimetic conditions for high throughput use for scientists and clinicians who study cancer, immunology, aging, diabetes, regenerative medicine, as well as many other fields, like drug discovery and toxicity.

BIBLIOGRAPHY

- Hench LL. The story of Bioglass®. *J Mater Sci Mater Med*. 2006 Nov 1;17(11):967–78.
- Kaur G, Pandey O p., Singh K, Homa D, Scott B, Pickrell G. A review of bioactive glasses: Their structure, properties, fabrication and apatite formation. *J Biomed Mater Res A*. 2014;102(1):254–74.
- Jones JR. Review of bioactive glass: From Hench to hybrids. *Acta Biomater*. 2013 Jan 1;9(1):4457–86.
- Rahaman MN, Day DE, Sonny Bal B, Fu Q, Jung SB, Bonewald LF, et al. Bioactive glass in tissue engineering. *Acta Biomater*. 2011 Jun 1;7(6):2355–73.
- Li A, Lv Y, Ren H, Cui Y, Wang C, Martin RA, et al. In vitro evaluation of a novel pH neutral calcium phosphosilicate bioactive glass that does not require preconditioning prior to use. *Int J Appl Glass Sci*. 2017;8(4):403–11.
- Durand LAH, Góngora A, López JMP, Boccaccini AR, Zago MP, Baldi A, et al. In vitro endothelial cell response to ionic dissolution products from boron-doped bioactive glass in the SiO₂–CaO–P₂O₅–Na₂O system. *J Mater Chem B*. 2014 Oct 15;2(43):7620–30.
- Ciraldo FE, Boccardi E, Melli V, Westhauser F, Boccaccini AR. Tackling bioactive glass excessive in vitro bioreactivity: Preconditioning approaches for cell culture tests. *Acta Biomater*. 2018 Jul 15;75:3–10.
- Thyparambil NJ, Gutgesell LC, Bromet BA, Flowers LE, Greaney S, Day DE, et al. Bioactive borate glass triggers phenotypic changes in adipose stem cells. *J Mater Sci Mater Med*. 2020 Mar 23;31(4):35.
- Choi JH, Gimble JM, Lee K, Marra KG, Rubin JP, Yoo JJ, et al. Adipose Tissue Engineering for Soft Tissue Regeneration. *Tissue Eng Part B Rev*. 2010 Aug;16(4):413–26.
- Cherubino M, Rubin JP, Miljkovic N, Kelmendi-Doko A, Marra KG. Adipose-Derived Stem Cells for Wound Healing Applications. *Ann Plast Surg*. 2011 Feb;66(2):210–5.
- Fitzsimmons REB, Mazurek MS, Soos A, Simmons CA. Mesenchymal Stromal/Stem Cells in Regenerative Medicine and Tissue Engineering. *Stem Cells Int*. 2018 Aug 19;2018:8031718.
- Kolan KCR, Semon JA, Bindbeutel AT, Day DE, Leu MC. Bioprinting with bioactive glass loaded polylactic acid composite and human adipose stem cells. *Bioprinting*. 2020 Jun 1;18:e00075.

- Kolan KCR, Semon JA, Bromet B, Day DE, Leu MC. Bioprinting with human stem cells-laden alginate-gelatin bioink and bioactive glass for tissue engineering. *Int J Bioprinting* [Internet]. 2019 Jul 8 [cited 2020 May 29];5(2.2). Available from: <http://ijb.whioce.com/index.php/int-j-bioprinting/article/view/204>
- Goerges AL, Nugent MA. pH Regulates Vascular Endothelial Growth Factor Binding to Fibronectin A MECHANISM FOR CONTROL OF EXTRACELLULAR MATRIX STORAGE AND RELEASE. *J Biol Chem*. 2004 Jan 16;279(3):2307–15.
- Mishra A, Ojansivu M, Autio R, Vanhatupa S, Miettinen S, Massera J. In-vitro dissolution characteristics and human adipose stem cell response to novel borophosphate glasses. *J Biomed Mater Res A*. 2019;107(9):2099–114.
- Wesson DE, Simoni J, Green DF. Reduced extracellular pH increases endothelin-1 secretion by human renal microvascular endothelial cells. [Internet]. American Society for Clinical Investigation; 1998 [cited 2020 Sep 8]. Available from: <https://www.jci.org/articles/view/854/pdf>
- Catoira MC, Fusaro L, Di Francesco D, Ramella M, Boccafoschi F. Overview of natural hydrogels for regenerative medicine applications. *J Mater Sci Mater Med*. 2019 Oct 10;30(10):115.
- Advances in crosslinking strategies of biomedical hydrogels - Biomaterials Science (RSC Publishing) DOI:10.1039/C8BM01246F [Internet]. [cited 2022 Nov 21]. Available from: <https://pubs.rsc.org/en/content/articlehtml/2018/bm/c8bm01246f>
- Gao T, Gillispie GJ, Copus JS, PR AK, Seol YJ, Atala A, et al. Optimization of gelatin–alginate composite bioink printability using rheological parameters: a systematic approach. *Biofabrication*. 2018 Jun;10(3):034106.
- Li Z, Huang S, Liu Y, Yao B, Hu T, Shi H, et al. Tuning Alginate-Gelatin Bioink Properties by Varying Solvent and Their Impact on Stem Cell Behavior. *Sci Rep*. 2018 May 22;8(1):8020.
- Bom S, Ribeiro R, Ribeiro HM, Santos C, Marto J. On the progress of hydrogel-based 3D printing: Correlating rheological properties with printing behaviour. *Int J Pharm*. 2022 Mar 5;615:121506.
- Jiao W, Li X, Shan J, Wang X. Study of Several Alginate-Based Hydrogels for In Vitro 3D Cell Cultures. *Gels*. 2022 Mar;8(3):147.

VITA

Bradley Allen Bromet earned his Bachelor of Science from the Missouri University of Science and Technology in Rolla, MO, USA in May 2019. He changed majors 3 times during that time before finding his niche in the biology department and joined Dr. Julie Semon's Lab of Regenerative Medicine in Spring 2018. She introduced him to Dr. Krishna Kolan, who was bioprinting cool things. Brad then decided to continue to mess around with science in her lab and continued his academic career by pursuing a Master of Science in Biological Sciences. He somehow lucked into getting a graduate research assistantship with Dr. Katie Shannon and the confocal microscope, which he found he liked, along with a couple of graduate teaching assistantships to help him along his way. After multiple authorships, awards, and proceedings, Brad has decided he has grown too big for S&T and is going to spread his wings and fly off to PhD world after getting accepted by multiple universities. He is tired and would like to ask his committee if they can just give him his master's degree in Biological Sciences from the Missouri University of Science and Technology in May 2023.